Gas Path Analysis on the GEnx-1B at KLM Engine Services

M. P. R. van Moorselaar

Technische Universiteit Delft

TU Delft

Gas Path Analysis on the GEnx-1B at KLM Engine Services

by

M. P. R. van Moorselaar

to obtain the degree of Master of Science
at the Delft University of Technology,
to be defended publicly on Monday September 24, 2018 at 11:00 AM.

Student number:	4139461	
Project duration:	September, 2017 – September, 2018	
Thesis committee:	Prof. dr. ir. P. Colonna,	TU Delft
	Dr. ir. W. P. J. Visser,	TU Delft, supervisor
	Dr. ir. W. J. C. Verhagen,	TU Delft
	Ing. M. Nollet,	KLM Engine Services

TU Delft

Executive Summary

Modern gas turbines are complex and expensive machines, requiring specialised maintenance to keep them in working order. Maintenance takes places at specialised shops such as KLM Engine Services (KLM ES). Part of KLM Engineering & Maintenance (KLM E&M), KLM ES provides maintenance services to aircraft engines belonging both to KLM and to external customers.

Gas Path Analysis (GPA) is a technique which can aid KLM ES in its maintenance process. As a gas turbine deteriorates over time, its performance will change. These changes in performance can be measured in the gas path of the engine. Using GPA the degraded component can be identified, after which corrective steps can be taken. This analysis gives more insight into the condition of a gas turbine than the traditional method in which only the Exhaust Gas Temperature (EGT) margin is taken into account. At KLM ES GPA is performed using Gas turbine Simulation Program (GSP), currently with the capability to analyse the General Electric (GE) CF6-80 and CFMI CFM56-7B.

Recently KLM ES has started maintenance on the GE GEnx-1B, powering the Boeing 787. The GEnx-1B is a state of the art aircraft engine, capable of collecting large amounts of performance data while in operation. KLM ES is not yet able to apply GPA to the GEnx-1B. The objective of this research is to extend the use of GPA at KLM ES to the GEnx-1B, by creating a model in GSP capable of providing accurate GPA results for the GEnx-1B using both test cell and on-wing measurements.

A GSP model has been created based on test cell measurements, taken at different power settings, of an average GEnx-1B. The range of power settings over which the model is capable of simulating the engine has been extended using take-off snapshots taken on-wing. Off-design performance simulation in GSP is based on component maps, describing the performance of the compressors and turbines of a gas turbine. Component maps describing the behaviour of the GEnx-1B components are proprietary to GE and unavailable in the public domain. Therefore maps representing a CF6-80, which are based on publicly available maps and are accessible at KLM ES, have been tuned to match the measured GEnx-1B performance. The tuned model is capable of simulating the reference engine in take-off conditions well. Some modelling errors remain, however these do not hamper the usability of the model of GPA.

Although the GEnx-1B is a much more modern engine than a CF6-80, it has fewer sensors installed in its gas path. Most importantly no pressure measurement is taken in the fan bypass, after the booster and after the High Pressure Turbine (HPT). During modelling this increased the uncertainty involved in tuning the component maps and required additional assumptions to be made to fix the model in the design point. Furthermore it has its effect on the application of GPA using GSP. The GPA method implemented in GSP is Adaptive Modelling (AM). AM is directly dependent on the amount of parameters measured in an engine, it requires an equal amount of available measurements as engine parameters it can adapt to compute an engine its condition. As previous work focused on engines with more measurements available, more research was required to investigate the possibility of applying AM to the GEnx-1B. It is found that the lack of a pressure sensor after the HPT affects GPA the most. With this sensor missing, deterioration on the Low Pressure Turbine (LPT) is contributed to an HPT efficiency loss by the AM component. Having no pressure measurement after the booster does not severely impact AM results. Lack of a thrust measurement, or equivalent pressure measurement, results in having no information available on the fan when on-wing snapshots are analysed. Overall it was concluded that the model would still be usable to analyse the condition of GEnx-1Bs in operation, or in the test cell after maintenance.

The model has been tested using snapshots of test cell measurements available from multiple engines and using on-wing take-off snapshots of the whole KLM fleet. Results based on test cell snapshots correlate well with the work done during the shopvisits and with the EGT margin as reported by the test cell software. Analysis of on-wing snapshots also shows a good relation with the EGT margin as computed by the engine. Furthermore deterioration is attributed to the components on which it would be expected. On-wing results are affected by scatter, which also influences the choice of reference dataset. A suggestion is made for a reference dataset, enabling the analysis of all KLM GEnx-1Bs considered. Overall it is proved that it is possible to analyse a modern engine such as the GEnx-1B with GSP, both in the test cell and in operation.

Preface

This report concludes both my year long research at KLM Engine Services and my time as a student at the Faculty of Aerospace Engineering at Delft University of Technology. It is also the starting point of a career in aviation and a fascination with aircraft engines.

Over the course of my graduation project I have learned a tremendous amount about both engines and the MRO world in general. I am grateful for having had the chance to graduate at KLM, in an operational environment where maintenance is performed daily on all kinds of engines. It has been inspiring to see the machines I have been researching each morning as I walked in.

I would like to express my gratitude to all my colleagues at KLM, who have assisted me during this project with their enormous amount of expertise. Specifically I would like to thank Michel Nollet for having been my supervisor, guiding me over the past year. Furthermore I would like to thank dr. ir. Visser for the scientific supervision from the faculty and prof. dr. ir. Colonna and dr. ir. Verhagen for taking place in my graduation committee. Finally I want to thank my friends and family for the support over the years and for having made my student life unforgettable!

M. P. R van Moorselaar
Schiphol-Oost, August 2018

Contents

List of Figures

List of Tables

Nomenclature

Acronyms

AFI	Air France Industries
AFKL	Air France-KLM
AI	Artificial Intelligence
AM	Adaptive Modelling
ANN	Artificial Neural Network
ARP	Aerospace Recommended Practice
BAI	Booster Anti-Ice
BPR	Bypass Ratio
CDG	Paris-Charles de Gaulle
CEOD	Continuous Engine Operating Data
CF	Calibration Factor
DOD	Domestic Object Damage
EGT	Exhaust Gas Temperature
EGTHDM	EGT Hot Day Margin
EGTSDM	EGT Standard Day Margin
ES	Expert System
ESN	Engine Serial Number
EEC	Engine Electronic Control
EWMA	Exponentially Weighted Moving Average
FADEC	Full Authority Digital Engine Control
FN	Net Thrust
FCM	Fault-Correlation Matrix
FNKSD	Corrected Standard Day Thrust
FOD	Foreign Object Damage
GA	Genetic Algorithm
GE	General Electric
GPA	Gas Path Analysis
GSP	Gas turbine Simulation Program
GUI	Graphical User Interface
HD	Hot Day
HPC	High Pressure Compressor
HPT	High Pressure Turbine
HPTACC	HPT Active Clearance Control
ICM	Influence-Coefficient Matrix
IGV	Inlet Guide Vane
ISA	International Standard Atmosphere
KLM	Koninklijke Luchtvaart Maatschappij (Royal Dutch Airlines)
KLM E&M	KLM Engineering & Maintenance
KLM ES	KLM Engine Services
LPC	Low Pressure Compressor
LPT	Low Pressure Turbine
LPTAAC	LPT Active Clearance Control
MC	Maximum Continuous
MM	Map Modifier
MRO	Maintenance Repair & Overhaul

NLR	National Lucht- en Ruimtevaartcentrum (Netherlands Aerospace Centre)
OEM	Original Equipment Manufacturer
OPR	Overall Pressure Ratio
OTR	Overall Temperature Ratio
PDF	Probability Density Function
PR	Pressure Ratio
PRSV	Performance Restoration Shopvisit
PTO	Power Take Off
QT	Quick Turn
SFC	Specific Fuel Consumption
SD	Standard Day
TO	Take-Off
VBV	Variable Bleed Valve
VFSG	Variable Frequency Starter Generator
VSV	Variable Stator Vane
WFKSD	Corrected Standard Day Fuel Flow
WPG	Workscope Planning Guide

Roman symbols

A	Area [m^2]
A	EWMA outcome
c_p	Specific heat at constant pressure [J/mol K]
D	Characteristic linear dimension [m]
F	Force [N]
h	Enthalpy [J]
M	Mach number [-]
$\dot{m}$	Mass flow [kg/s]
p	Pressure [Pa]
R	Specific gas constant [J kg^{-1} K^{-1}]
T	Temperature [K] or [°C]
v	Velocity [m/s]

Symbols as commonly used at KLM and GE, used as well in this thesis:

N	Rotational speed [rpm]
PS	Static pressure [Pa]
PT	Total pressure [Pa]
RHUM	Relative humidity [%]
TT	Total temperature [K] or [°C]
W	Mass flow [kg/s]
WF	Fuel flow [kg/s]
WA2	Total engine mass flow [kg/s]

Greek symbols

γ	Ratio of specific heats [-]
Δ	Difference
δ	Normalised pressure [-]
η	Efficiency [-]
θ	Normalised temperature [-]
μ	Mean
ρ	Density [kg/m^3]
σ	Standard deviation

Subscripts

0,	Total property
1, 2, 25...	Engine station numbering according to ARP 755A
a	Air
c	Compressor
c	Corrected
cc	Combustion
f	Fuel
g	Gas power point
g	Gas
is	Isentropic
j	Jet
m	Mechanical
ram	Ram
t	Turbine

1 Introduction

Invented in the 1930s, jet engines, and later more advanced forms of gas turbines used as aircraft engines, have become the standard form of propulsion for civil aircraft [26, 31]. Gas turbine technology has allowed aircraft to fly higher and faster than previously thought possible. Nowadays civil aircraft are powered by turbofan engines, an evolution of the basic jet engine. Turbofans are characterised by a large fan at the front of the engine, delivering most of the propulsive power, in addition to the propulsive jet of the jet engine.

Modern gas turbines are highly reliable machines, with aircraft engines staying on-wing for thousands of hours [34]. However, like all mechanical devices, gas turbines suffer from wear and tear, requiring occasional repair and maintenance. Furthermore they need the occasional inspection or maintenance for flight safety reasons. Modern gas turbines are complex pieces of machinery, requiring specialised knowledge in order to work with them. Due to this, gas turbine maintenance takes place in specialised shops. KLM Engine Services (KLM ES) is such a shop, based at Schiphol Airport.

KLM ES is part of Air France Industries KLM Engineering & Maintenance (KLM E&M), part of the Air France-KLM Group. About 180 engines visit the shop each year, both engines from KLM and from external customers. The shop has the capability to provide maintenance for the CFM56-7B, General Electric (GE) CF6-80 family and the GE GEnx-1B. At Schiphol KLM ES operates its own test-cell, where performance testing on the CFM and CF6 engines takes place. The GEnx-1B is tested in a different test cell at Charles de Gaulle (CDG), Paris.

Not only are modern aircraft engines complex, they are also expensive to acquire, operate and maintain. For the operator it is therefore important to have the engine on-wing as much as possible. Availability and maintainability are therefor important. This extends to the MRO (Maintenance Repair and Overhaul), in order to maintain customer satisfaction.

A tool which can aid KLM ES in the maintenance process is Gas Path Analysis (GPA). GPA can be used to get condition estimates of individual gas turbine components based on gas path measurements when the engine is in operation. Measurements can both be taken in a test cell, or during on-wing operation. The knowledge gained from applying GPA can be used to aid in determining the work to be done on an engine, to assess the effectivity of the work done, and to track the condition of different components.

The condition of a gas turbine in all its complexity is usually summarised in one value, the Exhaust Gas Temperature (EGT), or temperature behind the High Pressure Turbine (HPT). For each engine a redline is established, an EGT that cannot be exceeded. The difference between the EGT of the engine and the redline is referred to as the EGT margin and is the most important condition parameter for a gas turbine. The EGT margin does not provide information on the condition of each individual component, only on the overall condition of the engine. A component which performs badly can be compensated for by a component which performs much better, resulting in an average EGT margin. GPA can be used to provide more information on the condition of the individual components, rather than on the engine as a whole.

The current use of GPA at KLM is limited. GPA is applied only when an engine shows unexpected behaviour during the outbound test run, executed after maintenance on the engine is completed. If this unexpected behaviour is due to the gas path components, GPA can be used to diagnose the engine,

aiding in defining the additional workscope. KLM ES currently has the capability to use GPA in analysing the CFM56-7B and CF6-80 engines, which is done using the software package Gas turbine Simulation Program (GSP).

1.1. Research objective and questions

Maintenance on the GEnx-1B has only recently started at KLM ES. Although quite some engines have already visited the shop, KLM is still gaining experience with the GEnx-1B. Only Quick Turns (QTs) have been performed on the engine, consisting of light maintenance to correct unwanted behaviour of the engine, with no regard for the performance of the engine. More knowledge on the performance of the engine and its change over time must still be gained.

Not only knowledge must be gained on the GEnx-1B, as KLM ES currently also lacks the ability to apply GPA to the engine. This thesis is a first step into gaining the ability to apply GPA to the GEnx-1B at KLM ES. Although similar in layout to older engines, the GEnx-1B takes different measurements in its gas path, making it interesting to investigate whether previous research can still be applied to this engine. Furthermore, with the advent of faster computers and the ability to store more data, the GEnx-1B collects more data when in operation. The use of this data in combination with GPA might prove to be useful in analysing the performance of the engines while in operation.

The research objective of this research is thus defined to be: *To extend the use of GPA at KLM ES to the GEnx-1B, by creating a model in GSP capable of providing accurate GPA results for the GEnx-1B using both test cell and on-wing measurements.*

To fulfil this objective several research questions will have to be answered along the way. The overall research question can be summarised as: *How can Gas Path Analysis with Gas turbine Simulation Program be applied to the GEnx-1B at KLM Engine Services?* GSP is already used at KLM ES and is proven to be a good choice for GPA in a previously performed literature study. Furthermore an important part of the question is the fact that it will have to be answered in the MRO environment, where limited information on the engine is available.

In answering the overall research question several subquestions can be defined which will be answered along the way. These questions are stated below.

- How can the GEnx-1B be modelled in GSP for GPA purposes and what are the effects of having different measurements available?
- Is the created model providing accurate and usable GPA results, using both on-wing and test cell measurements?

1.2. Report structure

The report is divided into three parts. Part I contains necessary background information, giving the theoretical background of the thesis. This is followed by Part II in which the GSP model of the GEnx-1B is created. Finally the model its ability in applying GPA is tested in Part III, which is followed by the conclusions and recommendations.

Background knowledge in Part I is given on GSP in Chapter 2, followed by more information on gas turbine deterioration in Chapter 3. GPA is detailed in Chapter 4 and finally the GEnx-1B is detailed in Chapter 5.

The model creation in Part II starts with some preparation in Chapter 6, followed by the design point modelling in Chapter 7. The GEnx-1B model is then finished in Chapter 8, with the off-design modelling.

Part III starts with an intermediate step, investigating the use of Adaptive Modelling (AM), the GPA method applied in GSP, to an engine with fewer available measurements than currently used in literature in Chapter 9. This is followed by a sensitivity analysis of the GEnx-1B model in Chapter 10. Next the model is tested using simulated data in Chapter 11 and real engine data in Chapter 12. The report is concluded in Chapter 13, where recommendations will be given as well.

I

Background information

2

Gas turbine Simulation Program

Gas turbine performance calculations are often performed using computer software. In this chapter these software packages are investigated further. First an overview of the different modelling techniques is given, followed by an introduction to GSP, the software package that will be used in this research. The working principles of GSP are then investigated in more detail.

2.1. Gas turbine modelling techniques

A wide range of different computer models are available to predict the performance of gas turbines and to simulate their behaviour. An engine model can be defined as a mathematical description of an engine, representing its physical behaviour [27]. Models can both be used during the design phase of an engine and during its operational life. It is also possible to model components separately, rather than the engine as a whole.

Which kind of model is used depends on the use case. Which part of the life cycle of the engine the model will be used in, the level of fidelity needed and what part of the engine is of interest, are all examples of variables changing the kind of model to be used. Not only thermodynamic models are of interest also for example for vibrational analysis models. This will lead to additional parameters needed for accurate modelling. These models are usually mainly of interest to the engine designer [27].

In this report the focus will be on thermodynamic modelling of gas turbines for performance calculations. These models can be split into different categories, depending on how the spatial dimension of the engine is modelled. This can be done in either 0-D, 1-D, 2-D and 3-D. With an increase in spatial dimensions modelled, the required computing power increases as well. A description of the spacial dimensions is given below [27].

- **0-D** In 0-D models the flow properties are only calculated at discrete points inside the engine. These points usually correlate with the inlet and outlet of different components, such as the compressor. At these points only average properties are calculated.
- **1-D** In 1-D models the average flow properties are still calculated, however these properties are known continuously throughout the engine. Rather than computing the flow properties at discrete points, one dimension of the engine is computed continuously, for example the length.
- **2-D** In 2-D models the flow is assumed to be axi-symmetric. In these models the physics behind the processes in the gas turbine are modelled as well.
- **3-D** 3-D models do not use any simplifications and use the full equations of motion to represent the flow inside the turbine.

2.2. Background information on GSP

Engine manufacturers usually provide engine specific code to operators, to be used for health monitoring and diagnostics [27]. Furthermore engine specific codes and models are developed during the

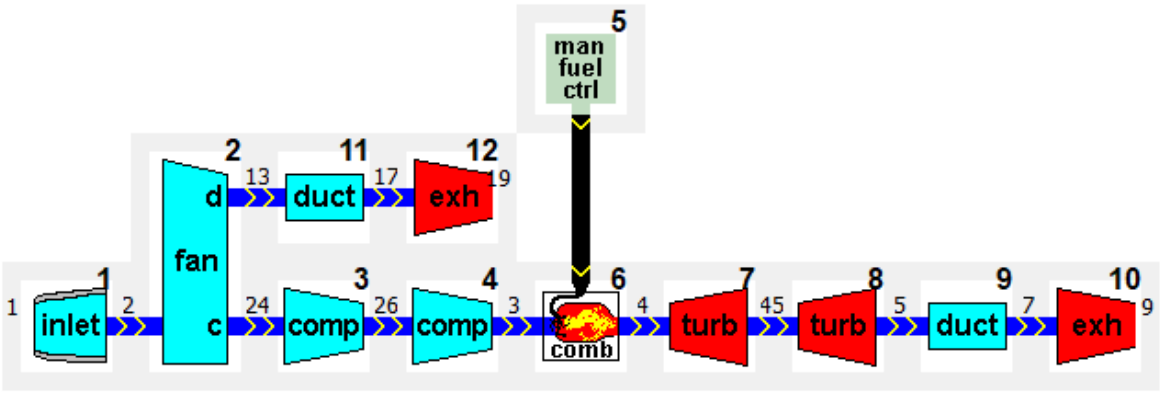

Figure 2.1: GSP model representation of a twin-spool turbofan.

engine design process, getting more advanced as the design process develops [38]. These more detailed codes and models however remain engine specific.

Outside of the Original Equipment Manufacturer (OEM) environment the need has arisen to be able to analyse the performance of different gas turbines. Ideally the simulation would be possible for any gas turbine, without the need for OEM information using a generic software package. This sparked the development of GSP, started at Delft University of Technology and the Netherlands Aerospace Centre (NLR). First work on creating such a program was already started in 1986 [38]. GSP has its origins in NASA's DYNGEN, after which it has been rewritten first in FORTRAN77 at NLR and finally in Borland Delphi for use on Microsoft Windows computers [15, 38].

GSP can be described as "a generic object-oriented gas turbine simulation environment" [39]. GSP can be used to simulate generic gas turbines, using its drag and drop interface, which allows the user to quickly generate different gas turbine geometries. Generic components which can be linked together, representing compressors, combustion chambers, nozzles and numerous other components are used in GSP. These can be combined using control components to simulate different operating points and conditions. GSP is build using an object oriented approach, the details of which are explained by Visser and, Visser and Broomhead in [38, 39].

Using the spatial discretisation terminology from Section 2.1 GSP can be described as an 0-D simulation program. Flow properties are only calculated at the inlet and exit of the components used [38]. The details of the flow inside a component are not computed.

For this thesis the most important part of using GSP is the flexible approach, allowing for the simulation of any gas turbine without any additional coding. Using the drag and drop GUI of GSP a gas turbine can be modelled with generic component blocks. This can be seen in Fig. 2.1. These components can be linked using gas paths and mechanical links. The components itself can be tuned to accurately model the gas turbine of interest [38, 39].

GSP can be used to perform design point calculations, steady-state off-design performance calculations and transient calculations. It is also possible to perform series of steady-state performance calculations, sweeping across parameters. Deterioration is modelled in GSP as an off-design condition [38].

2.3. Working principles of GSP

In this section the thermodynamic calculations and numerical techniques used in GSP are detailed. The exact implementation in the software itself is explained in detail by Visser in [38]. Background information on the thermodynamic principles of gas turbines and hence the performance calculations in GSP is found in Appendix C.

2.3.1. Design and off-design computations

In GSP a difference is made between design and off-design computations. In this section the difference is shortly explained, as this directly influences the modelling of the GEnx-1B in Chapters 7 and 8.

The design point of a gas turbine is the condition, ambient conditions and power setting, at which

Table 2.1: Parameter groups used for gas turbine performance analysis

	Dimensionless parameters	Quasi-dimensionless parameters	Corrected parameters
Pressure Ratio	$\frac{p_{0,2}}{p_{0,1}}$	$\frac{p_{0,2}}{p_{0,1}}$	$\frac{p_{0,2}}{p_{0,1}}$
Efficiency	η	η	η
Mass flow	$\frac{\dot{m}\sqrt{RT_{0,1}}}{D^2 p_{0,1}}$	$\frac{\dot{m}\sqrt{T_{0,1}}}{p_{0,1}}$	$\frac{\dot{m}\sqrt{\theta}}{\delta}$
Rotational speed	$\frac{ND}{\sqrt{RT_{0,1}}}$	$\frac{N}{\sqrt{T_{0,1}}}$	$\frac{N}{\sqrt{\theta}}$

all the engine its components run at their design operating point. That is the speed, pressure ratio and mass flow for which they are designed [26]. Which point this is can vary during the design process [43]. The design point for a model, or performance calculation, does not have to be the same point as used in designing the engine [38]. In previous studies at KLM ES take-off power at International Standard Atmosphere (ISA) sea level conditions has been chosen as the design point for the model [5, 34]. This point was chosen as it is the most demanding tested power setting in the KLM ES test cell.

Design point performance calculations can be computed without the need for any iterations, by computing the engine properties from inlet to exit. Completing the design point computations fixes the design/cycle of the model [26], due to which they can also be referred to as cycle reference computations [38]. Off-design computations are slightly more difficult, involving iterative loops. The design of the gas turbine is fixed, after which for given conditions an operating point must be found. This involves finding a point on the component maps of the different components (Section 2.3.3) which satisfy the compatibility conditions (Section 2.3.3).

2.3.2. Component performance

As shown in Fig. 2.1 and described above models in GSP are made up of individual generic components. The generic components can be altered to represent the gas turbine design of interest. This can either be a new design, or an existing one.

Upon adding a component its properties can be altered in the GUI (Graphical User Interface) by double clicking it. Here the design parameters can be changed, which dictate the design point of the component. For a compressor this would for example be the design pressure ratio and efficiency amongst others. Geometrical parameters can also be set, such as the component exit area. Doing so the design point of each component can be fully specified.

Off-design performance of components can be specified using component characteristics, or component maps. Using dimensionless parameter groups (Table 2.1) the performance of compressors and turbines can be described. These component characteristics can be described visually using compressor and turbine maps. On these maps curves are drawn relating the pressure ratio or efficiency against the mass flow for several constant spool rotational speeds. The curves for efficiency and pressure ratio can also be incorporated into one map, using lines of constant efficiency [26].

Having specified the design point of a component, this point acts as a cycle reference point [38]. The design point location on the component map is fixed by the GSP user. The program will then scale the map, such that the dimensionless parameters in the design point specified by the user match the values in the map in the chosen design point location. In this way a generic component map can be used, which is scaled by the program to match the engine design of interest.

Accurate component maps are essential in making correct performance computations for a specific gas turbine. The component maps however are proprietary to the OEM and are therefore not publicly available. When a model is created of an existing engine these maps have to be reverse engineered, by tuning publicly available maps until they match measured performance on the actual engine [1, 2, 5, 34, 36, 40]. This process will be described further in Chapter 8.

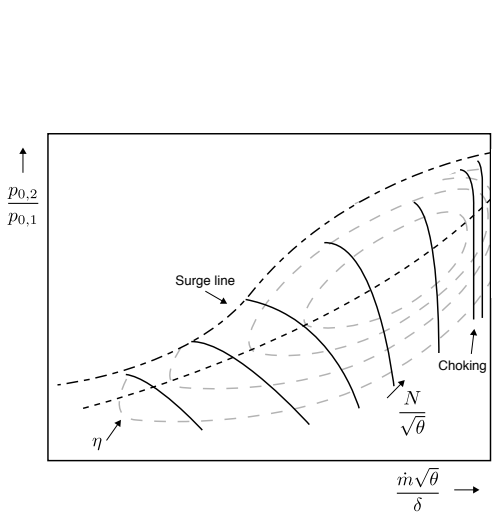

(a) Generic compressor map [31][Redrawn]

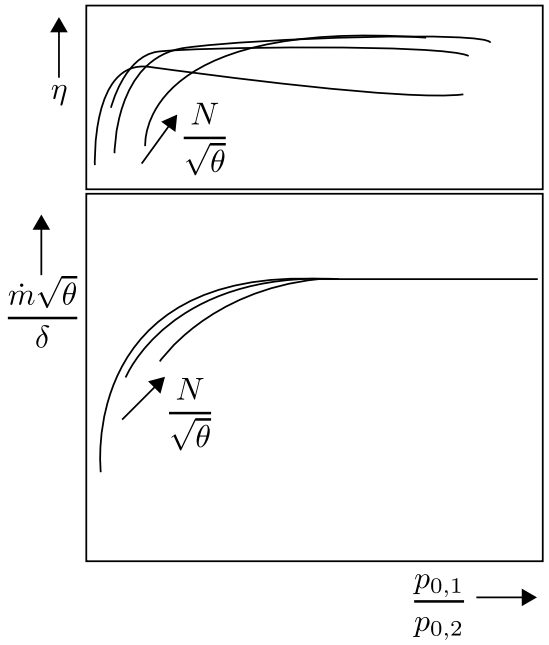

(b) Generic turbine map [26][Redrawn]

Figure 2.2: Example of an generic compressor and turbine map [26, 31]

An addition to the maps in GSP and other software packages are beta lines. These lines are not related to the component itself, but are used to load the component maps into the program. The beta lines can be seen as an array of addresses, specifying the location of the operating point in the compressor map. Doing so can avoid troubles with horizontal or vertical speed lines [38, 43]. Not all components need maps to describe their off-design performance, in these cases simpler relations are used. An example of this is a fixed pressure loss in a duct [38]. Between the lines on the map GSP interpolates linearly or quadratically. In this thesis, as in previous research, the interpolation is done in a linear fashion.

2.3.3. Compatibility equations

Running a gas turbine requires compatibility between the mass flow, work and rotational speed of different components in the gas turbine. Off-design performance calculations are based on matching the different components of a gas turbine with each other. Matching here refers to satisfying the compatibility conditions. For a physically accurate performance calculation, compatibility of mass flow, work and rotational speed is required between components [26].

For a twin-spool turbofan this has the following implications. The rotational speed of the fan, booster and Low Pressure Turbine (LPT) must be equal, as they are connect to the N1 shaft. The same goes for the High Pressure Compressor (HPC) and High Pressure Turbine (HPT). The power delivered by the LPT must be equal to the power required by the fan and booster, compensated for any mechanical losses. Te same counts for the HPC and HPT on the N2 shaft. The mass flow through the core engine must, after tertiary airflows have been subtracted or added, be equal through all components. Therefore the components on both shafts are aerodynamically coupled even though they are mechanically uncoupled [26].

The compatibility requirements in GSP are formalised for each component or shaft. These requirements are shown below [38].

First the mass flow compatibility between the inlet and exit of a component is described using Eq. (2.1). In this equation m_v refers to the mass inside a volume v, in this case the internal volume of the component.

$$\frac{\mathrm{d}m_v}{\mathrm{d}t} = \dot{m}_{in} - \dot{m}_{out} \tag{2.1}$$

The change in mass inside a volume can also be described using the relations between the different

gas properties, as shown in Eq. (2.2). The subscript $comp$ refers to the component itself, in this case the component volume.

$$\frac{\mathrm{d}m_v}{\mathrm{d}t} = \frac{V_{comp}}{\gamma RT}\frac{\mathrm{d}p}{\mathrm{d}t} \tag{2.2}$$

Next the conservation of energy is determined within a component using Eq. (2.3) and shaft Eq. (2.4).

$$\frac{\mathrm{d}m_v}{\mathrm{d}t}u + m_v\frac{\mathrm{d}u}{\mathrm{d}t} - Q = \dot{m}_{in}h_{in} - \dot{m}_{out}h_{out} + P_{abs} \tag{2.3}$$

$$I\frac{\mathrm{d}\omega}{\mathrm{d}t}\omega = P_{abs} - P_{del} \tag{2.4}$$

An additional equation is used for the conservation of momentum. This is needed when calculating propulsive thrust, or when a mixer is used to join multiple flows. For this Eq. (2.5) is used. Note that the pressures shown here are static.

$$\sum(\dot{m}_{in}v_{in} + A_{in}p_{in}) + F_x = \dot{m}_{out}v_{out} + A_{out}p_{out} \tag{2.5}$$

When using steady-state analyses, as is the case in the rest of this thesis, all time derivatives in Eqs. (2.1) to (2.4) will amount to zero, simplifying the equations. Finally additional equations are present in GSP to describe the relation of heat transfer between components. However in large gas turbines these effects are very small and usually ignored [38], which is also the case in this thesis. These equations are therefore not elaborated upon.

2.3.4. States and errors

Design point simulations in GSP are, as with manual calculations, straight forward requiring no iterations in most cases. Only if special components specifying design point equations are used iteration is needed. Calculations are performed from inlet to outlet, computing the design point performance of the gas turbine and fixing all the states needed to describe the gas turbine operating point.

Simulating a gas turbine in off-design conditions in GSP revolves around solving Eq. (2.6) [38]. Here $\bar{S}$ is a vector containing all the state variables s fully describing the state of the gas turbine. State variables can for example be mass flows, shaft rotational speeds and beta-line values. The vector $\bar{E}$ contains all the error variables e. In GSP the error equations are all variants of the compatibility equations from Section 2.3.3. If all errors are zero, as in Eq. (2.6), the compatibility equations are exactly satisfied.

$$\bar{E}\left(\bar{S}\right) = \bar{0} \tag{2.6}$$

All state and error variables are normalised using their design point value. This means that in the design point all state variables are equal to 1. This is done to maximise numerical stability [33]. The solution method used in GSP requires that the number of states and errors is equal.

The solution of Eq. (2.6) is not straightforward. No explicit equation exists to solve Eq. (2.6). The errors are determined by the states, through the operating point of the engine, which is determined by the states. To solve Eq. (2.6) in GSP, use is made of the Newton-Raphson iteration process [33, 38], which is a root-finding algorithm.

3

Gas turbine deterioration

Although modern gas turbines are highly complex, they are also highly reliable and durable. There can be years in between two overhauls of a modern turbofan engine [34]. Despite this modern gas turbines are not immune to deterioration. In this chapter a short overview will be given off different deterioration mechanisms that can influence a gas turbine and how they influence the performance. Following the deterioration mechanisms, the effect of deterioration on each individual component will be described.

3.1. Deterioration mechanisms

In this section different deterioration mechanisms which can affect the gas path during operational life will be described. In this chapter the focus will be on deterioration mechanisms affecting the performance of the gas path components of a gas turbine.

3.1.1. Fouling

In practice when running an gas turbine not only clean air enters the engine. Particles enter the engine as well, which then adhere to engine components, such as airfoils and annulus casings [21], due to oil or water mists [6, 16]. The adherence of particles to component surfaces is called fouling. Fouling is highly common in gas turbines and can be solved with washing in a large part of the cases [6, 21]. It is a form of recoverable deterioration. Fouling most severely affects the compressors [6].

Due to fouling material builds up on the gas turbine components, increasing the surface roughness of the component, altering the shape slightly and decreasing clearances inside the components [16, 21]. In compressors this can result in a decreased pressure ratio and a rise in exit temperature. This is due to for example increased surface friction and a decrease in efficiency due to shape changes of the airfoils. In the turbine the increased surface roughness and material may lead to a decrease in flow capacity [16].

3.1.2. Abrasion

Abrasion is the removal of material by rubbing two surfaces together. This can occur in gas turbines when a rotating surface rubs over a non rotating surface [16]. A likely place for this to happen is between the rotating blades in a compressor or turbine and the casing. Abrasion will in this case lead to increased tip clearances. Increased tip clearances lead to unwanted tip flows, leading to a loss in efficiency [16, 21], mass flow [21], pressure ratio in compressors and work output in turbines [16].

3.1.3. Erosion

Larger particles entering the gas turbine will not adhere to the surfaces causing fouling, but will rather remove material from the surfaces they hit [16, 21]. This process is called erosion. Erosion, like fouling and abrasion, causes an increase in surface roughness, changes in shapes and increased tip clearances.

Erosion of the compressor is more significant at the later stages, as pressures increase. In the compressor erosion will lead to decreased pressure ratios and mass flow, while also leading to a decreased

surge margin at the earlier stages [21]. In the turbine erosion may lead to an increase in mass flow, if the material is removed at the inlet [16], performance however will decrease [21].

3.1.4. Corrosion

Material from the gas path components can also be removed through chemical reactions with the flow, called corrosion [16, 21]. This is more likely to happen at the hot end of the gas turbine. The products of the reaction may then again adhere to the components, forming a scale [16]. This will lead to a reduction of performance.

3.1.5. Foreign/Domestic Object Damage

Finally damage can be caused by objects getting into the gas turbine. These may be foreign, leading to Foreign Object Damage (FOD), or parts of the engine itself leading to Domestic Object Damage (DOD) [21]. This deteriorates the performance of the engine. The exact damage done depends on the object and where it hits the internal components. This may lead to such an amount of damage that operation cannot longer continue.

3.2. Effects of component deterioration

The different deterioration mechanisms as described above have an impact on the performance of the different components of a gas turbine. In this section the changes in performance of a generic twin-spool jet engine due to deterioration of each component will be investigated. The generic layout of the engine is shown in Fig. 3.1 Deterioration is modelled as changes in component efficiency and component mass flow. The effects are based on the changes in component mass flow and efficiency. The effects of deterioration are analysed using simple component maps, the compatibility equations, matching procedures for off-design performance of a turbofan and are checked using GSP. In this way background knowledge is created to provide a knowledge base for interpreting the results from the AM component in GSP. The choice is made to analyse a turbojet rather than a turbofan to reduce the amount of interconnected parameters, the idea behind the deterioration effects however remain the same. It can also be argued that the fan of a turbofan does not deteriorate much during its operational lifetime, as will be discussed in Chapter 11[12].

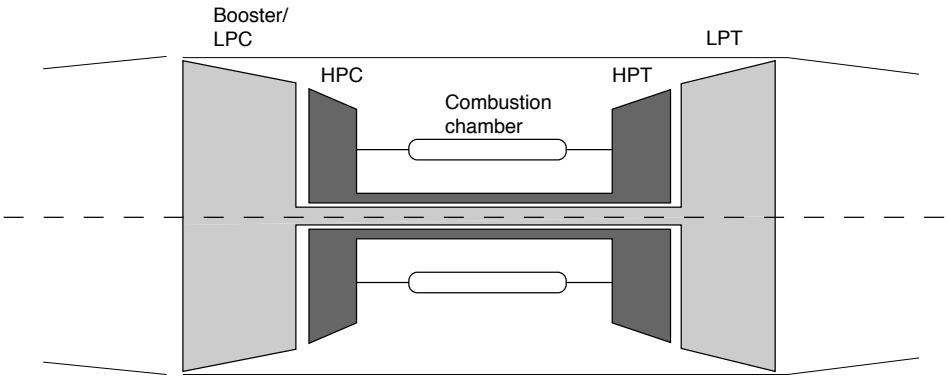

Figure 3.1: Gas path geometry of a twin spool turbojet [26, 31][Redrawn]

The performance effects of fouling, erosion and corrosion are quantified in Table 3.1 [6]. It shows that the change in component dimensionless mass flow is usually larger than the change in isentropic efficiency. This must be kept in mind when analysing the changes in the next sections. Furthermore it is found that the changes in turbine mass flow can be both positive and negative. For abrasion, or changes in tip clearances, the same effect is expected, although changes in efficiency are likely larger than with fouling [21].

3.2.1. LPC deterioration

The first component to be investigated is the Low Pressure Compressor (LPC). The engine on which the effect of deterioration is investigated is considered to be N1 controlled, as is the GEnx-1B (Chapter 5).

Table 3.1: Performance effects due to fouling, erosion and corrosion on component characteristics [6][Adapted]

Deterioration	$\Delta\dot{m}_c$	$\Delta\eta_{is}$	$\Delta\dot{m}_c : \Delta\eta_{is}$
Compressor fouling	↓	↓	± 3-8:1
Turbine nozzle guide vane fouling	↓	↓	± 2:1
Compressor erosion	↓	↓	± 2:1
Turbine erosion	↑	↓	± 2:1
Compressor corrosion	↓	↓	± 2:1
Turbine corrosion	↑	↓	± 2:1

LPC deterioration causes a reduction in component corrected mass flow and in a reduction of isentropic efficiency, as found in Table 3.1.

First the effects of mass flow reduction are detailed. A reduction in corrected mass flow through a compressor results in a reduction of the pressure ratio attained by the compressor [6]. This effect can also be seen in Fig. 3.2. LPC mass flow deterioration therefore reduces the pressure ratio over the LPC.

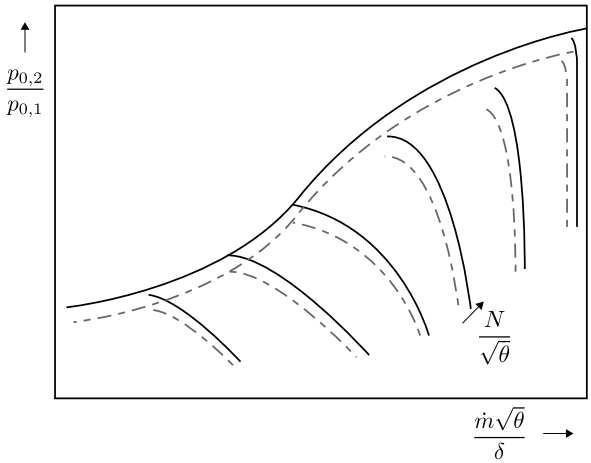

Figure 3.2: Influence of a reduction in mass flow capacity on a compressor map. The deteriorated map is shown with dashed lines

Following the LPC the flow enters the HPC. Assuming no losses, mass flow compatibility must exist between these two components. Written in terms of dimensionless parameters this compatibility is given by Eq. (3.1). Assuming that the efficiency of the LPC does not change significantly, Eq. (3.1) dictates that the corrected mass flow entering the HPC will rise. The temperature ratio and pressure ratio over the compressor are linked by the isentropic relationship, repeated here for clarity (Eq. (3.2)), from which it is clear that the change in temperature ratio is smaller than the change in pressure ratio.

$$\frac{\dot{m}\sqrt{T_{025}}}{p_{025}} = \frac{\dot{m}\sqrt{T_{02}}}{p_{02}} \cdot \frac{p_{02}}{p_{025}} \cdot \sqrt{\frac{T_{025}}{T_{02}}} \tag{3.1}$$

$$\frac{T_{025}}{T_{02}} = 1 + \frac{1}{\eta_{is}}\left[\left(\frac{p_{025}}{p_{02}}\right)^{\frac{\gamma-1}{\gamma}} - 1\right] \tag{3.2}$$

The increase in corrected mass flow through the HPC will cause an increase in HPC pressure ratio and non-dimensional spool speed [26]. The increased pressure ratio will also lead to an increased temperature ratio over the HPC, as shown by Eq. (3.2). Between the HPC and HPT both mass and work compatibility must exist, as they are located on the same shaft. Flow compatibility between the HPC and HPT is given by Eq. (3.3), work compatibility by Eq. (3.4), assuming no mass flow changes between the both components.

$$\frac{\dot{m}\sqrt{T_{04}}}{p_{04}} = \frac{\dot{m}\sqrt{T_{025}}}{p_{025}} \cdot \frac{p_{025}}{p_{03}} \cdot \frac{p_{03}}{p_{04}} \cdot \sqrt{\frac{T_{04}}{T_{025}}} \tag{3.3}$$

$$\frac{\Delta T_{HPT}}{T_{04}} = \frac{\Delta T_{HPC}}{T_{025}} \cdot \frac{T_{025}}{T_{04}} \cdot \frac{c_{pa}}{c_{pg}\eta_m} \tag{3.4}$$

The ratio p_{04}/p_{03} in Eq. (3.3) is assumed to be constant, as it is caused by the pressure losses in the combustion chamber. Furthermore it is assumed that the HPT is choked, thus having a constant dimensionless mass flow going through it. Using Eq. (3.3) it is then found that the temperature ratio T_{04}/T_{025} will rise. Rewriting Eq. (3.2) into Eq. (3.5), shows the relation between a change in pressure ratio and the temperature rise over the HPC. For the LPC the same sort of relation holds. The pressure ratio over the LPC however is much smaller, due to which the temperature difference is also smaller. The change in T_{025} will therefore also be small. From this it follows that the temperature difference over the HPC will increase, which leads to an increased temperature difference over the HPT, following Eq. (3.4). This will then lead to an decreased pressure ratio over the HPT, assuming the efficiency is not changing.

$$\Delta T_{HPC} = T_{03} - T_{025} = \frac{T_{025}}{\eta_{is}} \left[\left(\frac{p_{03}}{p_{025}} \right)^{\frac{\gamma-1}{\gamma}} - 1 \right] \tag{3.5}$$

A change in LPC efficiency has only a small effect on the operation of the engine. This can be explained using Eq. (3.2), remembering that the pressure ratio over the LPC is small. This will then lead to a small change in temperature ratio, the effect of which on the rest of the engine is almost negligible in comparison to the change in mass flow.

LPC deterioration will therefore lead to a decreased LPC pressure ratio, increased HPC pressure ratio, increased N2 speed and increased T_{04}/T_{025}. Due to this the EGT and fuel flow will increase. Furthermore the pressure ratio over the HPT will decrease.

3.2.2. HPC deterioration

Next the HPC will be considered, which is slightly more difficult than the LPC. The same equations and principles however apply as for the LPC. Following Table 3.1 the same deterioration principles apply, a reduction in both dimensionless mass flow and isentropic efficiency. It must be remembered that the spool speed of the HPC is not controlled actively.

The change in mass flow will be investigated first, starting at the LPC. The LPC will keep turning at a constant speed, as the assumed engine is N1 controlled. This will result in an increase in pressure ratio over the LPC, which also leads to a slightly increased temperature ratio.

Next the effect on the HPC is investigated. It is again assumed that the HPT is choked. Due to a decrease in mass flow the pressure ratio over the HPC will decrease. Assuming that HPC efficiency does not change much the temperature ratio over the HPC will decrease slightly. Using Eq. (3.3) it is then found that the temperature ratio T_{04}/T_{025} must increase, which is caused by an increase in fuel flow.

HPC deterioration will however combine the reduction in mass flow with a decreased isentropic efficiency. This will increase the temperature ratio and difference over the HPC. Furthermore it will cause a further reduction in pressure ratio, increasing the ratio T_{04}/T_{025} even further. Due to this the fuel use of the engine will rise, as does the EGT. As the work required by the HPC increases, the work delivered by the HPT must rise too. This will increase the temperature difference over the HPT, increasing the temperature ratio. Assuming constant efficiency this will also increase the pressure ratio, decreasing the pressure after the HPT. Changes to the LPT are only small.

The biggest changes in performance due to HPC deterioration are an increase in fuel flow, EGT and a reduction in pressure ratio over the HPC.

3.2.3. HPT deterioration

Turbine deterioration causes an efficiency loss and either an increase or decrease in mass flow through the component, as summarised in Table 3.1. The reduction of efficiency is investigated first, as this

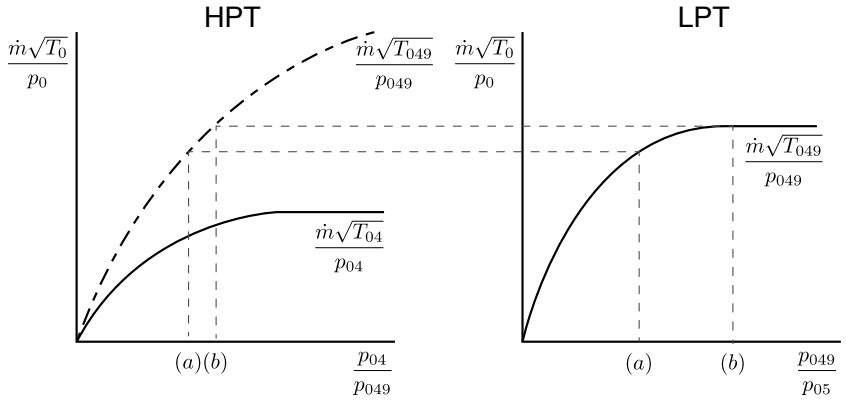

Figure 3.3: Matching of two turbines in series [26]

applies to all turbines with deteriorated performance.

A turbine transforms the potential energy in the flow into kinetic energy. A less efficient turbine will not perform as well at this, which will show in a reduced HPT pressure ratio, spool speed and a reduced temperature ratio. The HPC is connected to the same shaft and will therefore also run at a reduced speed. This leads to a reduction of dimensionless mass flow through the HPC and a decreased pressure ratio generated by the HPC. Investigating Eq. (3.3) assuming that the HPT is choked, it is found that the ratio T_{04}/T_{025} will increase. This will be caused by an increase in fuel flow. Changes in the LPC and LPT are comparable with a reduction of mass flow through the HPC as discussed before.

Before the changes in engine performance due to mass flow changes in the HPT can be discussed a short sidestep is made to discuss the matching of two turbines in series. Equation (3.6) shows the relation in dimensionless mass flow between the HPT and LPT (assuming no losses). Assuming that the efficiency of the HPT does not change much over the operating range, the LPT dimensionless mass flow becomes a function of only the HPT pressure ratio and HPT dimensionless mass flow, as the variation in temperature ratio over the HPT will be small. A choked LPT will therefore dictate the operating point of the HPT [26]. This is also shown in Fig. 3.3.

$$\frac{\dot{m}\sqrt{T_{049}}}{p_{049}} = \frac{\dot{m}\sqrt{T_{04}}}{p_{04}} \cdot \frac{p_{04}}{p_{049}} \cdot \sqrt{\frac{T_{049}}{T_{04}}} \tag{3.6}$$

Following the logic of the above relation the change in HPT performance due to a changing dimensionless mass flow capacity will be influenced by the presence of the choked LPT. Regarding Eq. (3.6), noting that the temperature ratio over HPT will be constant and that the dimensionless mass flow through the LPT will be constant, it is found that an increase in dimensionless mass flow over the HPT will lead to a decreased pressure ratio and vice versa.

Assuming that the turbine spool speed does not change due to a change in mass flow (only due to a change in efficiency, which is assumed to be constant) the HPC is only influenced by a change in dimensionless mass flow. At constant spool speed a reduction in inlet mass flow will lead to a higher pressure ratio, an increase in mass flow in a decrease in pressure ratio.

HPT deterioration in an actual engine will affect both the efficiency and mass flow capacity. This will result in a reduction of N2 speed, an increase in fuel flow and EGT. Furthermore the pressure ratios over the HPC and HPT are changed, depending on the change in mass flow over the HPT.

3.2.4. LPT deterioration

The LPT deteriorates in the same way as the HPT, with a decrease in efficiency and either a positive or negative change in component dimensionless mass flow. Again the efficiency change is discussed first.

The assumed engine is N1 controlled, so the spool speed of the LPT will remain constant. However, if left to itself a less efficient LPT will, like the HPT, turn at a slower spool speed. To keep the N1 speed constant more energy will have to be added to the flow, increasing the fuel flow and EGT.

Changes in mass flow for the LPT are influenced by the presence of the HPT. Again considering Eq. (3.6), assuming that the HPT is choked and operating at constant efficiency, it is found that with increasing LPT mass flow the HPT pressure ratio will increase and vice versa. The LPT still dictates the operating point of the HPT.

Decreasing the dimensionless mass flow through the LPT can be seen as using a nozzle with a decreased area. This will increase the restriction on the flow, hence reducing the HPT spool speed. This is also due to the reduced pressure ratio. The reduced spool speed will decrease the available mass flow through the HPC and reduce the pressure ratio over the HPC. This will reduce the work done in the HPC, allowing the work in the HPT to be reduced too as well as the ratio T_{04}/T_{025}, using Eqs. (3.4) and (3.6). The LPC is affected by the LPT too, an increase in mass flow decreases the pressure ratio over the LPC and vice versa.

Overall LPT deterioration will combine both a change in mass flow with a reduction in efficiency. This will increase the fuel flow and EGT, and the HPC, HPT and LPC performance, depending on the way the mass flow changes.

3.2.5. Discussion

In the above analysis many assumptions have been made and shortcuts have been taken. Furthermore due to different component maps actual engines might respond differently to different changes, or with a different severity. The main performance deviations due to deterioration however remain, as these follow from basic thermodynamic laws. From the analysis it can be seen that deterioration in one component affects the performance of all others. Furthermore different components affect the same performance parameters. Taking into account that in an actual engines all components will deteriorate in some way, the analysis becomes highly complex. This understates the importance of using software such as GSP to analyse the performance of an engine.

4

Gas Path Analysis

In this chapter the concept of Gas Path Analysis (GPA) will be explored. Different GPA methods will be detailed, even though at KLM ES GPA is applied using the method implemented in GSP. It is important to know the limitations of the applied method compared to others. After this the implementation of GPA in GSP will be explored further.

4.1. The principles of GPA

GPA is based upon the following principle: a physical fault, for example caused by any of the mechanisms in Chapter 3, will cause a change in component performance, which will cause a change in gas path parameters. This change can be measured, which allows for the isolation of the degraded component. This component can then be repaired if necessary. This is also shown in Fig. 4.1 [17].

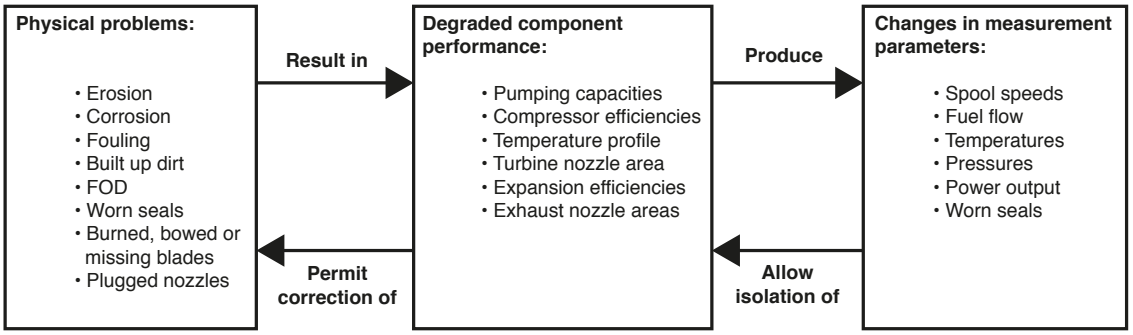

Figure 4.1: GPA principle [17][Redrawn]

The above relation can be used to monitor the performance of the engine gas path, or for differential GPA [34]. Differential GPA compares a reference gas turbine model parameters with those measured. In doing so an attempt is made to identify component conditions in comparison with the reference engine. The results must then be analysed taking the reference engine into account.

Not all engine faults can be found using GPA, only those that have a measurable impact on the gas path parameters can be identified. Unwanted vibrations, or material fractures not influencing the performance of the component cannot be identified [34].

GPA gives more insight into the condition of a gas turbine than the traditional method in which only the Exhaust Gas Temperature (EGT) margin is taken into account. The EGT Margin does not provide information on the condition of each individual component, only on the overall condition of the engine. A component which performs badly can be compensated for by a component which performs much better, resulting in an average EGT margin. GPA can be used to provide more information on the condition of the individual components, rather than on the engine as a whole.

4.2. GPA methods

In this section different methods of applying GPA will be detailed, with their respective advantages and disadvantages. At the end of the section a conclusion will be drawn to determine the most suitable method for use at KLM.

The different methodologies will be divided into two categories, model based and empirical as done by Verbist [34]. The model based methods are based upon a thermodynamic model of the gas turbine. Empirical models are based on Artificial Intelligence (AI), numerical methods used to perform GPA.

4.2.1. Model based: Linear

GPA has been introduced by Urban in 1967 for the first time, using a linearised model of the gas turbine to be analysed [17]. Linearised methods are based on the assumption that changes in the measured parameters are small around the steady-state operating point, hence they can be linearised [19]. The linear approximation used is given by Eq. (4.1) [17, 19]. Here $\bar{z}$ is the measurement vector, $\bar{x}$ the performance parameter vector and $\mathbf{H}$ the Influence-Coefficient Matrix (ICM). Multiplying both sides of Eq. (4.1) with $\mathbf{H}^{-1}$ gives Eq. (4.2), relating the performance parameter vector (denoting the condition [34]) and measurements through $\mathbf{H}^{-1}$. The inverse of the ICM is called the Fault-Correlation Matrix (FCM). Equations (4.1) and (4.2) can also be written as Eqs. (4.3) and (4.4) relating the differences to each other [17, 34].

$$\bar{z} = \mathbf{H} \cdot \bar{x} \tag{4.1}$$

$$\bar{x} = \mathbf{H}^{-1} \cdot \bar{z} \tag{4.2}$$

$$\Delta\bar{z} = \mathbf{H} \cdot \Delta\bar{x} \tag{4.3}$$

$$\Delta\bar{x} = \mathbf{H}^{-1} \cdot \Delta\bar{z} \tag{4.4}$$

The linear method has its advantages, as it is a simple and fast technique. Furthermore, it is able to detect multiple faults and give a degree of severity to the detected faults [17]. Unfortunately the linear method has its drawbacks.

Drawbacks can be found when investigating Eqs. (4.1) and (4.2). The conversion from ICM to FCM requires that the ICM is invertible, the ICM must be a square matrix, requiring equal measurements and performance parameters [19, 34]. This may not always be possible in an actual gas turbine. Accuracy of the method depends on the accuracy of the ICM [17]. The linear methods assumes that the used measurements are noise and bias free [17, 19, 34]. The method is not able to account for these inaccuracies, even though they are present in practical sensors. Filtering methods have been developed to overcome the limitations due to measurement errors, however these introduce their own disadvantages such as 'smearing' [17, 19]. Finally the linearity assumption is only acceptable in a small region around the steady state point [19]. This is shown visually by Verbist in Fig. 4.2[34].

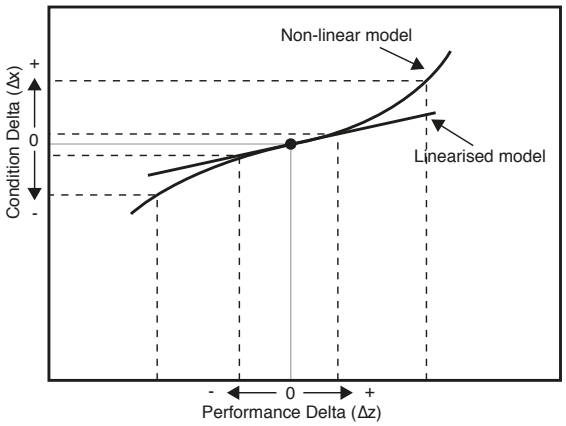

Figure 4.2: Accuracy differences between a linearised and non-linear model [34][Redrawn]

4.2.2. Model based: Non-linear

The performance of gas turbines cannot be described linearly without making use of large and not fully valid assumptions. This influences the results of the linear method described in Section 4.2.1. To take the non-linearity of gas turbines into account when applying GPA non-linear methods have been developed. Two methods will be described in this section. Both methods rely on optimisation in order to find the condition of the gas turbine [17], requiring an iterative approach.

The first method relies on the Newton-Raphson root finding method [19]. The linear method is applied repeatedly, converging towards the actual condition of the gas turbine while taking the non-linearity into account. This methods is also described by Escher and used in the Pythia software package [6].

The second modelling technique is Adaptive Modelling (AM), first described by Stamatis et. Al [29]. This methods relies on adapting the engine model to more accurately describe the measured performance [17, 34]. The model is adapted by changing the compressor and turbine maps. On a component map only two parameters are needed to fully describe the operating point of the component, hence with a limited amount of map modifiers the condition of a gas turbine can be fully described. The changes made to the maps correspond to the differences in component condition between the measured and reference engine.

Adaption of the model is done numerically. Adaption can be done either internally or externally [29]. The adaption is done internally if the AM equations are added directly into the simulation. External optimisation puts the AM equations outside of the model, externally iterating the simulation procedure [29]. The difference is represented visually in Fig. 4.3 [23]. In GSP GPA is performed using an internal AM strategy [40], more detail on which is given in Section 4.3.

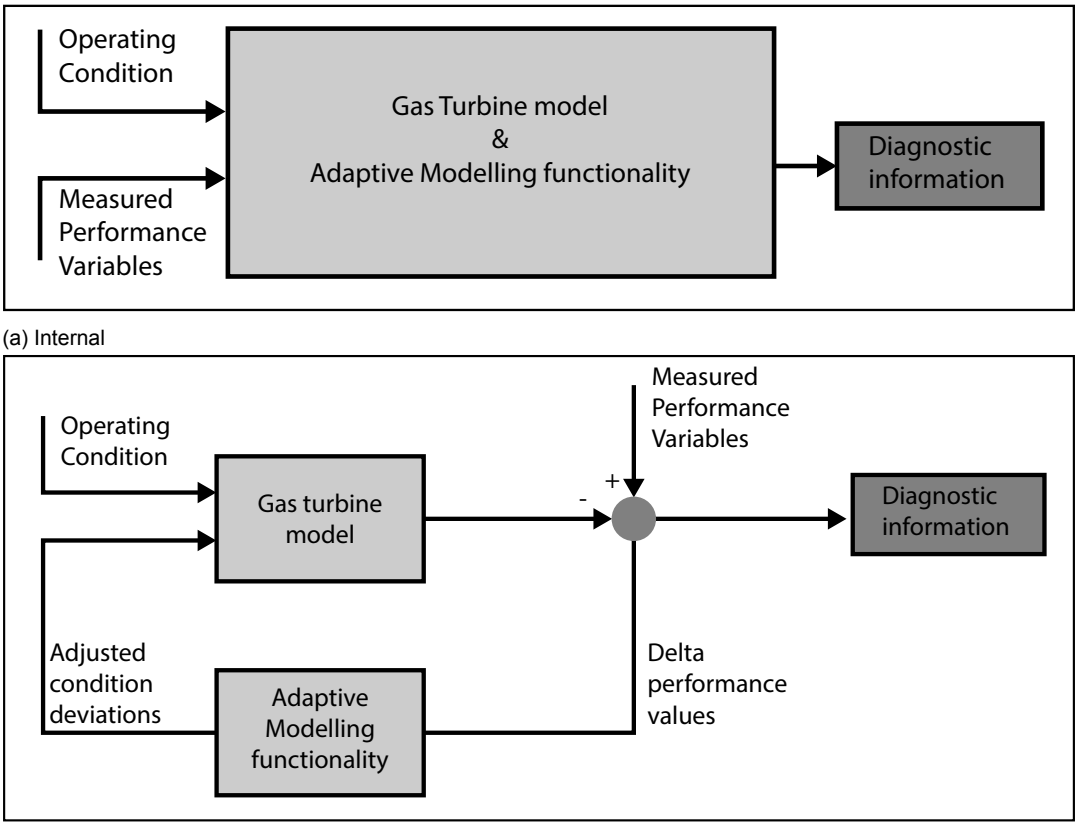

(a) Internal

(b) External

Figure 4.3: Internal and external AM strategies[23][Redrawn]

AM is, like linear models, a deterministic GPA method, meaning that a specific input always leads to the same specific output [34]. Due to this it is also not able to handle noise and bias well. The advantage however, is that it is still a simple method and that it can handle the non-linear behaviour of the engine.

4.2.3. Empirical: Artificial neural networks

Empirical methods have been developed to overcome the inherent problems of the model based methods: convergence issues and the inability to deal with measurement uncertainty [34]. Furthermore they are developed to overcome the need for large amounts of measurements and sensors, and the need for linearisation altogether [44].

The first set empirical, or AI based, methods are Artificial Neural Networks (ANNs). As the name already suggests, ANN aim to mimic the biological brain. Consisting of a series of parallel distributed processors it has the ability to store knowledge as experience and the ability apply this knowledge [17, 19]. Like the brain an ANN needs to be trained to produce useful output [17, 19, 34]. ANNs have the ability to learn and generalise [34]. Due to this property they are able to deal with cases not exactly available in the set of training data. This allows them to deal with sensor bias and noise. Although ANN is treated here as one class of methods, many different kinds of ANNs can be developed [17].

A trained ANN is able to deal with measurement errors and uncertainty. Furthermore calculation speed is high.

ANNs also have their disadvantages. Although a trained ANN performs quickly, training times are long and require vast datasets [19, 34]. Retraining might be required when operating conditions change [19]. Finally ANNs are unable to perform well outside of the scopes of their training dataset [19, 34].

4.2.4. Empirical: Genetic algorithms

Genetic algorithms (GAs) are a type of optimisation algorithms. GAs are based on evolutionary principles to find the optimal solution to a problem [34]. Starting with a range of solutions the first step is to apply a selection procedure to find the solutions that will advance to the next generation. Cross-over is then applied to these solutions, to form new solutions consisting of the combined information from the two parent solutions. Finally a mutation step is added to introduce new or lost information to the solution set [17].

GAs have first been applied to GPA by Zedda and Singh [44], noting positive results. Here it was noted that GAs are able to fully deal with measurement biases and noise. Furthermore GAs are not held back by non-continuous relations within the gas turbine as no differentiation is needed.

Analysis using GAs however is highly time consuming, limiting the practical use of GAs. Due to the high complexity of modern gas turbines many faults can occur, increasing the degrees of freedom for the analysis and thus decreasing the effectivity of GAs [19, 34].

4.2.5. Empirical: Expert systems

The final type of AI based GPA methods are Expert Systems (ESs). An ES consists of a knowledge base and an interference engine [17, 34]. Information is stored inside the knowledge base, which is accessed by the interference engine, using a range of different logics [17, 19, 34]. This way the system mimics the way in which a human expert would work [34].

The single largest advantages of using an ES for GPA is the ability of an ES to combine different diagnostic techniques [34]. This would for example allow for the possibility of combining GPA with vibrational analysis.

ESs like ANNs require vast datasets to perform properly, which is a disadvantage of the method [19, 34]. The response of the system might also change when new information is added to the knowledge base, as the system tries to incorporate this information into the analysis. As the response to previously analysed situations can also change, the system has to be revalidated in order to be used after information has been added [34].

4.2.6. Most suitable GPA method for KLM

Although the above description of the different GPA techniques hardly scratches the surface of the amount of research done, it can be used to determine the appropriate method of GPA for KLM. Comprehensive literature studies have been carried out by Li [17] and Marinai [19]. General advantages, disadvantages and properties of the GPA methods have been described above. Most research carried out has been applied to theoretical data only and/or only in a scientific environment. Verbist [34] has made an analysis of the requirements of an MRO, which are summarised below.

- The method used needs to be fast, especially as on-wing data is to be analysed.

- It is more important for the method to pinpoint the deteriorated component correctly than the amount of deterioration as further inspection will always be carried out.
- Large datasets are often unavailable, hence the method should be able to perform well without much data.

The first requirement, speed, eliminates GAs as an option as its computational times are high. The third method then eliminates the other empirical methods, as they are all reliant on large datasets to properly train the algorithm. This amount of data is unfortunately unavailable in the MRO environment [34]. The second requirement poses restrictions on the amount of 'smearing' that can take place, while asking for accurate predictions. Due to this linear methods, with or without the use of filters, are less appropriate. Also empirical methods do not work as well with slowly deteriorating components and engines with multiple faults [19].

This leaves the non-linear model based methods available for use at KLM. In GSP the AM method has been implemented [40]. This has been done in a highly flexible manner, another advantage in the MRO environment [34]. Another advantage of this method is that it is based on the physical model of the engine, relating the physical reality to the diagnosis. For the engineers at KLM this will increase the ease with which GPA can be used.

4.3. GPA implementation in GSP

In this section the GPA implementation in GSP is discussed. As mentioned before, the applied GPA method is AM using an internal calculation strategy [40]. The AM module in GSP has partially been developed at Delft University of Technology [22].

The AM component makes good use of the flexible architecture of GSP. By adding the AM component to any GSP model it can be turned into a GSA capable model, due to the object-oriented programming of GSP [38]. Because of this flexible way of working it is also possible to apply an internal problem solving method to any generic model [22]. The AM component is added to the GSP model using the drag and drop interface [38, 40].

Upon adding the AM component to the GSP model, additional equations are added to the set of states and errors as described in Section 2.3.4. The new set of equations is given by Eq. (4.5) [40]. Here f_1 till f_n are the error equations from the basic model, based on the continuity equations. The bottom half of the equation houses the added formulas for the AM component, f_{m1} until f_{mm}, Eq. (4.6). The parameters s_1 till s_n are the engine states that need to be solved for and the scalars s_{c1} till S_{cm} represent the condition factors that need to be solved for. The variable ε represents the iteration tolerance for the off-design calculations and ε_{m1} till ε_{mm} represent the tolerances set for the condition factors, which are manually set in the AM component [40]. From the way in which Eq. (4.5) is set up, it is clear that the number of measurements taken should be equal to the number of component conditions that can be adapted [22].

$$\begin{array}{cccc|cccc|ccc} f_1(s_1)+ & \cdots & f_1(s_n)+ & & f_1(s_{c1})+ & \cdots & f_1(s_{cm}) & = & \varepsilon \\ \vdots & & \vdots & & \vdots & & \vdots & & \\ f_n(s_1)+ & \cdots & f_n(s_n)+ & & f_n(s_{c1})+ & \cdots & f_n(s_{cm}) & = & \varepsilon \\ \hline f_{m1}(s_1)+ & \cdots & f_{m1}(s_n)+ & & f_{m1}(s_{c1})+ & \cdots & f_{m1}(s_{cm}) & = & \varepsilon_{m1} \\ \vdots & & \vdots & & \vdots & & \vdots & & \\ f_{mm}(s_1)+ & \cdots & f_{mm}(s_n)+ & & f_{mm}(s_{c1})+ & \cdots & f_{mm}(s_{cm}) & = & \varepsilon_{mm} \end{array} \tag{4.5}$$

$$f_{mi} = z_{i,model} - z_{i,meas} \leq \varepsilon_{mi} \tag{4.6}$$

Equation (4.5) has been translated into words by Pieters, which gives Eq. (4.7) [23]. From this it is clear that all parts of the AM calculation influence each other, showing the advantage of calculating everything in a single loop. Changing the component maps influences the operation of the engine, which still needs to be in equilibrium. Due to this the state variables of the engine change, which in turn influence the AM calculations. This is shown in the top right and bottom left of Eqs. (4.5) and (4.7).

Finally the changes in the component maps also influence the AM calculations themselves [23].

Basic engine model error equations	Effect of changed component maps on calculated engine equilibrium
Effect of state variables on additional error equations	Effect of changed component maps on additional error equations

(4.7)

Scaling of the original component maps is done using Map Modifiers (MM), computed using Eq. (4.8) [34]. The MM is given as a ratio of the reference value. The MMs are reported by GSP as component condition deviations, or performance deviations, reported as a percentage. This percentage is then a percentage difference of the reference value. It is important to note that GSP computes only a single MM for each map when analysing a data point. Differences caused by fouling in combination with variable geometry for example are not captured in the single analysis, but would require multiple analyses using multiple data points, giving multiple MMs. Overall it is not expected that this will introduce difficulties in applying AM.

$$\mathrm{MM} = \frac{\text{Adapted value}}{\text{Reference value}} \tag{4.8}$$

Each engine is different. This can be due to manufacturing tolerances, due to differences in the maintenance done on the engines or due to deterioration [34]. This can result in a difference between the engine and the baseline model, even when deterioration is not present. If the condition of an engine is to be compared with its own reference condition/performance the baseline model must be adapted. This is done in GSP using Calibration Factors (CFs) [34, 40]. These can used to align the model better to the engine of interest, preventing the AM calculation of being influenced by the differences between different engines. This effect is shown visually in Fig. 4.4a. The calibration factors are calculated using Eq. (4.9), where x_i is a parameter in the engine. The closer the baseline model describes the engine design performance the closer the calibration factors are to unity.

In Fig. 4.4a the measured power setting and the design point power setting were equal. Chances are however that a reference dataset is used which is measured at a different power setting than the design point of the model. For example when using an on-wing dataset, measured during a derated take-off. It is shown in Fig. 4.4b that this would lead to differences between the actual engine and the model. This is solved with an off-design calibration method in GSP, which takes the power setting of reference dataset into account [34]. This is shown in Fig. 4.4c, leading to proper calibration of the model even though the reference power setting is different from the design power setting. When necessary this calibration method will be used in the remainder of this thesis without explicitly mentioning it.

$$\mathrm{CF} = \frac{x_{i,meas}}{x_{i,model}} \tag{4.9}$$

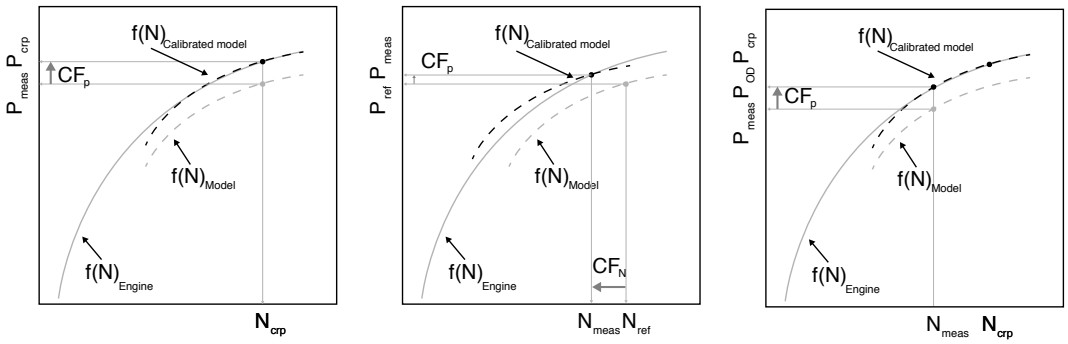

(a) Calibration at equal power settings

(b) Calibration at different power settings

(c) Off-design calibration at different power settings

Figure 4.4: Model calibration [34] [Redrawn]

5

The General Electric GEnx-1B

In this chapter the engine which is to be modelled in GSP is detailed, the General Electric GEnx-1B. This information will be helpful in the creation of the GSP model in Part II and the analysis of the AM results in Part III.

5.1. Overview

Designed and manufactured by GE Aviation, the GEnx-1B is one of the two engine options for the Boeing 787, the other option being the Rolls-Royce Trent 1000. The whole of the AFKL Boeing 787 fleet is powered by GEnx-1B engines. The GEnx-1B is a 'dual-rotor, variable-stator, high-bypass ratio turbofan' [10], and is shown in Fig. 5.1. It has been designed to be quiet, to have low emissions and a low Specific Fuel Consumption (SFC). The engine is controlled electronically by the Engine Electronic Control system (EEC), which is a Full Authority Digital Engine Control (FADEC) [10]. Another version of the GEnx is available, the GEnx-2B powering the Boeing 747-8. The GEnx-2B will not be modelled or researched in this thesis.

Figure 5.1: The GEnx-1B [9]

5.2. Layout and systems

Figure 5.1 does not show any details of the components of the engine, just the outside. In Fig. 5.2 more detail of the inside of the engine is shown. The engine will be discussed in some more detail in this section, all information is taken from the engine installation manual [10].

At the front of the engine the fan is visible, after which the flow is split into the bypass and core flow. About nine times as much mass flow goes through the bypass, again exiting the engine. The core flow travels through the booster and HPC where the pressure is increased. During this process

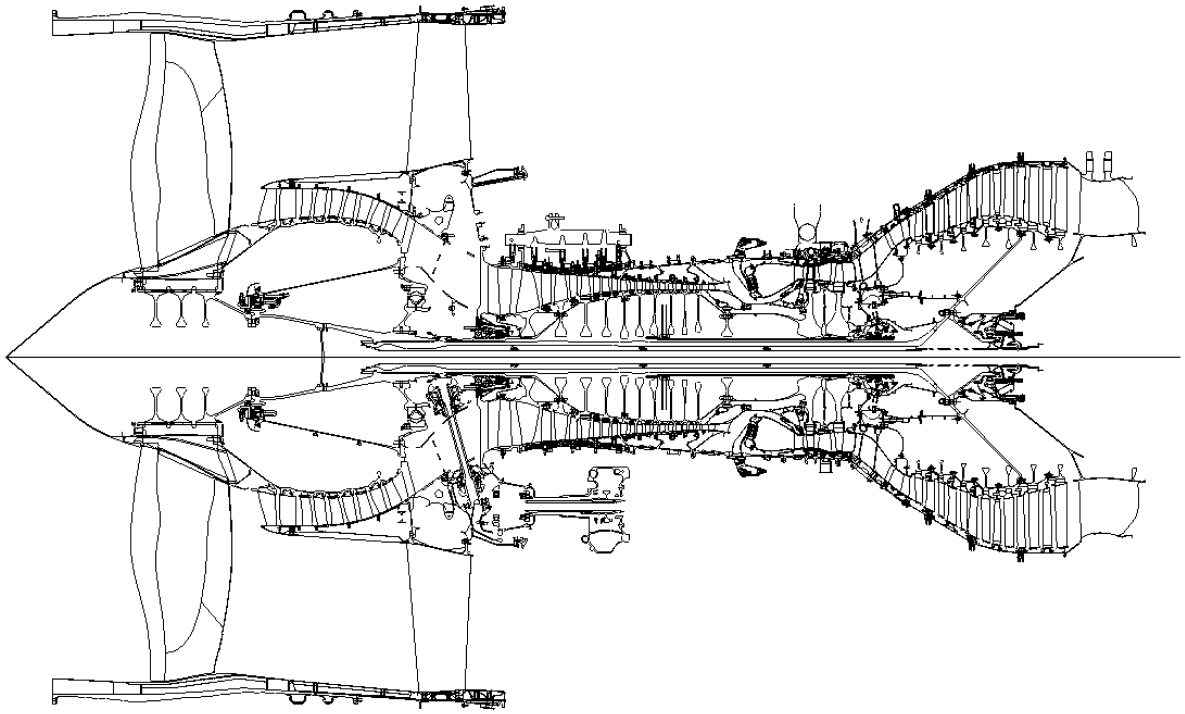

Figure 5.2: Layout of the GEnx-1B [10]

the pressure of the flow is increased approximately 40 times. Next in the combustion chamber heat is added to the flow, which is again extracted in the HPT and LPT. After this the core flow also exits the engine. The fan, booster and LPT are connected to the N1 shaft, the HPC and HPT to the N2 shaft and are considered the core engine. The shafts are counter-rotating. The rotation speed of the N1 system is the control variable of the engine.

Similar to the GE90, the fan is one of the most striking features of the GEnx-1B. It consists of 18 composite fan blades and is responsible for the largest part of the thrust produced by the engine. The booster consists of five stages, located behind the fan. Behind the booster Variable Bleed Valves (VBVs) are installed, allowing for a reduction in mass flow going towards the HPC.

The core engine starts with the HPC, which consists of 10 stages. The HPC is responsible for the largest part of the pressure rise in the engine. The stators of the first four stages are Variable Stator Vanes (VSVs). The Inlet Guide Vanes (IGVs) are also variable. All variable parts move at the same time, according to a fixed control schedule based on corrected N2 speed to ensure safe operation of the engine.

The hot section starts with the combustion chamber, followed by a two stage HPT. The HPT stage 1 blades and nozzles are cooled using air from the HPC exit, stage 2 is cooled using 7th stage HPC air. Finally the air flows through the 7 stage LPT, cooled using 4th stage HPC air. Both the HPT and LPT have Active Clearance Control (HPTACC/LPTACC), to keep the case in shape. This is provided using fan air flow.

Additionally 7th stage HPC air is taken for Booster Anti-Ice (BAI) and inlet cowl anti-ice. No bleed flow is provided to the aircraft, as the Boeing 787 does not require this [28].

5.3. Maintenance on the GEnx-1B at KLM ES

The GEnx-1B is maintained in the KLM ES engine shop at Schiphol, where work is done on both KLM engines and engines belonging to third party costumers. KLM ES has started to support the GEnx-1B in 2015. The GEnx-1B is still a new engine, therefore all engines under contract at KLM are still new. Due to this only some Quick Turns (QTs) have been performed, during which specific problems on an engine are fixed. The goal of a QT is not to restore the performance of an engine. Unfortunately this leads a lack of data which can be used for validation of the AM results, as no engine data is available

before and after a shop visit, and no data is available on the physical state of the engine when it is opened up in the shop.

After an engine has been repaired or overhauled at Schiphol it is shipped to Paris for testing at Air France Industries (AFI). Here the engine is tested according to a test schedule as determined by GE. The power setting on the engine is based on corrected fan spool speed, or N1 speed. The engine is set to a specific speed, within a small margin, after which measurements are taken. The highest speed is referred to as take-off (TO) power, the second highest as Maximum Continuous (MC). Only these two power settings are of interest for performance testing. Furthermore the engine is tested at Minimum Idle and Approach Idle. Acceleration performance, vibration and oil consumption tests are also performed.

II

Development of the GEnx-1B model

6

Preparation

This chapter is the starting point for the development of the GSP model representing the GEnx-1B, indicating the preparation done before the actual modelling was started. It includes the assumptions made about the engine and model, which influence the way the model works for the rest of the thesis. Furthermore the data gathered is detailed and finally the reference engine, the engine that will be modelled, is selected. With these steps out of the way, a start can be made with modelling the GEnx-1B in GSP.

6.1. Assumptions

Underlying GSP are several assumptions, which have been described in Chapter 2. As a model is a simplified depiction of the actual engine, more assumptions are introduced when creating a model, which are described in this section. The assumptions made remain valid throughout the remainder of the thesis and will have to be kept in mind when analysing results computed using the GEnx-1B model.

The assumptions stated below are made due to a lack of information about the detailed workings of the engine in the MRO environment. At KLM ES information is readily available about the performance of the engine in operation and about mechanical details and repairs. However it is unknown what each system does exactly at each operating condition. This information gap creates an additional challenge when creating a model in the MRO environment, leading to additional assumptions to be made. If the model were to be created by the OEM, these assumptions would not be necessary.

6.1.1. Design point

As stated in Chapter 2 the design point of a model can be different from the actual design point of the engine [38]. Take-off has been chosen as the design power setting for the engine. Take-off is defined here as the take-off power setting as tested in the test cell, being the maximum amount of thrust that the engine can deliver. This setting has been chosen as it is the most demanding from a performance point of view. It is expected that performance issues with a specific engine are clearest at this power setting. Designing the model at this point is then expected to give the most accurate analysis results.

6.1.2. Variable geometry

The GEnx-1B is outfitted with several variable geometry systems, such as VSVs and VBVs detailed in Chapter 5. During operation these influence how the engine performs. At KLM ES it is unknown on what schedules these systems operate, therefore the variable geometries are not modelled explicitly and are assumed to be nonexistent in the model. Removing the VSVs affects the way in which the off-design modelling of the engine is done in Chapter 8, where more information is given on this assumption. Removing the VBVs restricts the power settings in the engine that can be modelled, as these are opened near low power settings. This will not be possible using the GSP model.

6.1.3. Bleed air and cooling flows

Air is not only used for thrust generation in the GEnx-1B, it is also used to pressurise parts of the engine, for de-icing purposes, for cooling purposes and for active clearance control. On the Boeing

787 no bleed air is extracted for use in the aircraft (customer bleed)[28]. These systems extract air from the gas path, while not all of it returns to the engine. The amounts of air extracted from the gas path are controlled by the engine and not known to KLM ES. Only the maximum amounts of air allowable for extraction for booster anti-icing are available, shown in Table 6.1. Anti-icing systems are not used in the test cell. It is expected that the amount of cooling air will be almost a fixed ratio of the complete mass flow around take-off settings, influencing all operating points in the same way.

As the information is unavailable it is assumed that no parasitic airflows are present on the modelled GEnx-1B. As the AM module in GSP is a form of differential GPA this will not influence the results. The component efficiencies and pressure ratios set in the design point will be influenced. This however will not affect the model usability, as the computed temperatures and pressures will be equal to those present on the actual engine.

Table 6.1: Maximum permissible air bleed extraction for booster anti-icing [7]

$N1_c$ [%]	Stage 7 [% W_{25}]
0 - 31.3	5.0
31.3 to 66.4	4.7
>66.4	3.3

6.1.4. Rating

The GEnx-1B is available with different ratings, each having its own performance. Although mechanically equal, the rating is changed in the software using a rating plug, engine performance differs between the different ratings. The model will represent a GEnx-1B74/75/P2, as is used on KLM its Boeing 787-9. This will remain the same throughout the whole thesis. From this point onwards when referenced to a GEnx-1B a GEnx-1B74/75/P2 is meant.

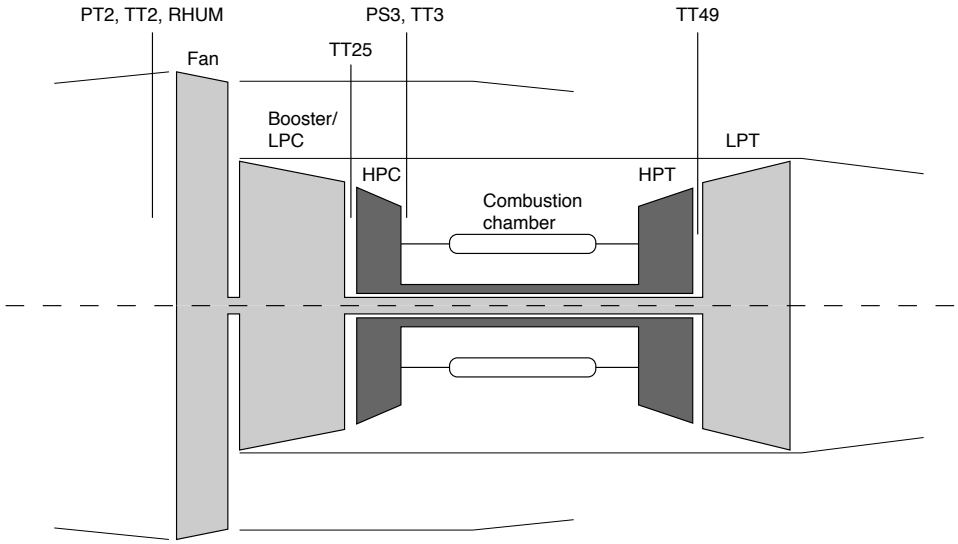

Figure 6.1: Gas path geometry of the GEnx-1B and the location of the gas path measurements [26, 31][Redrawn]

6.2. Acquired data

The model will be based on actual performance data gathered from both KLM and customer engines. The design point is modelled after the take-off (TO) point as measured in the test cell, located at CDG. Furthermore the maximum continuous (MC) measurement is taken from the test cell. The flight and ground idle measurements are not used, due to the assumptions as stated above. The MC snapshot is taken as a first off-design point to model.

All engines tested at CDG have been inducted into the KLM ES shop for maintenance and are tested upon release. Not all engines have undergone the same workscope. All engines have been inducted

Table 6.2: Available performance measurements for the GEnx-1B, on-wing and in the test cell

Parameter	Description	Unit	Test cell	On-wing
TT2	Total fan inlet temperature	[°C]	x	x
TT25	Total HPC inlet temperature	[°C]	x	x
TT3	Total HPC outlet temperature	[°C]	x	x
TT49	Exhaust Gas Temperature (EGT)	[°C]	x	x
PT2	Total fan inlet pressure	[psia]	x	x
PS3	Static HPC outlet pressure	[psia]	x	x
N1	Fan speed	[%/rpm]	x	x
N2	Core speed	[%/rpm]	x	x
WF	Fuel flow	[pph]	x	x
FN	Net thrust	[lbf]	x	
RHUM	Relative humidity	[%]	x	

for a QT, no Performance Restoration Shopvisits have been performed as of yet. This will potentially lead to increased engine to engine differences, however as all engines are rather new, before their first shopvisit, it is expected that differences are small. Additionally on-wing take-off data is available for the complete AFKL 787 fleet, starting from the most recent installation of the engine.

The measured parameters are located in Table 6.2, the location of the gas path measurements are shown in Fig. 6.1. The total pressure before the fan (PT2) is measured by the engine itself and by the test cell. It has been decided to use the test cell sensor where available, as it has been specifically calibrated during the test cell correlation to match GE standard conditions. Otherwise where available engine sensors have been used.

The performance equations from Chapter 2 all deal with total temperatures and pressures. The measured HPC outlet pressure however is a static measurement. A tube runs from the combustor diffuser to the Electronic Engine Control (EEC), where the static pressure measurement is taken. In order to compute the static pressure the flow path area is needed, as can be seen from Eq. (6.3), in which the only unknown is the area, A. GE unfortunately does not disclose the exact flow areas inside the engine. Furthermore because the geometry near the pressure tab is quite complex and near the combustion chamber, corrections will have to be made for factors unknown. Currently the area is estimated using a large drawing of the GEnx-1B available at KLM. This introduces an additional source of uncertainty and error into the model. When using the GSP AM component this is not a problem, as the error introduced by the area is the same in both the reference and adapted engine. Due to differential GPA this error will be negated.

$$p_0 = p + q \tag{6.1}$$

$$p_0 = p + 0.5\rho V^2 \tag{6.2}$$

$$p_0 = p + 0.5\rho \left(\frac{\dot{m}}{\rho A} \right)^2 \tag{6.3}$$

6.3. Reference engine selection

The reference engine selected in this section is the engine that the model will be based on. When analysing an engine using AM, its performance is compared with the performance of the reference engine. Comparing a mediocre engine with a perfect and a bad engine will result in two completely different results. For a meaningful result a good engine must show a good condition in the comparison and a bad engine a bad condition. The reference engine is therefore chosen to be as average as possible.

Reference engine selection is done based upon TO and MC data from the test cell. Five engines were available for selection. Engine data is shown in Table 6.3. Here the Engine Serial Number (ESN) is shown, the power setting, the amount of cycles it has run since new, the EGT standard day margin (EGTSDM), the corrected standard day net thrust (FNKSD), corrected standard day fuel flow (WFKSD),

the overall pressure ratio(OPR, PS3/PT2) and the overall temperature ratio (OTR, TT3/TT2). A standard day (SD) is the sea level conditions in the ISA.

Table 6.3: Data available for reference engine selection

ESN	Power Setting	Cycles since new [-]	EGTSDM [°C]	FNKSD [lbf]	WFKSD [pph]	OPR [-]	OTR [-]
95xxx1	TO	1465	18.413	78192	22102	45.836	3.1638
95xxx2	TO	1094	28.353	78096	22083	45.957	3.1574
95xxx3	TO	977	29.937	77965	22019	45.805	3.1760
95xxx4	TO	978	28.600	77511	21964	45.612	3.1900
95xxx5	TO	1602	16.810	78316	22299	45.706	3.3259
95xxx1	MC	1465	16.368	69826	19182	41.407	3.0719
95xxx2	MC	1094	27.674	69816	19140	41.539	3.0630
95xxx3	MC	977	28.449	69624	19093	41.330	3.0802
95xxx4	MC	978	26.367	69413	19077	41.265	3.0980
95xxx5	MC	1602	16.150	69874	19288	41.222	3.1165

Test cell results are converted to standard day (SD) and hot day (HD) values, for trending and comparison between tested engines. This is done to eliminate the influence of ambient conditions on the results. An engine is only accepted if it satisfies the thrust margin, with a predefined EGT margin at standard and hot day conditions. As engines are normally compared using their corrected performance it is a good starting point for the selection of the reference engines.

Looking at Table 6.3 differences in standard day thrust and fuel flow are small for all engines. Differences in EGT margin are more pronounced, with two engines performing significantly worse than the others. This might be explained by the 50% higher cycle count on these engines. Engineering experience at KLM shows that a 500 cycle difference normally does not result in a change of 10 degrees EGT margin. Furthermore no GEnx-1B engines have yet been taken into the shop due to performance issues, even though some are already older than these engines. It has therefore been decided to discard the 95xxx1 and 95xxx5 as possible reference engines, as they will likely not represent an average engine.

The 1.5 degree EGTSDM difference between the other three engines is small and would indicate engines of almost equal overall quality. As the quality of the individual components is analysed with AM, choosing the most averagely performing components would be best. This has been done by comparing the OPR and OTR. Choosing the most average engine here gives the 95xxx3, which has been chosen as the reference engine.

The 95xxx3 also has the most average SD thrust and fuel use of the remaining three engines. As an added benefit it is a KLM engine, due to which on-wing data is available as well. During its shopvisit the engine has had work done on the combustion chamber, HPT and small repairs on the LPT.

7

Design point modelling

Following the preparation in Chapter 6 the modelling of the GEnx-1B in GSP is started. The first step is to set the design point of the model, fixing the reference point for the off-design computations which will follow in Chapter 8. As stated in Chapter 2 design point equations are rather straightforward and do not require knowledge of the component maps. The design point however is the starting point for off-design modelling, fixing the engine its cycle reference point. In this chapter the steps taken to get to the design point are detailed, followed by an analysis of the model accuracy.

7.1. Methodology

In this section the steps taken to model the design point are detailed, starting with the general layout of the GSP model. This is followed by the steps that were taken to get to the design point model. Finally required additional assumptions are listed.

The calculation procedure inside GSP is detailed in Chapter 2. For the design point modelling it is important to restate that only the design point properties of the GSP components are adapted, as the component maps will not be used.

7.1.1. GSP model lay-out

At KLM ES GSP models of the GE CF6-80 and CFMI CFM56-7B are available, having been created in previous research projects [1, 2, 5]. The model of the GE CF6-80 has been chosen as a starting point, as it is an engine of similar configuration. Both engines are a high bypass, twin-spool turbofan, which are N1 controlled. Furthermore the GE CF6-80 model has been refined and researched extensively by Verbist during his PhD research, due to which it is assumed that it will likely be the most accurate model [34].

Using the generic components available in GSP the CF6-80 model has been rebuild for the GEnx-1B, to prevent errors from occurring due to copying of the model. The layout is shown in Fig. 7.1. Important to note is the absence of a compressor component for the booster. No measurements are taken between the fan and booster inlet on the GEnx-1B (as for the CF6-80 and CFM56). Previous research has shown that using a separate fan and compressor component for the fan and booster results in unstable AM results [5]. These are mitigated by combining the core of the fan and the booster into one component, the Low Pressure Compressor (LPC). The core pressure ratio and core efficiency of the fan component now represent the combination of the fan core and booster.

7.1.2. Procedure

The goal of the design point modelling is to exactly match the measured parameters on the reference engine at take-off power in the test cell with the values as computed by GSP. Test cell take-off settings correspond with the chosen design point. In Table 7.4 the measured values of the reference engine are found. Important to note here is that when a parameter is not measured, for example the booster exit pressure, it is not considered in the modelling procedure. The goal is only to match known parameters. The steps taken to determine the design point properties are stated below.

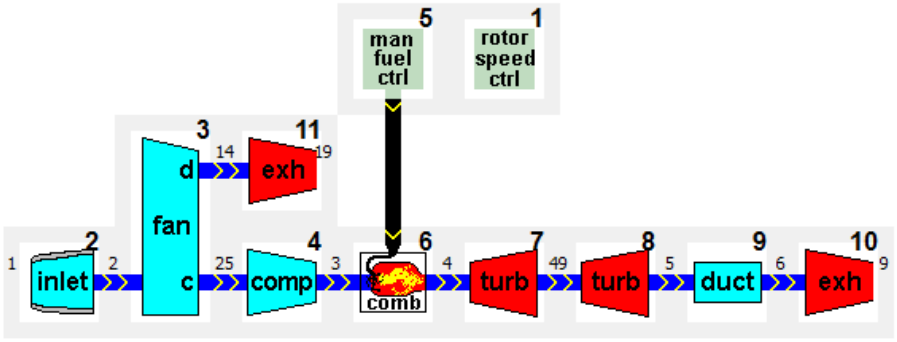

Figure 7.1: Layout of the GEnx-1B model in GSP

- Set known overall parameters
  - Adapt the ambient conditions to match the test cell conditions.
  - Set the fuel flow to the combustion chamber to what is measured in the test cell.
  - Set the overall mass flow. See Section 7.1.3 for details.
- Adapt the LPC core pressure ratio to match TT25
- Adapt the HPC pressure ratio to match PS3
- Adapt the HPC efficiency to match TT3
- Adapt the bypass ratio (BPR) to match TT49
- Adapt the LPC bypass pressure ratio to match the measured thrust

Following these steps is an iterative process which, when done by hand, can be time consuming. Therefore 'Design Point Equation' components in GSP have been used to adapt the components. These components allow the user to fix an output parameter and set a component property free to be adapted by GSP during design point calculations.

7.1.3. Additional assumptions

Comparing the list of adapted parameters as shown above to the complete set of parameters as needed to fully define the model, some are missing. The missing parameters have been assumed, due to a lack measured parameters in the GEnx-1B. In this section these assumptions will be described, their values are given in Table 7.1

The first category of model design point variables that have been assumed are the isentropic efficiencies for the LPC(both core and bypass), HPT and LPT. As no pressure measurement is taken after the booster, it is not possible to adapt both the efficiency and pressure ratio of the LPC core. It is therefore chosen to assume an efficiency and leave the control over the temperature to the pressure ratio. For both the HPT and LPT no pressure measurement is taken after the component, therefore the efficiency has to be assumed. Finally no pressure or temperature measurement is taken in the fan bypass. As the bypass flow is responsible for the largest amount of the thrust produced by the engine the thrust is left in control of the pressure ratio. The efficiency is again assumed. As the GEnx-1B is a newer, more advanced engine it is assumed that the efficiencies are higher than those as taken for the GE CF6-80C2.

Several other efficiencies have to be assumed as well. The nozzle efficiencies have also been based on the CF6-80C2 model. Furthermore the mechanical efficiency of both shafts and the combustion efficiency have been assumed, according to values found in literature [26] and the previous models.The inlet is assumed to be perfect, as PT2 and TT2 are measured in front of the fan face. These values are then set as the ambient pressure and temperature in GSP.

Although quite many, the influence of the assumptions on the usability of the model is limited. As stated in the beginning of Section 7.1.2 the model has to be able to mimic the measured parameters from the test cell. Parameters that are not measured do not need to be correct. For example the

Table 7.1: Design point model assumed values

Variable	Description	Unit	GEnx-1B	CF6-80C2
$\eta_{is,inlet}$	Inlet isentropic efficiency	[-]	1.000	1.000
$\eta_{is,LPC_{core}}$	LPC core isentropic efficiency	[-]	0.900	0.897
$\eta_{is,LPC_{bypass}}$	LPC bypass isentropic efficiency	[-]	0.920	0.905
$\eta_{is,HPT}$	HPT isentropic efficiency	[-]	0.930	0.9207
$\eta_{is,LPT}$	LPT isentropic efficiency	[-]	0.940	0.930
$\eta_{j_{bypass}}$	Bypass nozzle efficiency	[-]	0.915	0.915
$\eta_{j_{core}}$	Core nozzle efficiency	[-]	0.900	0.900
η_m	Mechanical efficiency	[-]	0.990	0.990
η_{cc}	Combustion efficiency	[-]	0.995	0.995

booster exit pressure is not measured. In the model its value is determined by matching the measured temperature, under influence of the assumed booster efficiency. Although the pressure might be off in comparison with reality, this will not influence the usability of the model as the actual value is unknown. Furthermore, when applying the model for AM purposes the reference engine and the adapted engine are both under the influence of the same assumptions, influencing both computations in the same way. Because AM is a form of differential GPA, the final error of this is zero as only the difference between the models is taken into account.

Assuming a perfect inlet and setting the conditions as measured at the fan face as ambient conditions has the advantage that the model can be more easily used with on-wing measurements. The bellmouth inlet in the test cell can be assumed to be perfect, however on-wing this is not the case due to the range of different flight conditions. Removing the inlet from the equation prevents this from causing any issues in the model.

7.2. Model

With the necessary assumptions made the model as shown in Fig. 7.1 can be finished. Following the steps in Section 7.1.2 the model has been adapted to fit the measured test cell values at take-off power settings for the selected reference engine. The input for the model is given in Table 7.2. The adapted model parameters are shown in Table 7.3 and the output in Table 7.4.

Table 7.2: Design point input parameters

Parameter	Description	Unit	Value
TT2	Total fan inlet temperature	[K]	285.59
PT2	Total fan inlet pressure	[bar]	0.9867
RHUM	Relative humidity	[%]	71.22
WF	Fuel flow	[kg/s]	2.6708
WA2	Total engine massflow	[kg/s]	1151.1166
N1	Fan speed	[%]	96.96
N1	Fan speed	[rpm]	2482
N2	Core speed	[%]	109.79
N2	Core speed	[rpm]	12491

The mass flow as shown in Table 7.2 cannot be measured directly. It is computed based on the ratio between the total and static pressure at the inlet, the inlet area and some empirical parameters. The relation is derived by GE for KLM, likely based on experimental results obtained during testing at GE facilities. As the equation is empirically determined, it introduces some additional uncertainty into the modelling. The thrust is influenced the most by the mass flow assumption. Following the procedure stated in Section 7.1.2 this directly influences the computed pressure ratio of the fan bypass section. Furthermore the computed BPR is influenced by the mass flow assumption. Again due to the comparison made between two engines both modelled under the same assumptions when applying

Table 7.3: GEnx-1B design point model parameters

Parameter	Description	Unit	Value
$PR_{LPC_{core}}$	LPC core pressure ratio	[-]	2.2296
$PR_{LPC_{Bypass}}$	LPC bypass pressure ratio	[-]	1.5482
PR_{HPC}	HPC pressure ratio	[-]	20.7521
$\eta_{is,HPC}$	HPC isentropic efficiency	[-]	0.872
BPR	Bypass ratio	[-]	9.0181

Table 7.4: Model output parameters and reference engine comparison

Parameter	Description	Unit	Model	Measured	Difference [%]
TT25	Total HPC inlet temperature	[K]	366.979	366.978	0.0002
TT3	Total HPC outlet temperature	[K]	907.028	907.050	-0.0025
TT49	Exhaust Gas Temperature (EGT)	[K]	1208.542	1208.593	-0.0042
PS3	Static HPC outlet pressure	[bar]	45.1959	45.1955	0.0009
FN	Net thrust	[kN]	318.554	318.563	-0.0030

AM in GSP, the influence on the GPA results will be small to nonexistent.

The results in Table 7.4 show that the values as computed by the model represent the measured values very well for the design point calculation. The difference between GSP and the measured values do increase when advancing further through the engine. This is likely due to the fact that more parameters are influencing these outcomes, making it harder for the algorithms in GSP to find an exact solution. The biggest deviation is in the computed EGT value, with a difference between the values of -0.0042%, which is very small.

Table 7.3 shows how the model has been adapted by the procedure as described above to match the test cell measurements. These values are as expected, looking at the similarities between the GEnx-1B and CF6-80C2. The biggest pressure increase is reached in the HPC, with a slight increase caused by the booster. The overall pressure ratio is almost equal to the value mentioned in GE promotional material [9], (46.3 vs 46.268 as computed by GSP). It is expected that the promotional values are computed at sea level standard day conditions, close to the conditions found in the test cell during testing. Unfortunately the division in pressure ratio attained by the HPC and LPC cannot be found directly. In literature on NASA its Energy Efficient Engine (E3) program however some information is found on the designed HPC [3]. The HPC had an efficiency and pressure ratio near to what is found by GSP for the GEnx-1B. The E3 programme has been carried out by NASA together with GE, which has used knowledge gained during the research program for the design of the GE90 HPC [8, 20], which has influenced the GEnx-1B HPC design as well. Based on this the computed compressor parameters are accepted.

Comparing the computed bypass ratio with the value given in GE promotional material [9] it shows that the computed bypass ratio is slightly lower, with about -0.90% difference. In the modelling procedure the bypass ratio is used to control TT49 (EGT), as indicated in Section 7.1.2. A lower bypass ratio indicates that more air flows through the core of the engine. With the given fuel flow, TT3 and TT25 combined with the assumed mechanical efficiency and combustion efficiency this means that more mass is needed in the core to lower TT49 to the measured level in the model. This can be explained in two ways. A first explanation can be that the assumed combustion efficiency is too high and that it must be lowered to 0.987. Based one literature this seems highly unlikely [26]. Another explanation is the use of cooling air on the actual engine, circumventing the combustion chamber and being injected into the HPT directly. This would lower the temperature in the actual engine, resulting in a higher bypass ratio with equal TT49. Cooling air is however assumed to be nonexistent in the model, accepting the 0.90% difference. It is assumed that this will not influence the results much, as seen in Table 7.4 as well.

Table 7.5: Difference between design point simulation in GSP and actual value for engines other than the reference engine

	Power	Difference [%]				
ESN	Setting	TT25	TT3	TT49	PS3	FN
95xxx1	TO	0.45	-0.23	-1.94	-0.11	1.22
95xxx2	TO	0.58	-0.05	-0.84	-0.36	0.96
95xxx4	TO	0.60	-0.36	0.79	0.46	-0.61
95xxx5	TO	0.29	-0.80	0.54	0.25	-0.97

7.3. Simulating different engines

The created design point model is simulates the measured values of the reference engine with great accuracy. The design point however has to represent a generic GEnx-1B engine, when tested at take-off settings in the test cell. This is tested by using the design point model to simulate the other engines tested in the test cell, found in Table 6.3. The model parameters as computed in the previous section, located in Table 7.3 have been kept constant, while adapting the input variables to match the tested conditions.

The results of this are found in Table 7.5. Differences are expected due to engine to engine variation and slight differences in power settings. This will cause differences is the performance of the individual engine components, leading to differences. It is found that indeed differences are present between the model and the actual engine. The largest differences occur for TT49 and FN, the values that depend on the most components and therefore assumptions. Overall the differences stay within 2.0%, from which it is concluded that set design point model represents a generic GEnx-1B at TO power in the test cell.

7.4. Conclusion

In this section the design point model of the GEnx-1B has been fixed, providing a reference point for the off-design calculations which will follow next. Due to a reduced number of measurements several assumptions have been made on the performance of engine components. The resulting design point model replicates the measurements made inside the engine with great accuracy, with the largest deviation being -0.0042%. Furthermore the design values as computed are realistic and match knowledge available on the design of the GEnx-1B and its predecessors.

8

Off-Design modelling

In Chapter 7 the design point of the GEnx-1B GSP model was determined. The actual engine however will operate at more than one power setting, in different conditions. In this chapter the model will be improved further, such that it is able to simulate the engine in different conditions. First the methodology is explained, followed by the results of the tuning procedure. Next the model accuracy is investigated, for both test cell and on-wing data of the reference engine.

8.1. Methodology and additional assumptions

In this section the methodology of the off-design modelling procedure is detailed. In Chapter 2 it has been mentioned that the off-design simulation procedure in GSP is dependent on component maps. The off-design modelling procedure is based on tuning maps that are publicly available, such that they mimic the performance of the actual engine. As for the design modelling, the model is only required to match the measured parameters. The component maps describing the performance for the GEnx-1B are not available outside the OEM environment, requiring adaption of publicly available maps.

Other than component map tuning, different methods to deal with different operating points have been proposed in previous research projects. The first one is the multiple reference point method, which proposes creating multiple design point models and interpolating the results between these models [32]. A second method is the baseline calibration method, in which separate calibration factors are computed to scale the design point model to different operating conditions [23, 32]. Both methods avoid having to tune the component maps, which has been proven to be a laborious task [1, 5, 36]. Both methods however will be less flexible for the end-user, either requiring multiple models to be maintained or additional software besides GSP. Therefore it has been decided to tune the component maps for the off-design modelling of the GEnx-1B.

A model is only within valid in the range over which it is tuned. This does not necessarily have to be the complete operating range of the engine. In case of the GEnx-1B only high power settings are modelled, as attained when taking off. For KLM two power settings are relevant for performance analysis,TO and MC, both tested in the test cell. Tuning for these two values will be done first. When trying to analyse on-wing data a larger range of power settings has to be analysed, due to de-rating when taking off. The component maps will also be tuned for these values. Tuning will be done based on the measurements for the reference engine, as selected in Chapter 6.

Tuning the component maps to analyse the complete operating range of the GEnx-1B will not be done. The objective of creating the model is to analyse the condition of an engine using the AM component in GSP. The condition however is independent of the power setting or ambient conditions. Furthermore, an engine its condition will stay, without any sudden events taking place, almost constant over the course of a single flight. So to analyse the condition of an engine it suffices to only analyse the engine at take-off.

The AM analysis will mainly be used to analyse the performance of an engine when tested in the test cell, in comparison to other engines. Accuracy around the TO and MC power settings as tested in the test cell is therefore the most important. On-wing it is expected that the analysis will be less accurate, due to a larger amount of uncertainties.

8.1.1. Tuning procedure

In this section the tuning procedure will be detailed. As a starting point the component maps as used for the CF6-80C2 model have been taken, which have been tuned in previous research projects, originating from open literature [1, 5, 36]. GSP automatically scales the component maps based on the computed design point, which has been established in Chapter 7, and the location of the design point on the map. The location on the map can be set by the user, by fixing the design point corrected spool speed and betaline. Due to this mechanism the maps of the CF6-80 model can be scaled to fit the GEnx-1B design point.

The relation between the map parameters spool speed, mass flow, pressure ratio and efficiency for the GEnx-1B will be different than those for the CF6-80, as a different compressor design is used. A component map is valid for one specific component geometry, thus the maps are tuned to fit the GEnx-1B geometry. This will be done by adapting the component maps until the parameters as computed by GSP match those measured in the engine.Tuning the maps is has been based on two methods, speed line re-labelling and relocating the speed lines.

Speed line re-labelling

Component maps are made up of lines of constant speed, each line corresponds to a specific non-dimensional spool speed. Between the speed lines GSP interpolates the values linearly. The first tuning method used, described by Verbist [34], is re-labelling these speed lines. The component map is adapted by changing the non-dimensional speed associated with a speed line. This changes the relation between mass flow, pressure ratio, efficiency and spool speed, changing the component its off-design performance. As GSP interpolates between the speed lines, changing one speed line alters the performance between that speed line and its two neighbours. Speed line re-labelling is the first method which has been applied in tuning the component maps.

Relocating the speed lines

The speed lines can also be moved, adapting the mass flow and/or pressure ratio to which they correspond. The efficiency can also be adapted. This again changes the component map and thus the performance of the component to which the map is assigned. This method has also been applied in adapting the component maps, often in combination with re-labelling the speed line.

Additional tuning options

The two methods described above rely on moving or re-labelling the speed lines, without changing the shape of the lines themselves. This is an additional method which can be applied to tune the component maps to fit the measured results. This would also allow for a complete representation of the component its performance. However, when installed in an engine the operating line of a component, for example the HPC, is restricted by the other components also installed on the engine. Due to this a single running line can be plotted over the component map, showing the operating conditions for normal operation of the engine. When deterioration is present in the engine there will be deviation from this line, however the complete shape of the component map does not necessarily have to be correct, as it is unlikely that the outer regions will be needed. Therefore shape of the speed lines has been kept the as in the CF6-80C2 maps.

Using the two methods above the component maps have been tuned. The adaption of the tables describing the maps has been done using custom scripts written in Python. The adaptions are set as percentages of the original value of the CF6-80 map.

8.1.2. Matching procedure

The component maps will be tuned to match the measured parameters on the reference engine, similar to the design point modelling procedure. To quickly analyse the differences caused by tuning the maps, the AM component of GSP is added to the model. As a reference data set the test cell result of the reference engine at TO settings is used, as this is the design point of the model. The AM module is then used to analyse MC results of the same engine, which will result in performance deviations. These deviations will be contributed to deterioration by GSP. However, in this procedure it is assumed that no deterioration is present on the engine, all differences between the MC and TO point are due to modelling errors. By tuning the component maps these errors are removed, causing the component

map to represent the behaviour of the engine [34, 36].The above procedure can be extended to the use of on-wing measurements, by using a point outside the TO-MC power setting range and repeating the procedure.

8.1.3. Variable geometry

A component map depicts the performance of a single geometry. For a component with variable geometry, for example the HPC of the GEnx-1B which has VSVs, the geometry is different for each variable geometry setting [43]. In theory this would mean that a new component map is needed for each VSV setting on the GEnx-1B.

When modelling the GEnx-1B in this research it has been decided to use only a single component map for the HPC. The VSVs in the GEnx-1B move according to a fixed control schedule based on the corrected N2 speed of the engine. Therefore it can be said that for each spool speed there is a predefined VSV setting, which corresponds to a certain behaviour of the compressor. This behaviour can then be matched by tuning the component map, which is valid each time the power setting is varied. The component map then describes a compressor which is only valid when the VSVs are varied in the exact same schedule. As this is the case for each GEnx-1B, this does not cause additional difficulties.

8.1.4. Data acquisition

The component maps will be tuned based on data of the reference engine. Data is available from the test cell and from the engine while installed on-wing. Only the test cell measurements at TO and MC power settings are used. This gives a discrete off-design point, for which the model can be tuned using the procedure above.

On-wing data is used to extend the range of power settings over which the model is tuned, and to check if the model is accurate between the discrete test cell measurements. On-wing the same measurements are taken as in the test cell, except for the thrust measurement which is unavailable. Collection of on-wing data is done automatically by the engine during take-off when certain conditions set by GE are met. At this point the engine is at almost constant conditions and the average of several measurements is taken.

The acquired data is cleaned prior to starting the modelling procedure, to ensure that the conditions in which the measurements were taken are similar. In the test cell no bleed air is extracted from the HPC for de-icing purposes. Therefore it has been decided to remove all on-wing data points in which the de-icing system was active, to keep the engine configuration on-wing equal to the configuration in the test cell. Furthermore as the test-cell is located at sea level, snapshots taken at very high altitudes have been removed, as conditions are significantly different there. All snapshots taken over 3000 ft have been removed, after it showed in the data that only few data points were collected above 3000 ft. This removed a few airports from the dataset. After cleaning the data 229 of the 295 data points were used for the analysis.

8.2. Model accuracy

In this section the outcome of the tuning procedure is shown, by looking at the accuracy of the tuned model in simulating the measured parameters on the engine. First the accuracy of the MC operating setting in the test cell is investigated in Section 8.2.1. The results of tuning the maps using on-wing results is shown in Section 8.2.2. Details of the adapted maps are shown in Section 8.4.

8.2.1. Test cell

A comparison between the tuned model and the test cell results for the MC power setting in the test cell is shown in Table 8.1. It is found that the model represents the engine well, staying within +/- 0.1% difference for all measured parameters. A comparison with Table 7.4 leads to the conclusion that accuracy of the model in the off-design MC point is much lower than for the design point. This is likely due to the added amount of uncertainty introduced by the component maps. Overall the model is accurate enough to be usable, as it is expected that to engine to engine differences and differences caused by deterioration are larger than 0.1%.

Table 8.1: Model output parameters and reference engine at MC in the test cell comparison

Parameter	Description	Unit	Model	Measured	Difference [%]
TT25	Total HPC inlet temperature	[K]	361.27	361.32	-0.0138
TT3	Total HPC outlet temperature	[K]	880.45	880.50	-0.0057
TT49	Exhaust Gas Temperature (EGT)	[K]	1157.37	1157.93	-0.0484
PS3	Static HPC outlet pressure	[bar]	40.81877	40.81852	0.0006
FN	Net thrust	[kN]	284.620	284.475	0.0510
N2	Core spool speed	[%]	108.410	108.396	0.0129
WF	Fuel flow	[kg/s]	2.3102	2.3094	0.0346

8.2.2. On-wing

The on-wing results are used to analyse the accuracy of the model over a range of operating points. The results of analysing 229 take-offs available for the reference engine with the GSP AM component and tuned maps are found in Fig. 8.1. As a reference dataset for the on-wing analysis the first available take-off of the reference engine has been used. This is done to prevent differences due to for example installation effects. In a previous study it has been shown that using a test cell measurement as a reference dataset for an on-wing analysis showed large condition deviations [34]. More information on this will be given in Chapter 12.

The results in Fig. 8.1 are shown as a percentage difference with the measured value. If the model would represent the measured results perfectly all data points would lie on the x-axis. A quick look at the figures shows that this is not the case. In the beginning of Section 8.1 it was established that deterioration of an component is independent of the operating conditions of the engine. From this it follows that the conditions as computed by GSP in Fig. 8.1 should be independent of the power setting, the x-axis.

The x-axes in Fig. 8.1 show the corrected spool speeds of either the LPC or HPC, $N1_c$ and $N2_c$. These values are calculated by GSP using Eq. (8.1)[14]. The reference values are the values used in the design point computation from Chapter 7.

$$N_c = \frac{\frac{N}{N_{ref}}}{\sqrt{\frac{T}{T_{ref}}}} \tag{8.1}$$

The results for TT25, TT3 and $N2_c$ deviations (Figs. 8.1a, 8.1b and 8.1e) look best. Not much scatter is present in the graphs and the performance deviations as computed by GSP are almost independent of the corrected spool speed.

The results for TT49 and WF (Figs. 8.1c and 8.1f) show more scatter than the previous figures. The TT49 deviations also have a slight dependency on $N2_c$, dropping slightly when $N2_c$ surpasses 100%. The WF results show slightly more scatter and almost no dependency on $N1_c$. The almost constant deviation from zero is due to the Calibration Factors (CFs), which are influenced by the choice of reference point (Chapter 8).

The strongest relationship between performance deviations and spool speed is found for PS3 in Fig. 8.1d. Here a linear relation can be found between the power setting and condition deviation. Especially above 100% $N2_c$ a larger deviation is found, as was also done for TT49 in Fig. 8.1c. The relation however is weak, especially considering the amount of scatter present in the results. Further tuning of the component maps has not resulted in the removal of the relation with corrected spool speed.

In all results a form of scatter is present, due to different operating conditions and added sources of uncertainty present in on-wing conditions. These sources will be further researched in Chapter 12. Scatter is therefore assumed not to be due to modelling errors.

The relation between power setting and performance deviations is likely caused by modelling errors. Judging from the results for TT49 and PS3 (Figs. 8.1c and 8.1d) there are errors present in the HPC map, which become stronger above 100% $N2_c$. Further tuning of the maps, using the methods as described in Section 8.1, has not solved this issue. Possibly the third method, further adapting the shape of the constant speed lines, can be of help. This is left as a recommendation for future work.

Another explanation for the deviation of PS3 is the lack of a PS25 measurement. As no information is available on PS25, the pressure ratio of the LPC is unknown. In Chapter 7 an assumption has been

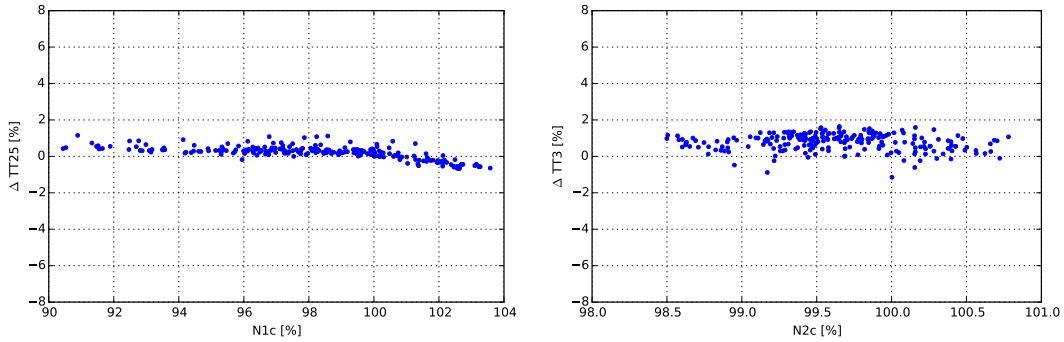

(a) $N1_c$ vs TT25 deviation

(b) $N2_c$ vs TT3 deviation

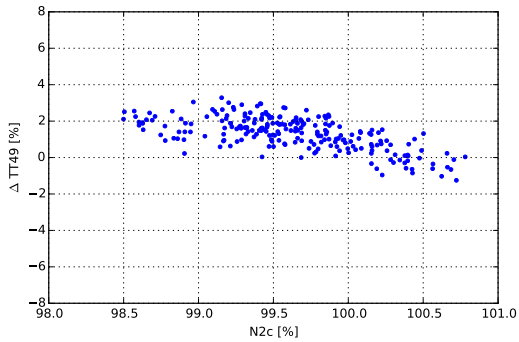

(c) $N2_c$ vs TT49 deviation

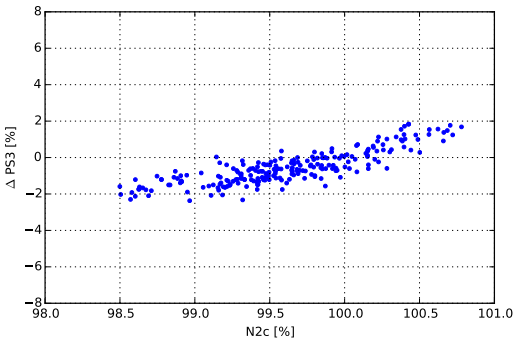

(d) $N2_c$ vs PS3 deviation

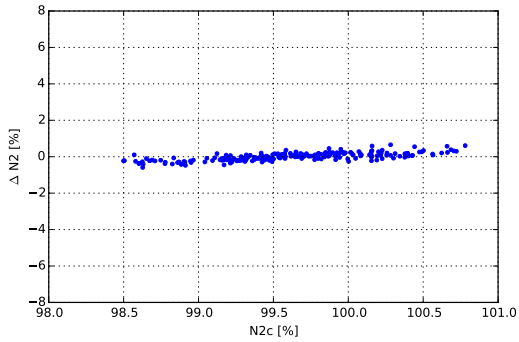

(e) $N2_c$ vs $N2_c$ deviation

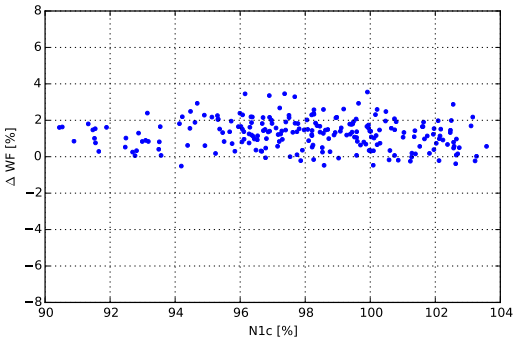

(f) $N1_c$ vs WF deviation

Figure 8.1: Accuracy of the model in simulating the on-wing measurements for the reference engine

made on the efficiency, computing the pressure ratio based on the known temperature TT25. The variation of both efficiency and pressure ratio with power setting for the LPC however is unknown. This might lead to a wrong computation of PT25 in GSP, which then leads to a different pressure ratio for the HPC in order to match the known value of PS3. If this would be unattainable with the compressor maps used this would lead to a condition deviations. Without a PS25 measurement however this cannot be verified. Another explanation could be in a slight deviation for the HPT mass flow or efficiency. Again due to a missing pressure measurement (PS49) this is not verifiable.

The model is accurate over the corrected spool speeds shown above. As the corrected speeds depend on the temperature, it is not possible to directly translate this to a specific power setting of the engine. Furthermore as Eq. (8.1) depends on a reference speed and temperature the range of power settings to be analysed also slightly depends on the chosen reference point.

8.3. Condition estimation accuracy

In the previous section the ability of the model to simulate a GEnx-1B has been tested, by investigating the accuracy with which the model can simulate measurements taken on the reference engine. This analysis has been performed using the GSP AM module, which next to performance deviations also computes a condition deviation of the modules in comparison with the reference engine. In Part III the workings of the AM component will be investigated further, in this section it can be assumed that it works properly. In Section 8.1.2 the assumption has been made that the reference engine is healthy with zero deterioration present. When tuning the maps it has to be made sure that this is also true, next to the proper estimation of the measured parameters. The condition deviation of the different modules in the on-wing condition is shown in Fig. 8.2.

The condition of the MC test cell measurement shows zero deterioration for all components. The AM component has a certain tolerance for differences in performance. This tolerance is the difference between the performance deviations of the calibrated reference engine and the analysed engine. If this difference is below 0.1% no adaption is made. As can be seen in Table 8.1 all differences are below 0.1% for the MC measurement, thus zero condition deviation is computed for all modules. The tolerance can be varied by the user. It is decided to not lower the threshold as this would likely lead to numerical instabilities. Furthermore small variations between engines are expected.

Judging from Fig. 8.2 the component conditions are computed well. As for the performance deviations in Fig. 8.1 some scatter is present in the data. Except for the computed HPC conditions the computed conditions show little to no relation with the power setting (as required) and are near zero.

The condition of the HPC as computed by the AM component shows different behaviour than the conditions of the other components. The estimated efficiency deviation in Fig. 8.2c is shifted down approximately two percent compared to the expected result of zero deviation. This is likely due to the chosen reference point, introducing errors into the analysis. At the end of Section 12.2.5 this is confirmed.

The HPC W_c deviations in Fig. 8.2b show the largest amount of scatter. Furthermore a weak relation with $N2_c$ can be found. These effects are likely due to small tuning errors in the LPC and HPC maps. The relation between the LPC map and the computed HPC condition deviations is found to be strong. This makes tuning the maps significantly harder, as the LPC outlet conditions (and thus the HPC inlet conditions) are not fully defined due to lack of a PS25 measurement. This added degree of freedom (mentioned before in Section 8.2.2) resulted in adaptions made to maps trying to match the performance of other components, without knowing the actual performance of each component. It is likely that due to this multiple possible combinations of LPC and HPC maps exist, which all match the measurements as available on the GEnx-1B. Only adding more measurements, preferably PS25, would solve this. This would add information on the LPC behaviour, allowing for more correct tuning of the maps. If possible in the future it is recommended to measure PS25 at several power settings and to retune the maps.

8.4. Tuned component maps

In this section the adaptions made to the maps will be described. The maps have been adapted following the procedure in Section 8.1, which involved re-labelling or moving the speed lines. Due to the used method the maps are highly similar. A comparison between the CF6-80 maps and the tuned GEnx-1B maps is shown in Fig. 8.3. The values corresponding to the speed lines are located in Table 8.2.

Table 8.2: Corrected spool speeds associated with each speed line for all components

	Speed line									
Map	1	2	3	4	5	6	7	8	9	10
GEnx-1B LPC C	0.359	0.528	0.661	0.791	0.845	0.956	1.000	1.038	1.155	-
CF6-80 LPC C	0.359	0.528	0.661	0.791	0.880	0.952	1.000	1.028	1.144	-
GEnx-1B LPC B	0.300	0.500	0.700	0.800	0.871	0.916	0.959	1.000	1.050	1.100
CF6-80 LPC B	0.300	0.500	0.700	0.800	0.850	0.906	0.951	1.000	1.050	1.100
GEnx-1B HPC	0.700	0.750	0.800	0.850	0.939	0.993	1.000	1.013	1.029	-
CF6-80 HPC	0.700	0.750	0.800	0.850	0.921	0.993	1.000	1.030	1.050	-

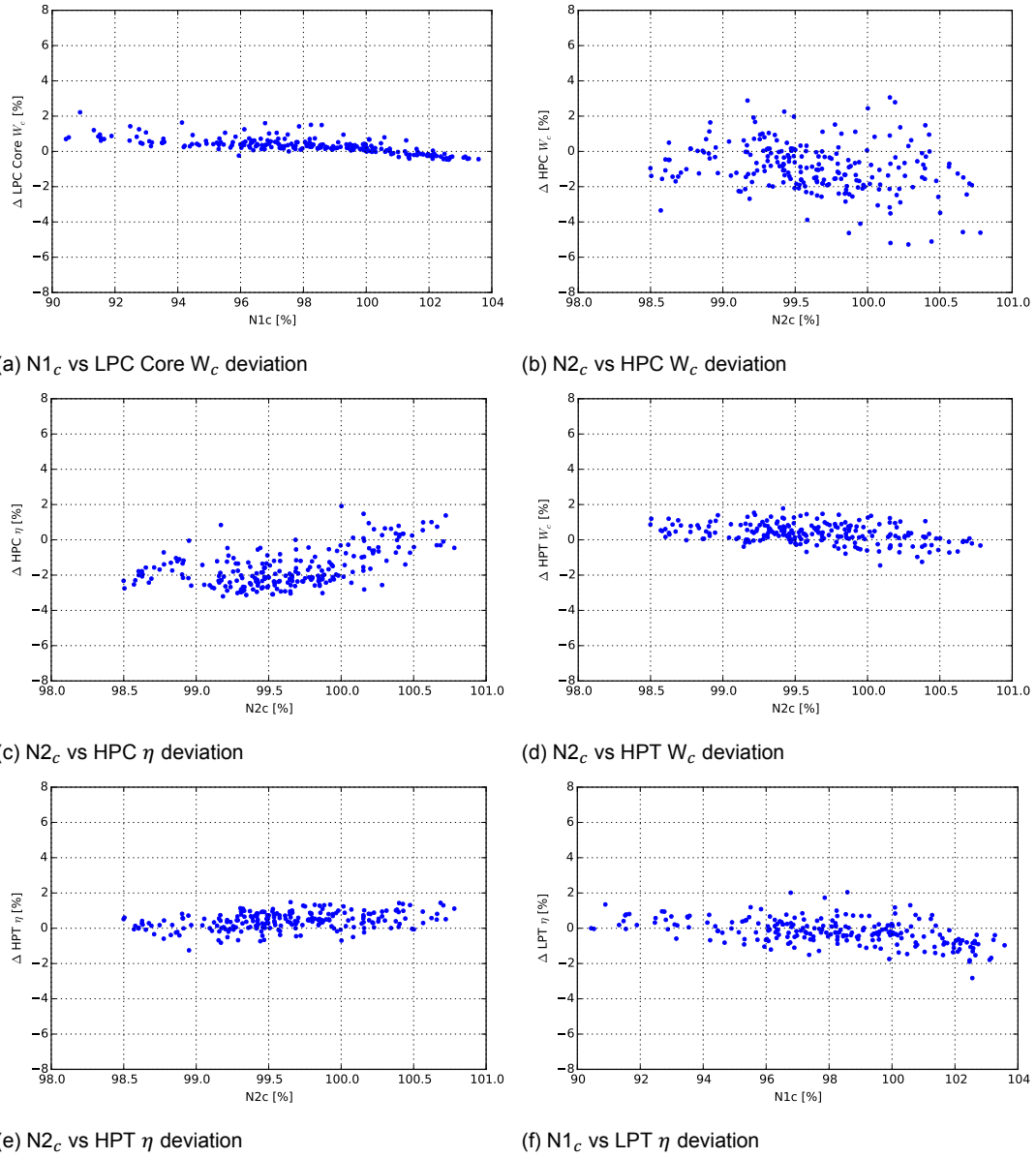

(a) $N1_c$ vs LPC Core W_c deviation

(b) $N2_c$ vs HPC W_c deviation

(c) $N2_c$ vs HPC η deviation

(d) $N2_c$ vs HPT W_c deviation

(e) $N2_c$ vs HPT η deviation

(f) $N1_c$ vs LPT η deviation

Figure 8.2: Accuracy of the model in simulating the engine condition for on-wing measurements of the reference engine

Tuning the maps has been an iterative process. Making a change in one component map influenced the operating line on another one, causing changes throughout the engine. When tuning using the MC test cell measurements the goal has been to reduce the computed deviations to zero, as it is assumed that there is no deterioration on the reference engine. Attempting to use the same technique using on-wing measurements however was unsuccessful, due to the amount of scatter present in the measurements. Instead a different method has been employed, in which an attempt has been made to remove any relationship between the computed performance and condition deviations, and spool speed, as has been discussed in Section 8.2.2.

The tuning process was not only iterative, but also involved some trial and error, which made the process time consuming. This same conclusion has also been drawn before, in an earlier thesis project [5]. Furthermore the lower amount of available measurements on the GEnx-1B has likely allowed for some additional freedom in tuning the maps. As not all parameters are measured, changes can be made influencing these parameters without penalty. This increases the uncertainty related to the maps, as it is not fully known if the maps accurately represent the real life performance of a GEnx-1B.

Tuning started with adapting the LPC bypass map, which has the biggest influence on the rest of

the engine. Adapting the performance of the LPC bypass mostly influences the BPR changing the performance of the rest of the engine. Using test cell results it was found that the computed thrust did not deviate much from the measured result, however the fuel flow was much higher. This indicated that the bypass efficiency was too low. GSP assigned this deviation to a (greatly) reduced LPT efficiency, which was deemed to be unrealistic. Adapting the bypass map resolved the LPT efficiency deviations. This same relation has been used in the on-wing results were no thrust measurement is available to assess the bypass performance.

Tuning the LPC core map reduced the deviations in all other parameters except for the N2 speed. This last deviation has been removed by tuning the HPC map. The last performance deviations have been removed by making a small adaption to the HPT efficiency. The LPT map has not been adapted.

The same relations have been used when tuning the maps using on-wing measurements. As no thrust measurement is available, the bypass map has been tuned using the computed fuel flow deviation and the efficiency deviation of the LPT.

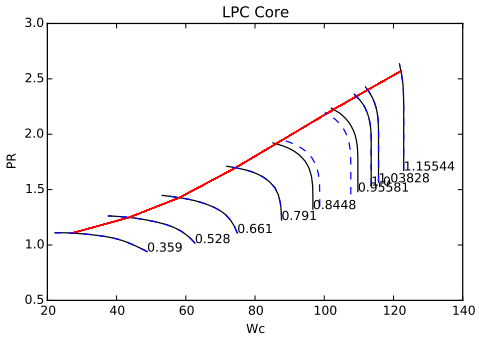

(a) LPC Core W_c vs PR

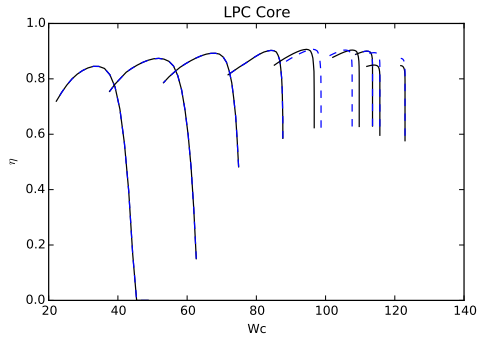

(b) LPC Core W_c vs η

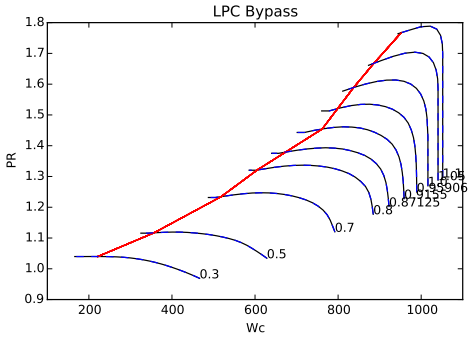

(c) LPC Bypass W_c vs PR

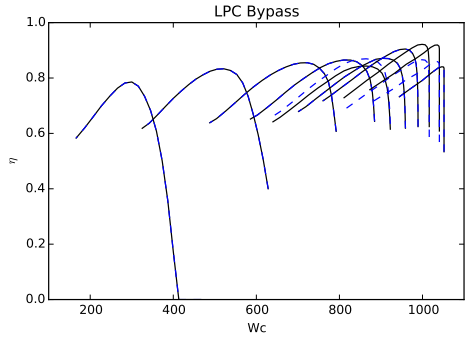

(d) LPC Bypass W_c vs η

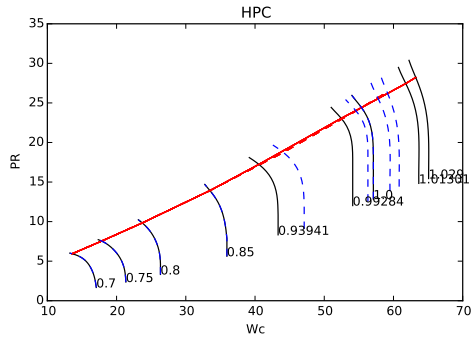

(e) HPC W_c vs PR

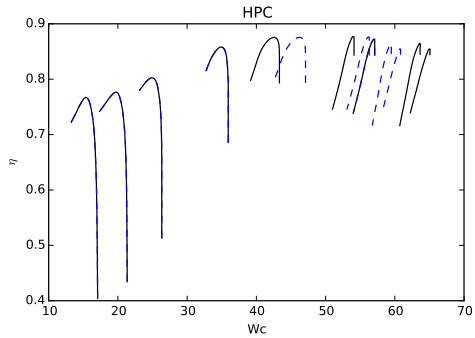

(f) HPC W_c vs η

Figure 8.3: Comparison of the original CF6-80 maps and the tuned GEnx-1B maps. In black continuous lines the GEnx-1B maps, in blue dashed lines the CF6-80 maps. Compressor surge lines are shown in red.

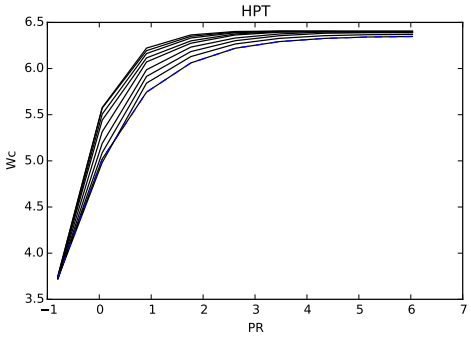

(g) HPT PR vs W_c

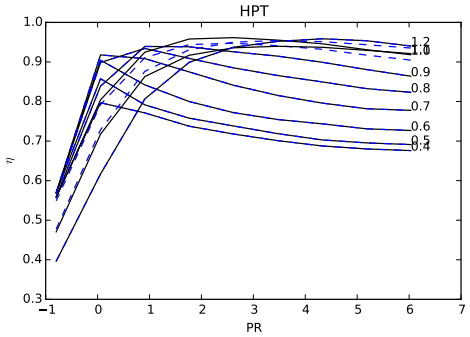

(h) HPT PR vs η

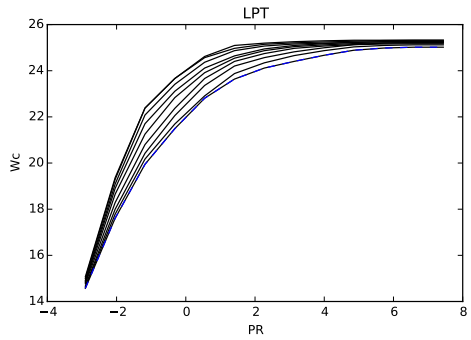

(i) LPT PR vs W_c

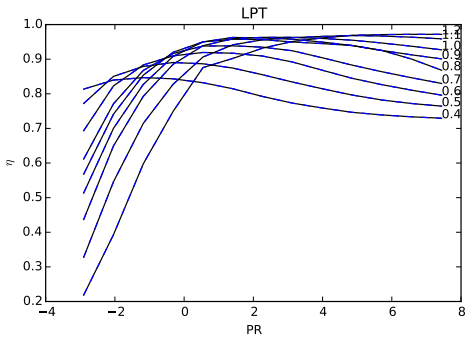

(j) LPT PR vs η

Figure 8.3: Comparison of the original CF6-80 maps and the tuned GEnx-1B maps. In black continuous lines the GEnx-1B maps, in blue dashed lines the CF6-80 maps. Compressor surge lines are shown in red. [Continued]

8.4.1. LPC Core

The shape of the LPC core map has been kept approximately equal as shown in Figs. 8.3a and 8.3b, the speed lines however have been re-labelled as found in Table 8.2. Two speed lines have been moved, as re-labeling these speed lines further changed the behaviour of the bypass too much, as this also changed the operating speed of the bypass portion of the fan.

Adapting the LPC has resulted in an increased pressure ratio and efficiency at spool speeds below the design point, which was at TO settings in the test cell. Especially the pressure ratio has increased, which indicates a fan core and booster on the actual engine which performs better when the power setting is reduced than the CF6-80 did. Unfortunately due to a lack of PS25 measurement this cannot be validated.

The pressure ratio above the design point reduces slightly in comparison with the CF6-80 map. This puts the increase in pressure with spool speed above the design point more in line with the relation below the design point. Overall the pressure ratio increases with spool speed, in a less dramatic fashion than for the CF-80, indicating more consistent performance.

The efficiency drops sharply when the corrected spool speed is higher than in the design point, which is likely not the case on the actual GEnx-1B. This adaption to the maps has been made to correct the computed HPC W_c deviation at higher power settings. Additional measurements, PS25 and PS49, might solve this.

8.4.2. LPC Bypass

The bypass map has been adapted to move the peak efficiency further towards higher spool speeds. Due to this the efficiency of the bypass is more constant over the range of power settings considered. The pressure ratio has not changed much. Considering the much improved fan design over the CF6-80, a more consistent efficiency for the fan is deemed realistic.

8.4.3. HPC

In Figs. 8.3e and 8.3f it can be seen that the HPC map has changed more than the other maps. Below the design point spool speed ($N2_c$=1) the lines of constant speed have been moved towards lower W_c values. The accompanying pressure ratios have also been lowered to keep the shape of the map equal, so that the curves of constant efficiency kept their shape. Above the design speed the speed lines have been re-labelled, and moved towards higher W_c values. The efficiencies have also been increased above the design speed.

The HPC map has been tuned last, as mentioned before in the beginning of Section 8.4. The adaptions to the HPC will therefore have to be investigated in light of the changed LPC in front of it. The range of spool speeds over which the HPC operates has slightly increased, caused by moving the lines of constant speed. Due to this the range of attainable pressure ratios has also slightly increased. Furthermore the efficiency at lower spool speeds has increased.

In comparison with the CF6-80 maps, the biggest difference is in the range of spool speeds attained. The GEnx-1B map and CF6-80 map (when scaled), attains about the same pressure ratio and efficiencies, the spool speeds however differ. This is also as expected when looking at the changes made to the map.

8.4.4. HPT

The HPT map has been tuned slightly, reducing the efficiency. After tuning the LPC core and bypass, and the HPC the EGT remained too high. By reducing the HPT efficiency this has been solved. It is however not expected that the HPT is less efficient in the actual engine. Likely the EGT is lower due to cooling air circumventing the combustion chamber being ejected into the HPT. These cooling flows however have not been modelled, due to which the HPT efficiency has been lowered slightly.

8.5. Conclusion

Despite the unavailability of the original component maps, the off-design performance of the GEnx-1B can be simulated well using the tuned publicly available maps. The CF6-80 LPC (core and bypass) HPC and HPT maps have been adapted to match the measured GEnx-1B parameters.

The component maps have first been tuned to match the MC measurement taken in the test cell for the reference engine. Matching only a single point, it has been possible to match the measurements with a high degree of accuracy, staying within +/-0.1% of the measured value. The reference engine in the test cell at the two highest power settings can therefore be simulated accurately.

The maps have been tuned over a larger range of power settings using on-wing data. Scatter was present in the results, leading to more difficulties in tuning the maps. Therefore it has been decided to tune the maps such that no relation is found between the operating settings and the computed deviations, as it is assumed that the engine condition is constant over the take-offs considered. Overall this has been successful, with small dependencies on corrected spool speed remaining for the deviation of PS3 and TT49. Furthermore it was found that the HPC corrected mass flow capacity deviation showed a high degree of scatter. Further tuning of the component maps using the proposed methods has not solved this issue.

The lack of a pressure measurement between the LPC and HPC has increased the amount of uncertainty involved in tuning the maps. The LPC map cannot be fully tuned as the change of pressure ratio with power setting is not known. Due to this the inflow conditions for the HPC are also unknown, leading to an increase in uncertainty. This is likely an explanation for the small errors in the HPC results.

Overall it is concluded that despite the small modelling errors the maps are accurate enough to simulate the GEnx-1B in off-design conditions. In Part III this will be investigated further. In future research it is recommended to try to further improve the component maps, it is possible that improvements can be made by changing the shape of the speed lines. Furthermore the maps might be tuned better if a PS25 measurement is available.

III

Applying AM to the GEnx-1B

9

Applying AM to an engine with a limited amount of available measurements

When modelling the design point in Chapter 7 a large amount of assumptions had to be made, due to a lack of measurements in the GEnx-1B gas path. Furthermore in Chapter 8 it was found that the lack of measurements introduced more freedom and thus uncertainty when tuning the component maps to simulate a GEnx-1B.

In Chapter 4 it was shown that AM requires an equal amount of measurements and adapted engine parameters to function. As fewer measurements are available on the GEnx-1B than on older engines, the AM procedure is hampered in comparison to previous research. In previous research AM has been proven to be working on the CF6-80. In this chapter it will be investigated if the reduced amount of measurements influences the use of AM, by adapting the previously used CF6-80 GSP model.

9.1. Research rationale and objective

The use of AM at KLM ES using GSP has been researched before in several research projects, as described in Chapter 4. Although a model has been made of the CFM56-7B [2], most research has been focused on the CF6-80 [1, 5, 34]. It is shown that it is possible to analyse engines, using both test cell and on-wing data. The goal of this thesis research is to apply the same techniques to the GEnx-1B.

Fewer gas path measurements are taken on the GEnx-1B than on older engines, leading to an increased amount of assumptions required and more freedom in tuning the component maps. A comparison between the available measurements on the GEnx-1B and CF6-80 is found in Table 9.1. The amount of pressure sensors decreased the most. Due to the smaller amount of measurements, information about the performance of the fan is missing, which in previous research has always been available both on-wing and in the test cell. Furthermore less information is available on the LPC core, HPT and LPT, which caused difficulties when tuning the component maps.

Looking forward to analysing the GEnx-1B using the AM component in GSP, additional difficulties appear. As a smaller amount of measurements is taken, fewer parameters can be adapted during the AM procedure. This leads to a smaller amount of information available about the engine its condition and to a less constrained solution space. It is therefore unknown if the AM component will correctly estimate an engine its condition, both with and without deterioration present. Furthermore it must be investigated which parameters can be removed when analysing an engine, without introducing large uncertainties into the analysis. In previous projects this problem has not been addressed, due to the abundance of available measurements. When starting this research it was expected that a newer modern engine would measure more parameters onboard than engines of a previous generation. In an older thesis project by Pieters at the Royal Netherlands Navy an analysis has been made to investigate GPA with fewer parameters than on the CF6-80 [23, 41]. In this research it was concluded that the root cause of the performance deviation has to be included adapted parameter set. In the research by Pieters more measurements were taken than on the GEnx-1B, hence this research.

The objective of this chapter is to investigate the possibility of applying AM to an engine with a limited amount of available measurements. Furthermore it is investigated which parameter combinations

Table 9.1: Comparison between the available measurements on the GE CF6-80 and the GEnx-1B in the test cell

Parameter	Description	GEnx-1B	CF6-80
TT2	Total fan inlet temperature	x	x
TT25	Total HPC inlet temperature	x	x
TT3	Total HPC outlet temperature	x	x
TT49	Exhaust Gas Temperature (EGT)	x	x
TT5	Total LPT outlet temperature		x
PT2	Total fan inlet pressure	x	x
PS14	Static pressure duct		x
PS25	Static booster outlet pressure		x
PS3	Static HPC outlet pressure	x	x
PS49	Static HPT outlet pressure		x
N1	Fan speed	x	x
N2	Core speed	x	x
WF	Fuel flow	x	x
FN	Net thrust	x	x
RHUM	Relative humidity	x	x

provide useful results for the AM analysis. This will close the research gap between previous research on applying AM in the MRO environment and applying it to a modern engine such as the GEnx-1B. A look forward to the CFMI LEAP-1B powering the Boeing 737MAX which will be maintained at KLM ES in the future shows that this engine will have a sensor set comparable to the GEnx-1B. The research here will therefore be of interest to more future engines than just the GEnx-1B.

9.2. Methodology

The methodology is based around a single assumption: the GSP model as created for the CF6-80 is correct and the AM module produces an accurate analysis of the its engine condition. The model as used by Verbist in his research is taken as a baseline, to which models with a reduced amount of measurements will be compared [34].

The GSP AM component is used in combination with the baseline model to analyse a range of CF6-80C2B1F engines. Data selection details are located in Section 9.2.2. The AM module allows the user to choose which measurements are to be used in the analysis and which engine parameters can be adapted to match the measured performance. Removing a measurement from the analysis, by deselecting it in the AM module, is equal to removing it from the engine. Removal of a measurement must be balanced by the removal of an engine parameter which can be adapted by the procedure. By progressively removing sensors from the analysis, the CF6-80 model is adapted so that it can only use the measurements available on the GEnx-1B.

The analysis will first be performed on engines which are considered healthy by AM component in combination with the baseline model. These engines will then be analysed using different combinations of sensor data and adapted component conditions. Next the results are analysed to investigate their accuracy, based on the change in average deterioration and standard deviation. In this way the effect of a less constrained solution space can be determined. If successful the useful cases will be used to analyse engines on which deteriorated performance is simulated. It is expected that the results will only perform well if the root cause is included in the analysis, as determined by Pieters [23, 41].

9.2.1. Case definitions

Fourteen different combinations of measurements and engine condition parameters have been defined. The different combinations, or cases, can be found in Table 9.2. The amount of measurements has been reduced starting at the rear of the engine, moving forwards until the used measurements represented the GEnx-1B. In one case a measurement has been added: TT5 the LPT exit temperature, to investigate the effect of further constraining the solution space. Furthermore PS14 is not used in any of the cases, as FN is measured in the test cell. As the bypass is responsible for the largest part of the thrust, adding both FN and PS14 has been shown to be too restrictive for the algorithm to find a

Table 9.2: Parameter combinations tested, measurements at the top, adapted component properties at the bottom

Name	TT25	PS25	TT3	PT3	TT49	PS49	TT5	FN	WF	N2
9 - Baseline	x	x	x	x	x	x		x	x	x
10	x	x	x	x	x	x	x	x	x	x
9 - No FN	x	x	x	x	x	x	x		x	x
8	x	x	x	x	x			x	x	x
8 - Alt	x	x	x	x	x			x	x	x
8 - No FN	x	x	x	x	x				x	x
7	x		x	x	x			x	x	x
7 - Alt	x		x	x	x			x	x	x
7 - η	x		x	x	x			x	x	x
7 - W_c	x		x	x	x			x	x	x
6	x		x	x	x				x	x
6 - Alt	x		x	x	x				x	x
6 - W_c	x		x	x	x				x	x
6 - No WF	x		x	x	x			x		x

	LPC Core		LPC Bypass		HPC		HPT		LPT	
Name	η	W_c	η	W_c	η	W_c	η	W_c	η	W_c
9 - Baseline	x	x		x	x	x	x	x	x	x
10	x	x	x	x	x	x	x	x	x	x
9 - No FN	x	x		x	x	x	x	x	x	x
8	x	x		x	x	x	x	x	x	
8 - Alt	x	x		x	x	x	x	x		x
8 - No FN	x	x			x	x	x	x	x	x
7		x		x	x	x	x	x	x	
7 - Alt	x			x	x	x	x	x		x
7 - η	x			x	x	x	x	x	x	
7 - W_c		x		x	x	x	x	x		x
6		x			x	x	x	x	x	
6 - Alt	x				x	x	x	x		x
6 - W_c		x			x	x	x	x		x
6 - No WF		x			x	x	x	x	x	

solution. PS14 and FN can however be used instead of one another, as has been shown by Verbist in previous research [34]. Focussing on the test cell measurements PS14 can be left out.

Many more combinations can be thought off, however it has been chosen to keep all parameters related to the core engine, the HPC and HPT, in the analysis. These modules are hardest to reach and likely to deteriorate the most. To keep the model as useful as possible these components have therefore been kept in the analysis. Furthermore the sensors as available on the GEnx-1B have been kept in place.

The cases with 6 parameters represent the GEnx-1B on-wing, removing the thrust measurement from the analysis. The fuel flow has also been removed once instead of the thrust measurement, to compare the influence of these parameters. Removing the thrust measurement also leads to removing the condition of the LPC bypass, as this part is responsible for most of the thrust. In previous research a thrust measurement (or equivalent) has always been present in the analysis. It is of interest to see if the fuel flow alone restricts the analysis enough.

As mentioned in Section 9.2 some of the cases from Table 9.2 will also be used to analyse engines with simulated deterioration. This will be done by modifying the test cell results of the reference engine by applying simulated deterioration in GSP. The different types of deterioration simulated are shown in Table 9.3. The first cases focusses specifically on a single component, to see if the parameter selection can correctly pinpoint deterioration in each component. The other cases combine deterioration in several components, to investigate if the correct amounts of deterioration are linked to each component by

Table 9.3: Simulated deterioration cases CF6-80C2

	LPC Core		HPC		HPT		LPT	
Name	$\Delta\eta$	ΔW_c	$\Delta\eta$	ΔW_c	η	W_c	η	W_c
1 - LPC	-0.33%	-1%						
2 - HPC			-1%	-3%				
3 - HPT					-1%	-2%		
4 - LPT							-1%	-2%
5 - LPC + HPC	-0.33%	-1%	-1%	-3%				
6 - HPC + HPT			-1%	-3%	-1%	-2%		
7 - HPT + LPT					-1%	-2%	-1%	-2%
8 - LPC + HPC + HPT	-0.33%	-1%	-1%	-3%	-1%	-2%		
9 - LPC + HPC +HPT + LPT	-0.33%	-1%	-1%	-3%	-1%	-2%	-1%	-2%

the AM module. The cases are based on the effects of deterioration found in Chapter 3. The amount of deterioration applied to the LPC is less, as it was found that deterioration such as fouling affects the HPC more.

9.2.2. Data acquisition

Data has been gathered from the extensive history of CF6-80C2 testing at KLM ES. 251 different test cell runs have been gathered, including both inbound and outbound test runs of B1F rated engines. From this set of runs a selection of 158 engines has been made, based upon the condition of the LPT as determined by the AM-component in GSP. Some LPTs showed large deviations in computed condition, these test runs have been removed from the selection. Due to this the condition of the other components also became more constant. The exact condition of the analysed engines is not of importance, as the difference between the different parameter selections from Table 9.2 is of interest. A large amount of engines is beneficial, as is a low spread in the original measurements. Both allow for easier determination of any differences.

As a reference engine ESN 70xxx1 has been chosen. The reference case is an outbound test run after the engine had work done on all modules. All modules except the LPC have been given an overhaul shop visit, the LPC has been given a performance restoration shop visit. For an engine with this amount of work done, the reference engine had the most average EGTHDM, of 67 degrees Celsius.

9.3. Results

In this section the results of trying to apply the AM component in GSP to an engine with fewer available measurements is presented. First the results of applying the different cases from Table 9.2 to healthy engines are shown. This is followed by the selection of cases which will be investigated further. In Section 9.3.2 the selected cases will be used to analyse engines on which deterioration has been simulated.

9.3.1. Parameter selection

The 14 different parameter combinations from Table 9.2 have all been used analyse the 158 healthy CF6-80C2 engines as mentioned in Section 9.2.2. The effects on the average amount of deterioration computed by the AM component is found in Table 9.4 and the effect on the standard deviation of the results in Table 9.5. The values shown are the difference with the baseline parameter set.

The effects of removing or adding measurements will be investigated first. Adding TT5, the temperature after the LPT, leads to a shift in the average LPT efficiency deviation and an increase in the standard deviation. This is likely due to a more constrained LPT condition, due to which the LPT has to be adapted more to match the measured temperatures. This will lead to a shift and an increase in standard deviation as differences between the engines will be clearer. The effect on other components is rather small.

Removing FN while keeping TT5 in the measurement set changes the LPC mass flow deviations, for both the core and bypass. The changes for the bypass are expected, as without a thrust or bypass

Table 9.4: Difference in average computed deterioration with the baseline parameter set

	LPC Core		LPC Bypass		HPC		HPT		LPT	
Name	η	W_c	η	W_c	η	W_c	η	W_c	η	W_c
9 - No FN	0.00	-0.54		-0.90	0.00	0.01	0.00	0.01	-1.12	0.01
10	0.01	0.04		-0.03	0.00	0.01	0.00	0.01	-1.12	0.01
8	0.00	0.00		0.00	0.00	0.00	-0.18	0.00	0.18	
8 - Alt	0.00	0.00		0.00	0.00	0.00	-0.60	-0.01		1.19
7		0.15		0.00	-0.27	-0.50	-0.18	0.00	0.18	
7 - Alt	0.41			0.00	-0.15	-0.29	-0.60	-0.01		1.19
7 - η	0.41			0.00	-0.15	-0.29	-0.17	0.00	0.18	
7 - W_c		0.15		0.00	-0.27	-0.51	-0.60	-0.01		1.19
6		0.27			-0.27	-0.51	-0.18	-0.01	0.47	
6 - Alt	-0.04				0.02	0.03	-0.33	-0.01		0.65
6 - W_c		0.27			-0.27	-0.51	-0.33	-0.01		0.65
6 - No WF		0.22			-0.29	-1.06	-0.47	-0.58	0.99	

pressure measurement the changes in this component are unconstrained. This will then also lead to a mass flow deviation in the core flow. The changes for the LPT remain the same, likely due to the added TT5 measurement. From this it is concluded that if FN is included in the measurement set, the mass flow deviation through the bypass must be included as well. Adding TT5 results in a larger amount of uncertainty, it is however uncertain if the actual LPT conditions are computed with increased accuracy.

Moving to the 8 variable cases the total pressure measurement after the HPT is removed, PS49. TT5 is again not considered, as set in the baseline. Removing PS49 has two effects on the AM results. The average difference in HPT efficiency as found by the AM component increases, while also increasing the scatter in the results. Changes in HPT mass flow capacity are not found. For the LPT both the average mass flow and average efficiency deviations increase, with the standard deviation increasing as well, showing increased scatter. The effects on both the HPT and LPT increase when the LPT mass flow is adapted rather than the efficiency. The accuracy of the LPT results will have to be investigated further, as the changes are rather large.

Removing PS25, the pressure measurement after the booster, or LPC core, creates the 7 variable cases. This has effects on both the LPC core and HPC. For the HPC both the mass flow and efficiency deviations as computed by the AM component shift, with a larger increase in scatter when the LPC mass flow deviation is removed from the dataset. From this it is concluded that the LPC mass flow deviation should be included for the most accurate results. This is also expected from the analysis made in Chapter 3, where it was found that efficiency deterioration only has a small effect on the performance of other components. Removing PS25 does not affect the hot section of the engine.

Finally the thrust measurement is removed, as well as the bypass mass flow deviation, mimicking the GEnx-1B on-wing. Doing so changes the LPC and LPT performance, which is expected as their conditions are less constrained. With the parameter set as defined above, using the LPT efficiency and LPC mass flow, the core engine is not affected by removing the thrust measurement. To what extend the LPC and LPT results are still usable will have to be investigated. The alternative dataset breaks with the trend as found in the previous results and seem to increase the accuracy of the results in comparison to the 7 or 8 variable set. This seems unlikely and will be investigated next. Removing the fuel flow rather than the thrust results in unusable results.

In the analysis above a look has been taken at the differences over the whole dataset, without taking specific cases into consideration. Overall the results can be trusted, however when analysing specific measurements different parameter combinations might be more accurate than would be expected based on the results above. In previous research by Pieters it was found that the most accurate results are obtained when the root cause of the performance deviation is included in the measurement set [23, 41], which has not been tested.

9.3.2. Simulated deterioration

The analysis in Section 9.3.1 has resulted in five parameter sets which are of interest in researching the effect of removing measurements from the dataset. In this section engines with simulated deterioration

Table 9.5: Difference in standard deviation of the computed deterioration with the baseline parameter set

	LPC Core		LPC Bypass		HPC		HPT		LPT	
Name	η	W_c	η	W_c	η	W_c	η	W_c	η	W_c
9 - No FN	0.00	0.70		1.66	0.00	0.00	0.00	0.00	2.23	0.00
10	0.00	0.03		-0.03	0.00	0.00	0.00	0.00	2.23	0.00
8	0.00	0.00		0.00	0.00	0.00	0.13	0.00	0.10	
8 - Alt	0.00	0.00		0.00	0.00	0.00	0.19	0.00		0.67
7		-0.09		0.00	-0.06	0.33	0.13	0.00	0.10	
7 - Alt	0.41			0.00	0.33	0.88	0.19	0.00		0.67
7 - η	0.41			0.00	0.33	0.88	0.13	0.00	0.10	
7 - W_c		-0.09		0.00	-0.05	0.33	0.18	0.00		0.66
6		-0.17			-0.06	0.33	0.13	0.00	-0.07	
6 - Alt	0.02				0.13	0.47	0.28	0.00		0.36
6 - W_c		-0.17			-0.05	0.33	0.28	0.00		0.36
6 - No WF		-0.17			-0.04	1.15	0.30	0.35	1.10	

present are analysed, to investigate if the chosen parameter set is capable of detecting the deterioration accurately. The simulated deterioration cases are found in Table 9.3.

The results of this analysis are show in Fig. 9.1. In the figure the simulated values are shown, together with the deterioration as estimated by the AM component using different parameter sets. It shows that the baseline parameter set is capable of detecting all the simulated deterioration cases with good accuracy. Although small errors show, the main trend is visible, which is what is most important in the MRO environment.

The removal of the PS49 measurement, going to the 8 variable case, removes the ability of the AM component to detect LPT faults, instead attributing these to a reduction in HPT efficiency. Possibly due to a less constrained measurement set. This allows for more freedom in adapting the component map of the HPT, without affecting the measurements behind it. It is likely that the TT49 measurement is more sensitive to HPT efficiency adaptions than to LPT adaptions. Due to this the AM procedure adapts the HPT efficiency rather than the LPT condition. If PS25 is included in the analysis this does not happen as changing the HPT efficiency has a different effect on the pressure than changing the LPT condition. Smearing the LPT deterioration onto the HPT efficiency also appears when multiple components are deteriorated including the LPT.

Further removing PS25 and FN slightly increases the differences between the estimation by the AM component and the actual applied deterioration. No large differences are introduced. The alternative 6 parameter set shows large errors as soon as deterioration is present on the LPC, making it unusable. This might be due to not including the root cause of the performance deviations.

9.4. Conclusions for the GEnx-1B

As mentioned before, the GEnx-1B is comparable to the 7 variable case when tested in the test cell and the 6 parameter variable set when located on-wing. Provided that an model of similar accuracy is available for the GEnx-1B, conclusions can be drawn based upon the results from the previous section.

It can be concluded that the AM results for the GEnx-1B will be less accurate than those for the CF6-80. The overall trend, indicating which components are deteriorated, is still visible. This is deemed more important than indicating the exact percentage with which a component is deteriorated, as it is more important to apply corrective action to the correct component. This is the case for both test cell results and on-wing measurements.

Furthermore it must be concluded that the AM component will not be able to properly indicate LPT deterioration on the GEnx-1B, instead indicating a reduction in HPT efficiency. This will reduce the usability of the model. Fortunately consultation with KLM engineers revealed that, based on experience, the LPT is not as sensitive to deterioration as other components. Possibly because the component is shielded from the environment by the preceding components. This is backed by the Workscope Planning Guide (WPG) provided by GE for the GEnx-1B, which states that the LPT only needs to be overhauled every three shopvisits, approximately once every 15 years [12]. For the other components

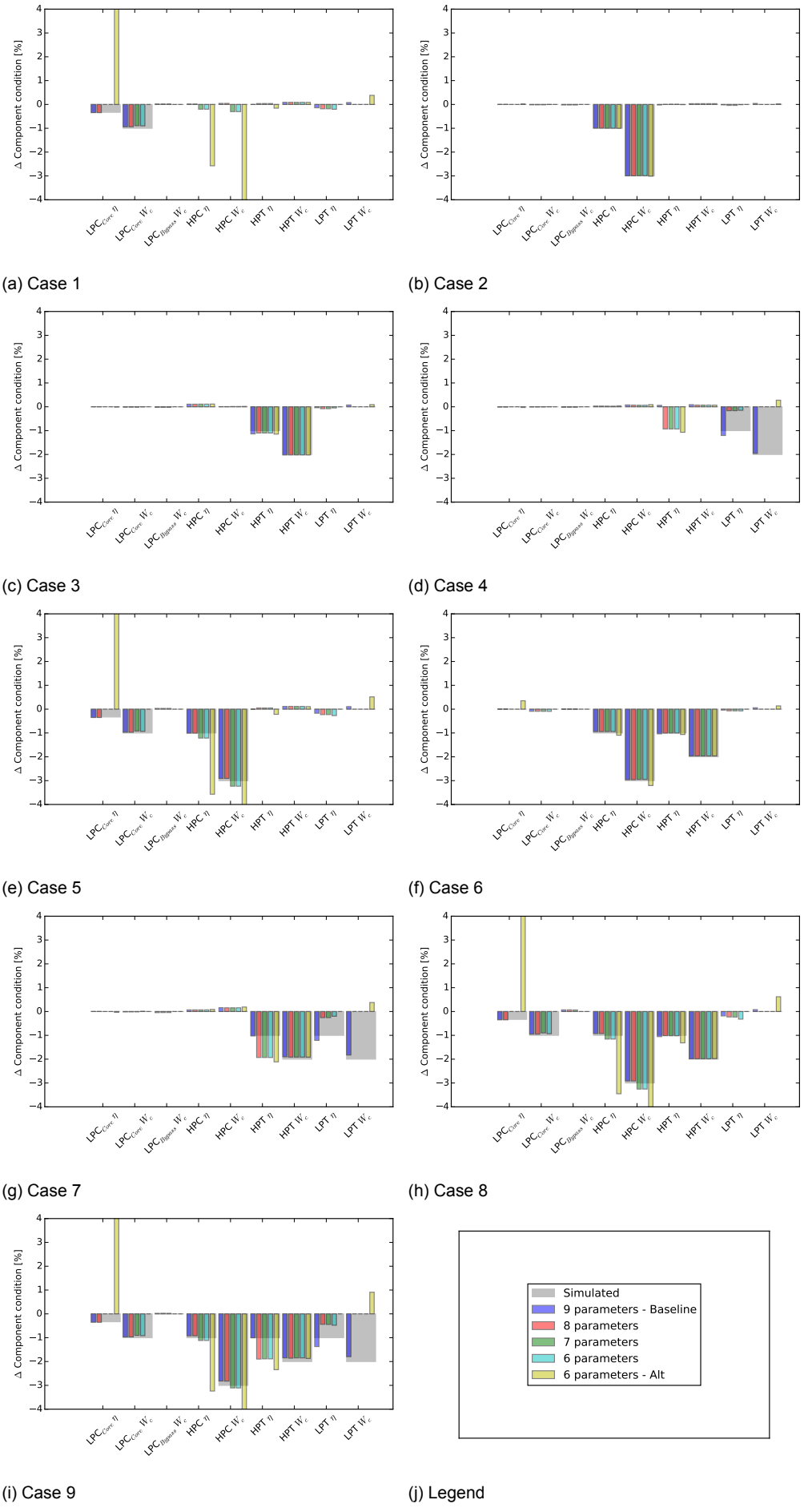

(a) Case 1 (b) Case 2

(c) Case 3 (d) Case 4

(e) Case 5 (f) Case 6

(g) Case 7 (h) Case 8

(i) Case 9 (j) Legend

Figure 9.1: Analysis of an engine with different types of simulated deterioration (cases from Table 9.3) using different parameter sets

this frequency is higher. Experience on older engines showed that the overhaul after such a long time was mainly for mechanical defects not influencing the performance of the LPT. From this it is concluded that even though the LPT cannot be analysed it is still of interest to apply the AM component to the GEnx-1B. However it must be understood that HPT and LPT results are less reliable.

10

Sensitivity analysis

The GEnx-1B GSP model has been finished with the end of Part II and in Chapter 9 it is confirmed that the AM component can work with the GEnx-1B model. In this chapter a preliminary analysis is performed, investigating the sensitivity of the analysis to perturbations in the input data. The rationale for doing so is explained first, followed by the methodology and results.

10.1. Rationale

Adaptive Modelling is a form of deterministic GPA, as mentioned before in Chapter 4. A specific input condition given to the model gives a single outcome, which is the same each time that the analysis is performed. Due to this measurement error will directly influence the outcome of the AM analysis [17].

Sensor measurements are influenced by noise and bias. Bias is the average deviation of a sensor measurement from the true value. Noise is random scatter of each individual measurement point around the average value. Noise can be described using an appropriate Probability Density Function (PDF) [17, 18]. This is shown visually in Fig. 10.1. Different filtering techniques have been developed to cope with measurement uncertainties in applying GPA [17], however these will not be elaborated upon in this thesis.

If a differential GPA model has been created using data from a specific sensor set and the measured data which is used to perform the analysis is taken with the same sensor set, bias does not have to be taken into account [5]. When comparing different engines with each other this is only the case if the sensor bias on both engines is equal. As the same sensor types are used on all GEnx-1B engines, it is expected that the influence of sensor bias is small.

In this chapter the effect of measurement noise on the computed condition deviations will be investigated. This will give an indication of how much the analysis outcome is affected by sensor noise.

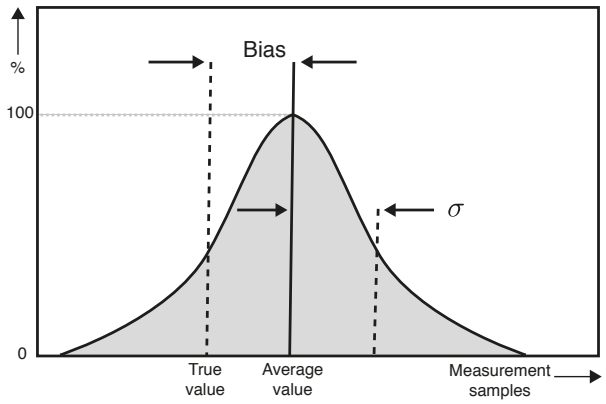

Figure 10.1: Noise and bias [18][Redrawn]

10.2. Methodology

Each sensor in either the test cell or on the engine itself is influenced by its own amount of measurement noise. The amount of noise present in an individual measurement is unknown. However, for each used sensor a known accuracy range is available. Sensor accuracies are given in Table 10.1. It is assumed that the sensor noise can be described by a normal probability distribution. Furthermore it is assumed that the accuracy values from Table 10.1 are 2σ, two times the standard deviation of the probability distribution. The quoted accuracies are therefore approximately the 95.5% confidence intervals, meaning that 95.5% of the measurements made are influenced by noise not larger than the given value [4].

Table 10.1: Sensor accuracies for the GEnx-1B and test cell [11, 13]

Parameter	Accuracy
TT2	$\pm$ 0.5°C
PT2	$\pm$ 0.1% of reading
RHUM	$\pm$ 3%
TT25	$\pm$ 0.13°C
TT3, TT49	Greater of $\pm$ 1.1°C or $\pm$ 0.4% of reading
PS3	Greater of $\pm$ 0.0344 bar or $\pm$ 0.75% of reading
FN	$\pm$ 0.2% of reading
WF	$\pm$ 0.3% of reading
N1, N2	$\pm$ 7.2 rpm

The GSP AM component relies on the data of multiple sensors when estimating an engine its condition, all influenced by the sensor accuracies from Table 10.1. The objective of this sensitivity analysis is to find a confidence interval between which the estimated condition deviations lie, influenced by the random errors introduced by noise affecting all sensors. This is done by means of a Monte Carlo simulation.

During a Monte Carlo simulation a process which is influenced by multiple stochastic processes with known probability distributions is simulated multiple times in order to obtain statistical information about the outcome of the process. The process in this case is the computation of an engine its condition using the AM component. The influencing stochastic process is the noise influencing the individual sensors. By simulating this process multiple times a probability density function is obtained for the outcome of the simulated process under influence of chance. The simulation itself is performed with GSP, perturbations to the sensor set have been applied using a Python script.

The simulation is performed with test cell data of the reference engine. It is expected that the mean of the obtained PDFs lie around zero, which is the true value.

10.3. Results

2500 trials have been analysed using AM. The number of trials is considered to be adequate, as the mean and standard deviation of the outcomes have converged [34]. In Fig. 10.2 the behaviour of the computed HPT efficiency deviation is shown, which was the slowest to converge. After approximately 1000 trials both the mean and standard deviation have converged.

The mean and standard deviations for all components are located in Table 10.2. In Fig. 10.3 the normal probability density functions corresponding to Table 10.2 are plotted, combined with a weighted histogram of the computed results.

The mean computed deterioration based on the 2500 trials is near zero for all components. This corresponds well with the actual deterioration, which is zero as the perturbations have been added to the reference dataset. The small deviations are contributed to the randomness of the simulation.

Whereas the mean of the deterioration is almost equal for all components, the standard deviation is not. The standard deviation is an indication of sensitivity of the condition deviation to random perturbations. The higher the standard deviation is, the more sensitive a specific condition deviation is to uncertainties.

The LPC mass flow deviations for both the core and bypass are found to be the least sensitive to measurement noise, followed by the LPT efficiency deviation. The mass flow and efficiency deviations

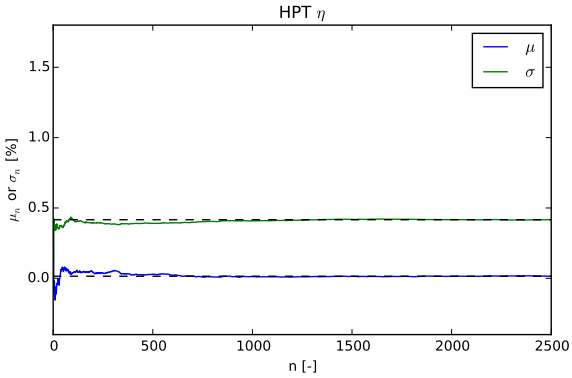

Figure 10.2: Behaviour of the sample mean and standard deviation of the computed HPC mass flow deterioration in relation to the number of trials in the Monte Carlo simulation

Table 10.2: Computed mean and standard deviations for each condition deviation as computed by GSP, obtained using the Monte Carlo simulation using 2500 trials. The perturbed data set is the TO test cell measurement for the reference engine

Condition deviation	Mean μ [%]	Standard deviation σ [%]
LPC Core W_c	0.0048	0.0708
LPC Bypass W_c	0.0083	0.0996
HPC W_c	0.0116	0.5338
HPC η	0.0144	0.4254
HPT W_c	0.0054	0.5190
HPT η	0.0152	0.4167
LPT η	0.0076	0.2680

for the HPC and HPT are slightly more sensitive to measurement noise, with a standard deviation of about 0.50%. This value is about as high as for the most sensitive parameter found by Verbist for the CF6 (LPC core efficiency) [34, 36]. This increased sensitivity was contributed to a lack of measurements taken in the engine, due to which the numerical procedure could not estimate the component condition with equal accuracy as for other components. This is also highly likely on the GEnx-1B.

The greater sensitivity found for the N2 system is likely due to the missing PS25 and PS49 measurements, due to which the inlet and outlet conditions of the N2 system are not fully defined. Measurement noise seems to have a much smaller effect on the computed LPC conditions. As the component is not adapted much, the noise introduced in the ambient conditions might directly influence the inlet conditions for the HPC, further increasing its sensitivity to measurement error. This is not corrected for using a PS25 measurement. Furthermore the HPT outlet pressure, PS49, is not measured. Due to this the state of the N2 shaft is not fully defined which leads to an increased number of possibilities for the AM component.

In Fig. 10.3 the results from the Monte Carlo simulation have been plotted against their assumed normal PDFs. Overall the computed deviations follow the normal PDFs well, as is expected normal input data was used. Some condition deviations, such as the HPT mass flow in Fig. 10.3e, show larger peaks near the mean than would be expected considering the normal PDF. An explanation might be that the total performance deviation, including the random perturbations, falls within the 0.1% interval allowed by GSP. When this is the case no deteriorations are computed.

The histograms for the HPT and LPT efficiency deviations (Figs. 10.3f and 10.3g) are slightly skewed towards values with a larger condition deviation. In Chapter 9 it was already established that correctly estimating the conditions of the GEnx-1B LPT would not be possible, due to a missing PS49 measurement. It is expected that this also influences the results in Fig. 10.3.

10.3.1. Results at MC power settings

Previous results have been gathered by adding measurement noise to the TO measurement set from the test cell for the reference engine. To investigate if the computed sensitivities are dependent on the

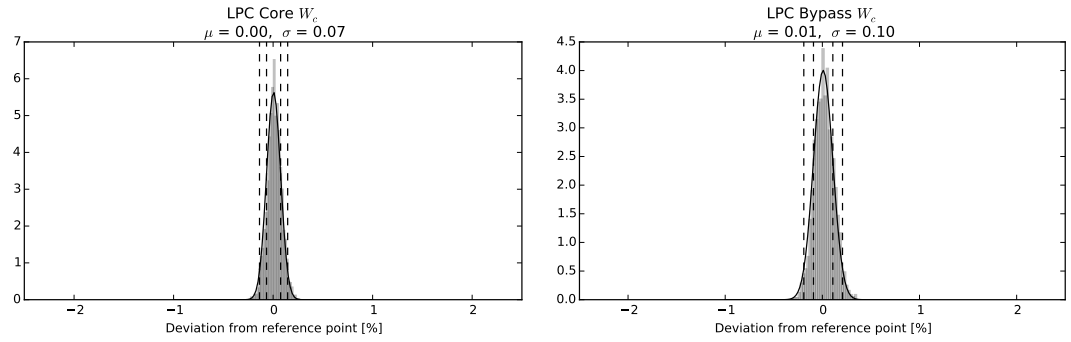

(a) LPC Core W_c

(b) LPC Bypass W_c

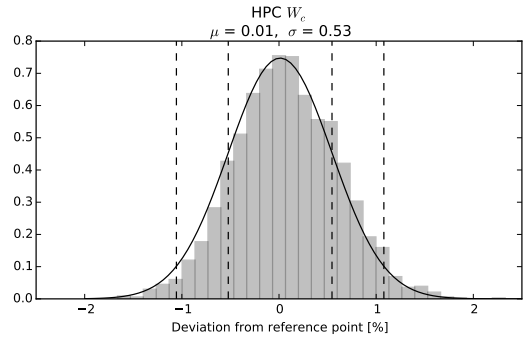

(c) HPC W_c

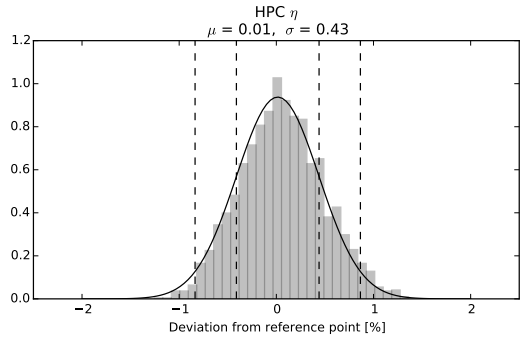

(d) HPC η

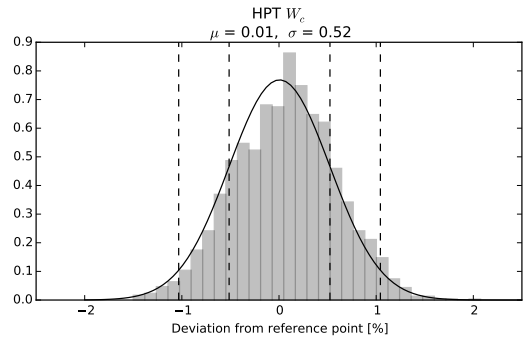

(e) HPT W_c

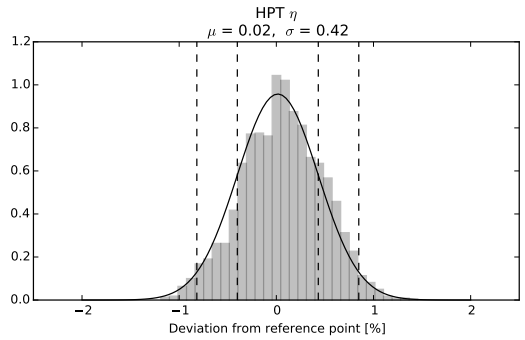

(f) HPT η

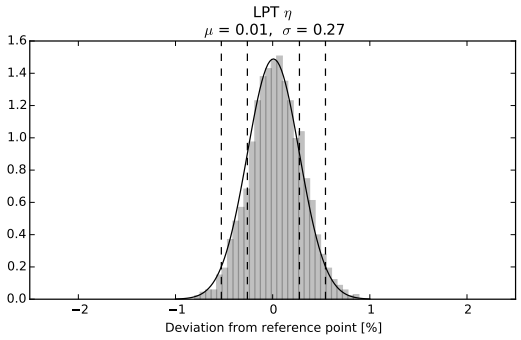

(g) LPT η

Figure 10.3: Probability density functions for each condition deviation obtained using a Monte Carlo simulation with 2500 trials. The bars show the distribution of the computed results, the continuous lines the probability density function of the related normal distribution and the dashed lines indicate -2, 1, 1 and 2 σ from the mean μ. Reference data set is the TO test cell measurement for the reference engine.

power setting investigated the same procedure has been repeated, this time adding the measurement noise to the MC measurement of the reference engine, again taken in the test cell. The results are shown in Table 10.3.

Table 10.3: Computed mean and standard deviations for each condition deviation as computed by GSP, obtained using the Monte Carlo simulation using 2500 trials. Perturbed data set is the MC test cell measurement for the reference engine

Condition deviation	Mean μ [%]	Standard deviation σ [%]
LPC Core W_c	0.0480	0.0861
LPC Bypass W_c	0.0365	0.1546
HPC W_c	0.0248	0.5189
HPC η	-0.0074	0.4238
HPT W_c	-0.0418	0.5081
HPT η	-0.0926	0.4169
LPT η	0.0254	0.2864

Comparing Table 10.3 and Table 10.2 it is found that the standard deviations do not differ much. This indicates that the sensitivity to uncertainty of the analysis does not change depending on the power setting, and thus on the region of the component map investigated.

The MC means lie slightly further away from zero than those obtained for the TO analysis. An explanation for this deviation can be found in the way GSP works. As stated before the AM component with the settings used does not try to match performance deviations below 0.1%. Due to the added measurement noise the performance deviations become larger than 0.1%, causing the AM component to start adapting components. It is likely that for small performance deviations above 0.1% larger condition deviations are computed, causing the mean to shift. From this it can be concluded that the component maps are not fully accurate near the MC point. Deviations however are small and will likely not influence the use of the model, as it is expected that differences due to deterioration are larger than the perturbation introduced here.

10.4. Conclusions for the GEnx-1B

In Chapter 8 it was already suspected that the HPC results would be the most sensitive to uncertainties, as these results showed the most scatter. Using the Monte Carlo simulation this has been confirmed., with thee HPT showing similar behaviour. The sensitivities of the HPC and HPT are about equal to the most sensitive component in the research of Verbist [34], likely due to fewer measurements available before and after the components.

From the sensitivity analysis above it is found that around 95.5% of the measurements affected by uncertainties due to sensor inaccuracies lie within $\pm$ 1% of the actual value (2σ). As the AM analysis at KLM ES will mainly be used as an indicator on which component is deteriorated, rather than the amount of deterioration present on the component, this accuracy is deemed enough.

Used snapshots from both the test cell and taken on-wing average sensor readings over a period of time. This lowers the influence of measurement noise. In the KLM test cell at Schiphol measurements are taken for 10 seconds after which all values which lie beyond 3σ are discarded. The average of the remaining values is taken as the final measurement. Sensor frequency differs per sensor, but averages around 10Hz. Averaging of 100 values (10Hz for 10s) for each measurement using the same accuracies as before (Table 10.1) and using this data as input for the Monte Carlo simulation showed that with 2500 trials almost all points showed zero deterioration, the actual case. Unfortunately it is not known if the given accuracies take averaging into account. When averaging only 10 values, so 1 Hz for 10 seconds, a similar response is seen.

From the above analysis it is concluded that the accuracy of a single snapshot used in the AM component is high enough, even more so if averaging is applied. Especially if on-wing measurements are to be used, which are influenced by many other factors increasing the uncertainty of the measurement Chapter 12. The differences in sensitivity between the different components is important to know, such that the results can be interpreted better.

11

Applying AM to simulated deterioration data

In Chapter 10 the GSP AM component has been applied to the GEnx-1B model for the first time. The Monte Carlo analysis was not performed to find deteriorated components, or to assess the ability of the model to find deterioration. This will be investigated in this chapter, using simulated deterioration. The methodology is detailed first, followed by the obtained results.

11.1. Methodology

The objective of the analysis in this chapter is to find the usability of the GSP AM component in combination with the GEnx-1B model. For maximum usability the AM component needs to be able to correctly identify deteriorated components and the amount of deterioration using both test cell and on-wing measurements. Determining the precise amount of deterioration is less important than correctly identifying the deteriorated component, as corrective action will have to be taken nonetheless. False positives, identifying deterioration when there is none, are detrimental to the usability of the model. A false positive when acted upon will lead to additional maintenance costs, rather than the prevention of such costs.

Currently only test cell results are analysed using AM at KLM ES, and only if during the outbound test run an engine does not meet its specified performance. The AM analysis is then used to investigate the engine performance and aid in determining the additional or corrective maintenance steps to be taken. In this case it is important not to show false positives, to avoid unnecessary work. Furthermore the use of test cell measurements is the most important. On-wing measurements and the analysis of engines while still on wing is not done yet, this will be investigated during this thesis.

Although KLM has a whole fleet of Boeing 787s with GEnx-1B engines in operation, each with its own amount of component deterioration, data from these engines cannot be investigated if it is unknown if the AM analysis will be able to correctly identify component deterioration. To overcome this knowledge gap the workings of the model will first be verified using simulated deterioration data.

In GSP deterioration can be added as an off-design condition to each component, changing the model its corrected mass flow, efficiency and pressure ratio [38]. In this case only mass flow and efficiency deterioration has been added. The simulated deteriorations are added to the design point model, which is then simulated using GSP. Next the corresponding measurements are recorded in a file that can be read by the GSP AM component. These files are subsequently analysed. This is the same procedure as followed in Chapter 9.

All defined cases will be analysed twice. Once using the measurement set as available from the test cell, thus including FN. All cases will also be analysed without FN present in the measurement set, simulating on-wing conditions.

11.1.1. Case definitions

Using GSP deteriorations to the mass flow and efficiency have been added to the LPC core, LPC bypass, HPC, HPT and LPT. Investigating all possible (1024) combinations will not be done. Especially

Table 11.1: Simulated deterioration cases GEnx-1B

		LPC Core		LPC Bypass		HPC		HPT		LPT	
	Case	$\Delta\eta$	Δ W$_c$	$\Delta\eta$	Δ W$_c$	$\Delta\eta$	Δ W$_c$	$\Delta\eta$	Δ W$_c$	$\Delta\eta$	Δ W$_c$
I. Basics	1	-0.33%	-1%								
	2			-1%	-3%						
	3					-1%	-3%				
	4							-1%	-2%		
	5							-1%	2%		
	6									-1%	-2%
	7									-1%	2%
II. Core-	8	-0.33%	-1%			-1%	-3%				
	9							-1%	-2%	-1%	-2%
	10	-0.33%	-1%							-1%	-2%
	11					-1%	-3%	-1%	-2%		
	12	-0.33%	-1%			-1%	-3%	-1%	-2%		
	13	-0.33%	-1%			-1%	-3%	-1%	-2%	-1%	-2%
III. Core+	14							-1%	2%	-1%	2%
	15	-0.33%	-1%							-1%	2%
	16					-1%	-3%	-1%	2%		
	17	-0.33%	-1%			-1%	-3%	-1%	2%		
	18	-0.33%	-1%			-1%	-3%	-1%	2%	-1%	2%
IV. Full-	19	-0.33%	-1%	-1%	-3%	-1%	-3%				
	20			-1%	-3%			-1%	-2%	-1%	-2%
	21	-0.33%	-1%	-1%	-3%					-1%	-2%
	22			-1%	-3%	-1%	-3%	-1%	-2%		
	23	-0.33%	-1%	-1%	-3%	-1%	-3%	-1%	-2%		
	24	-0.33%	-1%	-1%	-3%	-1%	-3%	-1%	-2%	-1%	-2%
V. Full+	25			-1%	-3%			-1%	2%	-1%	2%
	26	-0.33%	-1%	-1%	-3%					-1%	2%
	27			-1%	-3%	-1%	-3%	-1%	2%		
	28	-0.33%	-1%	-1%	-3%	-1%	-3%	-1%	2%		
	29	-0.33%	-1%	-1%	-3%	-1%	-3%	-1%	2%	-1%	2%

considering that each combination can be investigated with a near endless number of deterioration values. To keep the research manageable assumptions have been made on the deterioration encountered in operation, using which different cases have been identified. These assumptions and cases will be described in this section.

From the information gathered on deterioration in Chapter 3, summarised in Table 3.1 on Page 11, it is found that component deterioration affects both corrected mass flow capacity and efficiency. Using this information it has been assumed that component deterioration always involves a change in both mass flow capacity and efficiency, greatly reducing the amount of combinations possible. The amount of deterioration has been determined using Table 3.1. Finally it has been assumed that all performance deviations are due to deterioration in the components as mentioned above, no deterioration in for example the combustion chamber is assumed.

With the assumptions above taken in mind 29 different cases have been defined. The different cases have been divided into five categories as shown in Table 11.1. The first category ‘I. Basics’ contains seven cases, which have the purpose of investigating the ability of the model to detect the different types of deterioration. Note that for the turbines both an increase and decrease in mass flow capacity is simulated. The next two categories ‘II. Core-’ and ‘III. Core+’ investigate the ability of the model to analyse the core engine, not taking the fan duct into account. The first one assumes a decrease in turbine mass flow capacity, the second an increase. Both turbines have been adapted in the same way. The cases within the categories simulate the following types of deterioration: only the cold section is

affected, only the hot section is affected, the N1 system is affected, the N2 system, a combination of all parameters except for the LPT and all parameters. The final two categories of deterioration are the same as the previous two, however taking a deteriorated bypass section of the LPC into account.

11.2. Results

Results of the analysis with simulated deterioration are located in Figs. 11.1, 11.2 and B.1 to B.3. In the figures the simulated amount of deterioration is plotted, as well as the amount of deterioration computed by the AM component for both measurement sets. When analysing the results it must be kept in mind that not all component conditions are adapted by the AM component, only those as used in Chapter 10, which correspond to parameter set 6 or 7 in Chapter 9, specifically Table 9.2 on Page 47.

11.2.1. Results category ‘I. Basics’

Starting with Fig. 11.1 the results of simulating the ‘I. Basic’ cases from Table 11.1 are investigated. Starting with case 1 in Fig. 11.1a, the mass flow deviation is found by the AM component for both the test cell and on-wing case. The deterioration is slightly underestimated, which will not hamper the usability of the model. The LPC core efficiency is not included in the parameter set which can be adapted by the AM component. Due to this other components are adapted to match the performance parameters. This leads to a small amount of deterioration on the HPC. It is expected that this will not influence the model its usability.

Results for the deterioration of the bypass, Fig. 11.1b, show very different results for the different parameter sets. Including the thrust (FN) as available in the test cell shows good agreement between the deterioration as computed by the AM component and the deterioration applied. The efficiency reduction in the bypass is contributed to an efficiency reduction of the LPT. This is according to expectation as the LPT has to generate the energy for the fan, since they are located on the same shaft. The fan efficiency reduction however is not in the parameter set adapted by the AM component, thus the energy loss is placed somewhere else. Using the on-wing measurement set the deterioration is not detected, as it is not included in the parameter set. The thrust measurement is also not included, which leads to erratic behaviour of the AM component, contributing the performance losses to the other components on the N1 shaft. It is likely that if the fan is deteriorated it is necessary to use a thrust measurement to find the correct amount of deterioration on the other components as well. This will be investigated in the categories ‘IV. Full-’ and ‘V. Full+’.

The figures corresponding to the N2 system, Figs. 11.1c to 11.1e, show that the AM component can detect the simulated deteriorations with high accuracy, both for an increase and decrease in HPT mass flow capacity.

Finally the results for the LPT deterioration are shown in Figs. 11.1f and 11.1g. If the LPT mass flow capacity decreases the performance deviations are contributed to the HPT. If the mass flow decreases the deviation in LPT efficiency is found, albeit twice as much. From Chapter 9 it was already expected that the LPT results would not be reliable, due to the missing PS49 measurement.

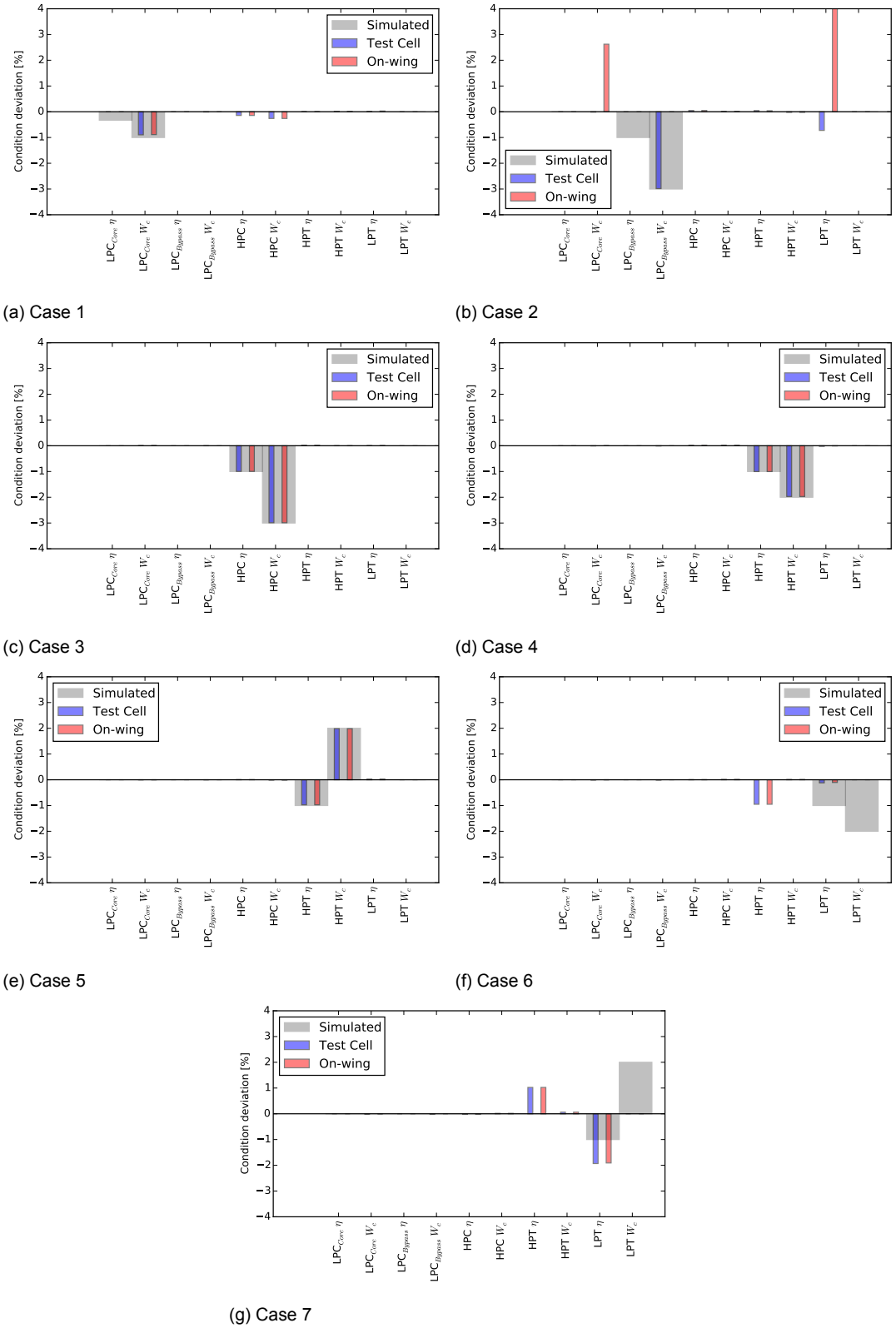

(a) Case 1

(b) Case 2

(c) Case 3

(d) Case 4

(e) Case 5

(f) Case 6

(g) Case 7

Figure 11.1: Analysis of an engine with different types of simulated deterioration ('I. Basics' cases from Table 11.1) for either test cell or on-wing measurements

11.2.2. Results for the other categories

In Fig. 11.2 the results for the second category are shown, in which different combinations of deteriorated components are investigated. In this category the bypass is assumed to be healthy and turbine deterioration to have caused a decrease in mass flow capacity.

First considering deterioration to the cold section, Fig. 11.2a. As expected from the results of case 1 and 3 (Figs. 11.1a and 11.1c) the simulated deterioration is found on both components. The HPC deterioration is slightly overestimated, likely due to the effects as seen above in case 1.

Closer inspection shows that the results of case 8 match the addition of case 1 and 3. Further inspection of the cases in Fig. 11.2 shows that the results can be predicted accurately by addition of the basic components from category 'I. Basics' of which the different cases are composed. This is also the case for the other categories. From this it can be concluded that using the results in Fig. 11.1 the results of all other cases can be predicted as well. Results for the other categories are located in Figs. B.1 to B.3 in Appendix B.

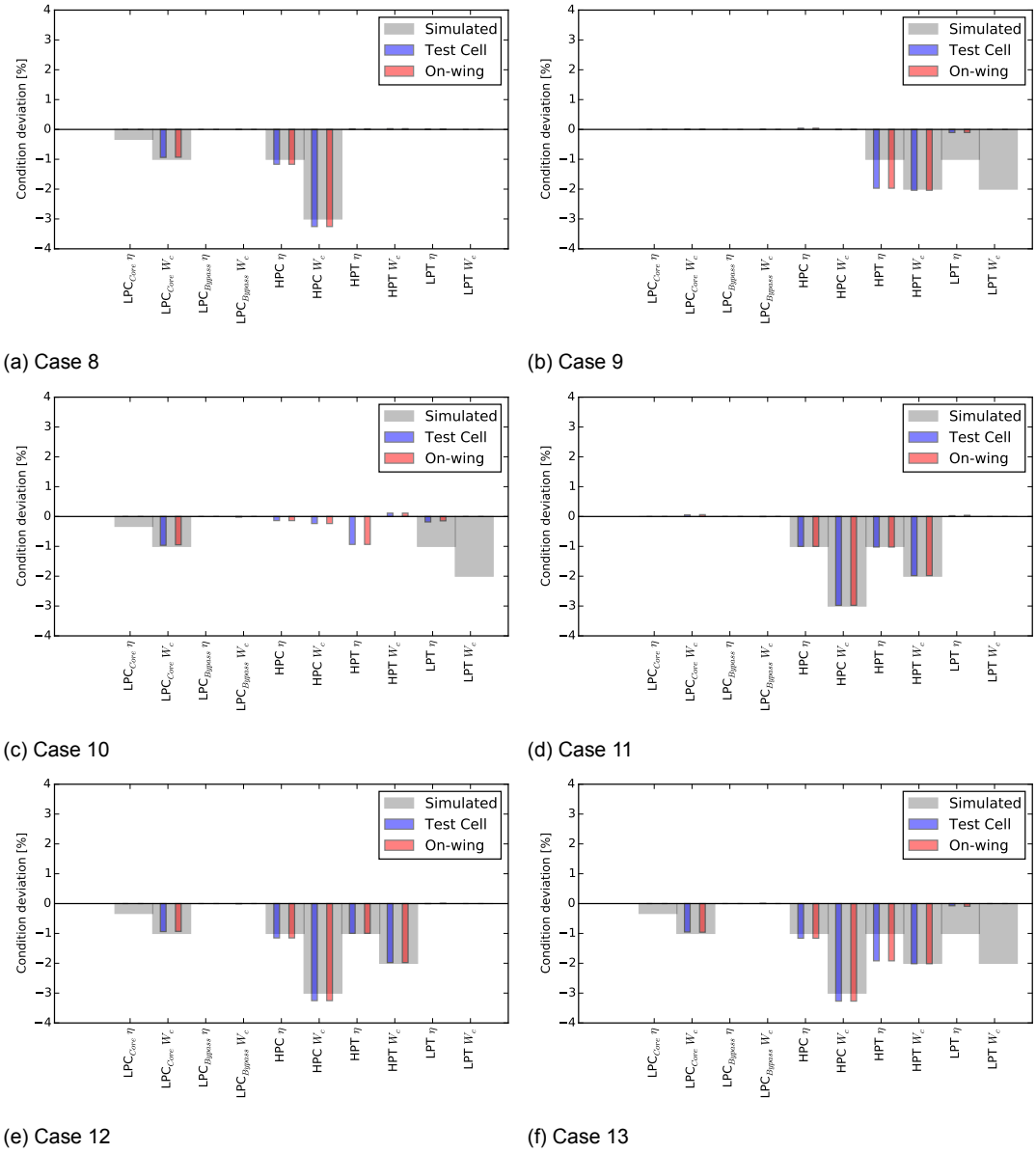

(a) Case 8

(b) Case 9

(c) Case 10

(d) Case 11

(e) Case 12

(f) Case 13

Figure 11.2: Analysis of an engine with different types of simulated deterioration ('II. Core-' cases from Table 11.1) for either test cell or on-wing measurements

11.3. Conclusions for the GEnx-1B

Based on the results gathered in Section 11.2 some conclusions can be drawn on the application of GPA to the GEnx-1B. As was already suspected in Chapter 9, results for the LPT will be unreliable. If deterioration is present on the LPT, the reduction in performance will be contributed to the HPT and partially to the LPT, depending on the change in LPT mass flow capacity. Due to this LPT deterioration will influence the results of the AM analysis, which could lead to erronous results. However as was already stated in Chapter 9, the LPT is not so sensitive to deterioration, confirmed by both KLM engineers and the GE WPG [12].

From Fig. 11.1c it must be concluded that detecting deterioration of the LPC bypass, the fan on the actual engine, will not be possible using on-wing data. Instead erroneous results for the booster and LPT will be found. Fortunately performance deterioration of the fan is rare. As for the LPT an overhaul level workscope is only needed once every three shopvisits, or around 15 years. Looking further into the details of this workscope as recommended by GE, only small repairs to the abradable surface around the fan are found. These repairs only have to take place ‘on condition’. No further work has to be done on the fan itself [12]. From this it is concluded that the fan is not sensitive to deterioration and can be assumed to be in good condition when installed on the engine. Due to this it will not be of influence on the use of the AM component with on-wing data.

12

Applying AM to real engine data

In Chapter 11 the AM functionality of GSP in combination with the GEnx-1B model has been tested using data containing simulated deterioration. This analysis led to a positive outlook on the use of AM when analysing GEnx-1B engine data. The next step is to investigate the analysis of real engine data, gathered in either the test cell or during operation. This investigation is the topic of this chapter. First analysis of test cell measurements is investigated, followed by the analysis of on-wing data.

12.1. Test cell measurements

Having completed a shopvisit, each engine is tested in the test cell. The GEnx-1B is tested in the AFI test cell at Paris CDG. Here the engine is run through a series of tests, to validate if the engine is working correctly and to measure the engine its performance. If the engine does not meet its specified performance, KLM would like to apply AM to investigate the engine in more detail. In order to do so correct analysis of test cell results is necessary, which is investigated in this section.

12.1.1. Objective and requirements

The objective of this research is to verify that the AM component, in combination with test cell measurements, works correctly. In Chapter 11 it has been verified, with simulated data, that using test cell snapshots it is possible to detect deterioration on all the engine components except for the LPT. Differences exist between simulated data and real engine data. Furthermore the use case in analysing real engine data is slightly different. The differences are detailed next.

Power setting

In Chapter 11 deterioration has been simulated on the reference engine at TO power setting as measured in the test cell. This exact point on which the design point model is based. Due to engine to engine differences the power setting of an engine other than the reference engine is likely to be different, even when tested at TO settings. This should not hamper the model its ability in determining the deterioration of the engine. The model has also been tuned for correct analysis of an engine at the MC power setting, as described in Chapter 8. This power setting should also be correctly analysed by the AM component. Both these differences will be tested in this chapter.

Reference engine selection

The reference case to which the analysed engine is compared has thus far been the design point measurement. The reference engine has a direct influence on the results of the AM analysis, as the results are reported as differences in performance between the analysed and reference engine. In an operational setting it might be of interest to analyse an engine in comparison to a different engine than the one the model has been based on. For example one might be interested in the change in condition between an inbound and outbound test, to get a grip on the effect of a specific shop visit. To quickly make this analysis it is easier to use one of the two tests as the reference case. The reported results by the AM component would then immediately be of interest with no additional analysis needed.

Despite the influences above the model is required to perform consistently. No differences should occur due to analysis at different power settings, as deterioration is assumed to be a unaffected by power setting. Furthermore, differences between engines should remain equal when different reference data sets are used. If the results are not constant this is likely due to tuning errors in the component maps. It is expected that slight differences will appear between the different analyses. Although it has been tried in Chapter 8 to model the engine such that no differences occur between the power settings as analysed in the test cell, this has only been done for the reference engine. It is expected that due to engine to engine differences some engines will run a bit faster or slower in the test cell. It is expected that due to this small differences can occur, as was also seen for the on-wing analysis in Chapter 8.

12.1.2. Data acquisition

All available test cell measurements for the GEnx-1B since the test cell has officially been correlated have been used for the analysis. These engines are the same as used for the reference engine selection in Chapter 6, located in Table 6.3. The tested engines are repeated in Table 12.1 with their date of testing and EGTSDM for further referencing.

Table 12.1: Engines available for the analysis of test cell results

ESN	Test date	EGTSDM [°C]
95xxx1	26-06-2017	18.413
95xxx2	22-08-2017	28.353
95xxx3 [reference]	14-09-2017	29.937
95xxx4	23-09-2017	28.600
95xxx5	29-11-2017	16.810

12.1.3. Results

The engines in Table 12.1 have been analysed using AM at different power settings and using different reference engines. First the differences between different power settings are analysed, followed by the same analysis using different reference engines.

Power setting

All engines have been analysed using AM, using the 95xxx3 as the reference engine. Results are shown in Table 12.2. In this table the difference in component condition between the analysed engine and the reference engine is shown. This analysis has been performed twice for each engine, once at TO settings and once at MC. The difference between the analyses at different power settings is also shown. As the model is based on the 95xxx3 all Calibration Factors (CFs) were unity.

As stated above the results of the analysis should be equal, independent of power setting. A quick look at Table 12.2 shows that this is not the case. Results for the LPC core are rather constant, showing little deviation between the power settings. Same goes for the HPT mass flow deviation. All other components show a larger deviation, the largest one being the HPC mass flow deviation.

In Fig. 12.1 the results from Table 12.2 are plotted per engine. As stated before in the MRO environment it is more important to correctly identify the deteriorated component than it is to identify the amount with which the component is deteriorated [34]. From Fig. 12.1 it is clear that the overall image of the condition of the engine is equal, independent of which power setting is analysed. Small variations in component condition will not greatly influence the decision process of the KLM ES engineer. From this it is concluded that the results are useable, even with the found differences in place.

Differences can be contributed to two separate factors. The first factor are small modelling errors present in the component maps, due to which deterioration is dependent on power setting, as was already discovered in Chapter 8. A second possible explanation is the way in which GSP adapts the maps, using Map Modifiers (MM) as explained in Chapter 4. A single map modifier is computed for the complete map, depending on the amount with which the map has to be adapted in the analysed point. It is possible that the deterioration is slightly dependent on the region of the map analysed, for example due to moving variable geometry. This would then lead to different results for the two power settings analysed. Likely a combination of the two factors is present in the results, with the largest contributor being the modelling errors.

Table 12.2: AM results for different engines, tested in the test cell at TO and MC. Reference engine: 95xxx3 TO (Reference engine)

	LPC		HPC		HPT		LPT
	ΔW_c C	ΔW_c B	$\Delta\eta$	ΔW_c	η	W_c	η
95xxx2 @TO	-0.47	0.30	0.47	-0.57	0.42	-0.35	0.16
95xxx2 @MC	-0.52	0.02	0.67	-1.21	0.54	-0.41	-0.07
Δ TO - MC	0.04	0.29	-0.19	0.64	-0.12	0.05	0.23
95xxx5 @TO	0.03	0.40	-1.33	-2.26	-0.21	-0.02	-0.05
95xxx5 @MC	-0.07	0.26	-1.28	-2.51	0.44	-0.01	-0.16
Δ TO - MC	0.10	0.14	-0.05	0.26	-0.64	-0.01	0.11
95xxx1 @TO	-0.19	0.60	-0.32	-0.35	-0.18	-0.95	0.92
95xxx1 @MC	-0.23	0.27	-0.02	-0.31	-0.09	-1.07	0.76
Δ TO - MC	0.03	0.33	-0.30	-0.03	-0.09	0.12	0.16
95xxx4 @TO	-0.77	-0.32	-1.04	-0.62	0.38	-0.04	-0.34
95xxx4 @MC	-0.92	-0.43	-0.58	-0.22	0.67	-0.07	-0.56
Δ TO - MC	0.14	0.11	-0.45	-0.39	-0.29	0.03	0.22

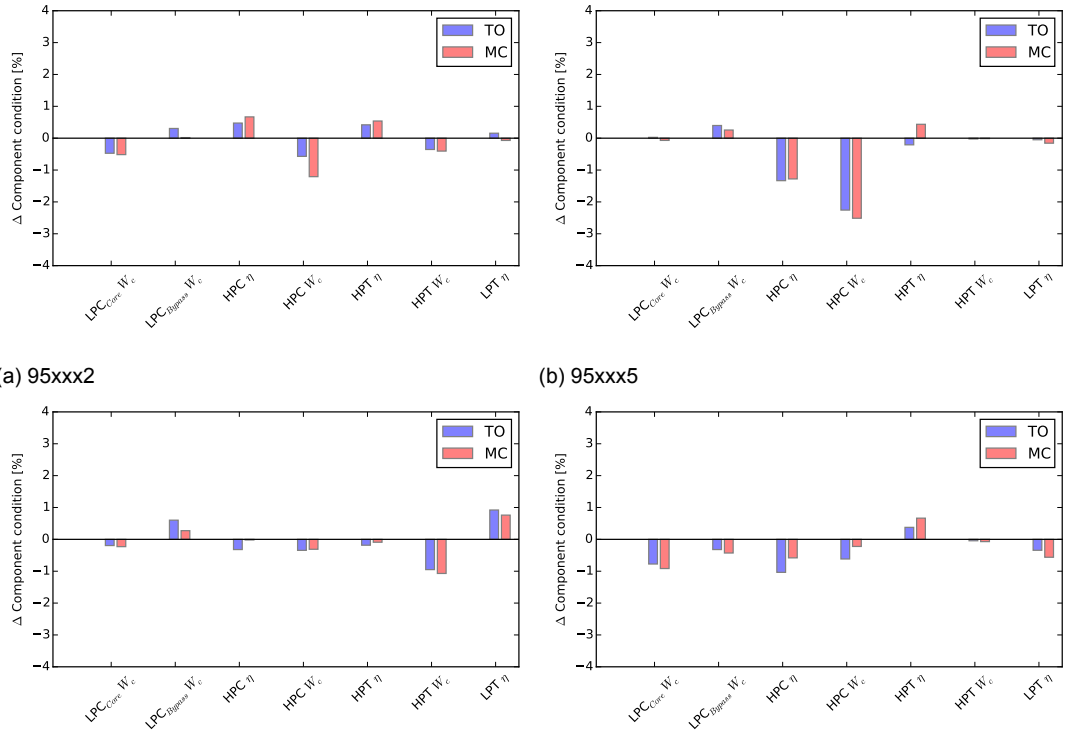

(a) 95xxx2

(b) 95xxx5

(c) 95xxx1

(d) 95xxx4

Figure 12.1: AM results for different engines, tested in the test cell at TO and MC. Reference engine: 95xxx3 TO (Reference engine). Results from Table 12.2

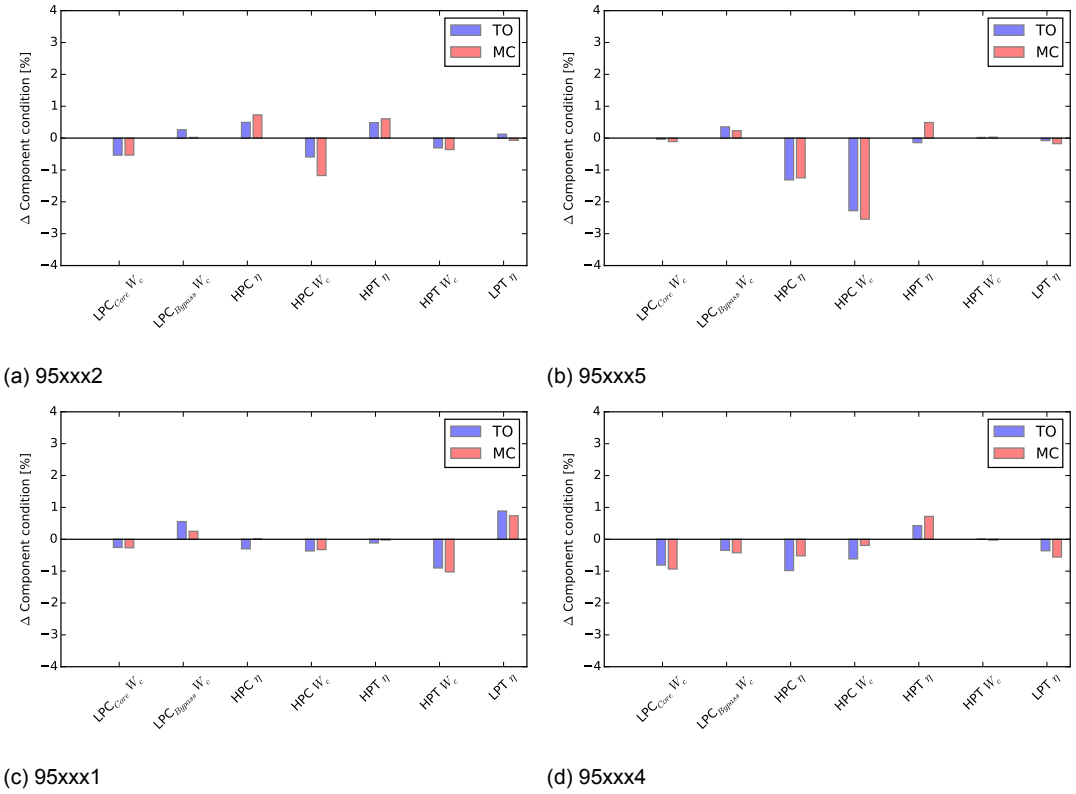

(a) 95xxx2

(b) 95xxx5

(c) 95xxx1

(d) 95xxx4

Figure 12.2: AM results for different engines, tested in the test cell at TO and MC. Reference engine: 95xxx3 MC (Reference engine)

Different reference engine

As stated above it might be useful to use a different engine as a reference for the analysis. In this case the model should still properly analyse the engine. This has been tested in two ways. First the reference engine is used at a different power setting. Next one of the other engines is used for the analysis.

In Fig. 12.2 the results of the AM analysis using the reference engine at MC power is shown. The exact same analysis as in Fig. 12.1 is made, but at a different power setting. Assuming that no deterioration is present on the reference engine (independent of power setting), the results in Figs. 12.1 and 12.2 should be equal. Comparing both figures it is found that this is true.

The similarity between Figs. 12.1 and 12.2 is as expected. The model has been tuned such that the reference engine (95xxx3) is simulated with great accuracy at both TO and MC power settings. Using the off-design calibration setting in GSP, it is found that the calibration factors are very close to unity when using the MC measurement set as reference data. Due to this the model using in the AM analysis is equal to the model used above, leading to similar results.

The analysis can also be done using a different reference engine. As AM is a form of differential GPA, this will lead to different results, as the difference between the measured engine and a reference is given as a result. Using one of the engines from the previous section to analyse the reference engine however would have to lead to the same albeit opposite result. From Fig. 12.1 it follows that the 95xxx5 in Fig. 12.1b has the clearest deterioration present. Using this engine as a reference engine, calibrating the model such that it represent this engine using the AM component and analysing the 95xxx3 gives the results as shown in Table 12.3.

The absolute difference between the deteriorations should be zero in Table 12.3. This is not the case. Differences are likely caused by small differences in the component maps at the analysed points. In Chapter 10 it was determined that the HPC and HPT are more sensitive to changes in their surroundings, likely they are also more sensitive to different operating points being analysed. Overall the same conclusions on the engine its condition would be drawn based on the results.

Table 12.3: AM results analysing two engines, using both as a reference engine. Engines: 95xxx3 and 95xxx5

	LPC		HPC		HPT		LPT
	ΔW_c C	ΔW_c B	$\Delta\eta$	ΔW_c	η	W_c	η
Ref 95xxx3	-0.07	0.26	-1.28	-2.51	0.44	-0.01	-0.16
Ref 95xxx5	0.05	-0.23	1.56	2.31	0.02	0.00	0.33
Absolute Δ	0.02	0.02	-0.28	0.20	0.41	0.01	-0.17

From this it is concluded that is is possible to use the build in function to calibrate the model to different engines. Some accuracy will however be lost, as the tuned maps when scaled do not fully represent the engine for which the calibration has taken place, as found in Table 12.3. This is likely due to errors in the tuned component maps, due to which the model reacts differently at different corrected spool speeds. It is likely that this also causes part of the differences found in Fig. 12.1. Further tuning of the maps however has not solved this issue.

12.1.4. Physical analysis

In Section 12.1.3 the results of the AM analysis have been investigated without taking the condition of the engine into account, it has only been analysed if the AM component works as expected. In this section the results from Table 12.2 and Fig. 12.1 will be investigated, to see if they can be related to knowledge about the anaylsed engine and its physical condition.

From Table 6.3 it follows that two engines (95xxx2 and 95xxx4) have a performance which is comparable to the reference engine (95xxx3). From Figs. 12.1a and 12.1d it is found that these engines do not show any significant component performance deviations in comparison to the reference engine. This is as expected, as the condition of the engines were highly similar, as shown in Table 6.3. Some components perform slightly better, some slightly worse, which balances out the performance.

The 95xxx5 has a 10°C lower EGTSDM than the reference engine. From this it can be deduced that the engine will have one or multiple components which perform worse than on the reference engine. In Fig. 12.1b it is clearly visible that the difference in performance with the reference engine is contributed to an HPC which performed worse by the AM component. Both the reference engine and the 95xxx5 had no work done on the HPC during their shopvisits. Engine to engine differences and/or differences in operational life can possibly explain the difference in HPC performance between the engines.

The other engine which had a reduced EGTSDM is the 95xxx1, the results of which are located in Fig. 12.1c. Unlike for ESN 95xxx5 no clear component condition deviations are visible, with the biggest deviations present on the HPT and LPT. A decreased mass flow capacity is computed for the HPT and an increased LPT efficiency. From the analysis in Chapter 11 it was however found that the LPT results were unreliable and were likely to interfere with differences in the HPT condition. Some more investigation into this engine is likely required.

Further investigation into the 95xxx1

Both the 95xxx5 and 95xxx1 belong to the same operator, are of approximately equal age and have had the same work done on the engine during its shopvisit at KLM. It is therefore expected that there must be some similarity between the conditions of both engines. As this is not visible in Figs. 12.1b and 12.1c an extended analysis will be performed on the 95xxx1.

In Table 12.4 the performance deviations as computed by the AM component of the 95xxx1 in comparison with the reference engine are shown. It strikes that the difference in TT49 (EGT) is small at TO, although from the EGTSDM as computed in the test cell software, using GE guidelines, indicates a larger difference in TT49. It is suspected that this difference is due to small mistakes in the component maps as tuned in Chapter 8, due to which the TT49 value is computed as too low at the conditions in which the 946641 has been tested. At MC the difference is positive, although slightly smaller than expected looking at the EGTSDM, a 0.28% difference results in an absolute difference of 3.4K, a bit less than expected.

The largest performance deviation found in Table 12.4 is in the fuel use at TO, which is lower than for the reference engine. It is likely that this is the reason for the increased LPT efficiency as computed by the AM component. It is however also possible that the efficiency of the LPC is slightly higher on the 95xxx1 than on the reference engine due to engine to engine variations. It is assumed that the fan

Table 12.4: Computed performance deviation of the 95xxx1 in comparison with the reference engine

Power setting	ΔTT25	ΔTT3	ΔPS3	ΔN2	ΔTT49	ΔWF	ΔFN
TO	-0.44%	0.20%	0.40%	-0.10%	0.04%	-0.44%	0.24%
MC	-0.33%	0.26%	0.39%	-0.10%	0.28%	-0.08%	0.49%

efficiency is equal for both engines, as fans are not as sensitive to deterioration as stated in Chapter 11. From this follows that the engine will have to be analysed with the LPC core efficiency as one of the parameters to be adapted by the AM module. In Chapter 9 it was concluded that this would give less accurate results, however Pieters has concluded that for the analysis to be accurate the root causes of the performance change must be included [23, 41].

Before the effects of adding the LPC core efficiency are analysed, an hypothesis is made about the expected condition of the engine, based on information available on the work done during the the shopvisits at KLM ES. The reference engine has had no work done on the HPC, whereas the 95xxx1 has had the stage 10 blades replaced. Stage 10 is the final stage of the HPC, which as a smaller effect on the performance of the HPC than the preceding stages [26]. As the 95xxx1 is slightly older it is expected that some deterioration is present on the engine in comparison to the reference engine. Especially as the engine has been flown by the same operator as the 95xxx5, on which a large amount of deterioration is present on the HPC. The reference engine had its HPT stage1 and 2 blades and nozzles replaced, whereas no work has been done on the 95xxx1 HPT. It is therefore expected to see a reduction in HPT condition.

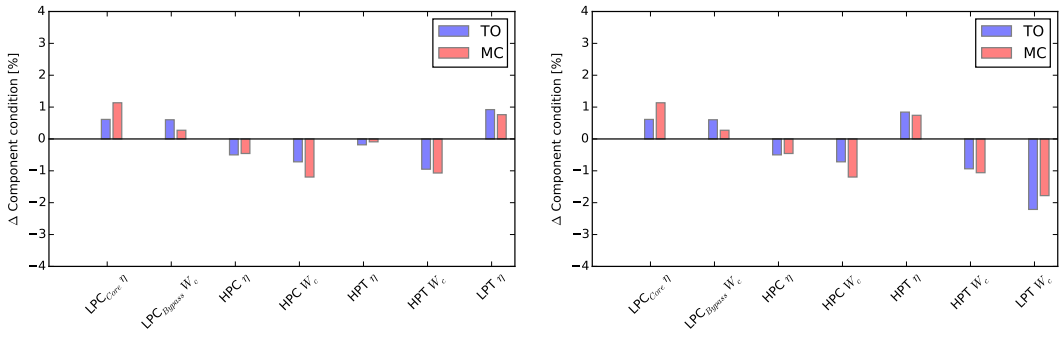

(a) Analysis using LPC$_{core}$ η

(b) Analysis using LPC$_{core}$ η and LPT W$_c$

Figure 12.3: AM analysis of the 95xxx1 using different parameters than in Fig. 12.1c

Figure 12.3 shows the results of the AM analysis using two different parameter sets. Replacing the LPC mass flow deviation with the LPC efficiency results in the outcome shown in Fig. 12.3a. Here it is visible that more deterioration is found on the HPC than using the original parameter set in Fig. 12.1c, as is expected. Replacing the LPT efficiency deviation with the mass flow deviation leads to the analysis in Fig. 12.3b, where an improved condition for the HPT is found. This is not as expected, due to which this analysis is discarded. From the results in Fig. 12.3 it is suspected that the booster of the 95xxx1 is of better condition than the booster of the reference engine. Including the LPC efficiency in the analysis then gives more realistic results for the HPC. It is concluded that the reduced EGTSDM is due to a reduction in HPC and HPT performance. Taking from Chapter 11 the LPT results are not fully trusted and likely due to numerical variations.

The results in this section all look plausible, being likely explanations for the observed performance differences between the engines. Unfortunately it is not possible to validate these results. All engines have been shipped out to their respective owners after testing and are currently in operation. Due to this it is not possible to physically check if differences are present between the engines. Furthermore as all engines have been in the shop for a Quick Turn (QT) and are relatively new it is not possible to fully correlate the work done, or operational history, with the found results. It is left as a recommendation to keep monitoring the engines and to try to correlate the work done in the shop with found AM results in the future. The use of on-wing data in combination with test cell data will likely prove to be useful.

12.2. On-wing measurements

While in operation the GEnx-1B takes measurements continuously, monitoring its status. Aside from Continuous Engine Operating Data (CEOD), the engine also produces snapshots at specific moments in flight. As mentioned in Chapter 8 one of these moments is take-off. In this section these snapshots will be analysed using GSP, investigating the use of the GEnx-1B model with the AM module to analyse on-wing measurements. A start with this has already been made in Section 8.3, in which on-wing measurements of the reference engine have been analysed.

12.2.1. Objective

The objective of this section is to investigate the use of AM in analysing on-wing measurements for the GEnx-1B. Currently GSP is not used to analyse on-wing data on a regular basis at KLM, although this has been investigated by Verbist [34, 35, 37]. As all GEnx-1B collect data while in operation, compared to only part of the CF6-80C2 engines, analysing this data will be of interest for KLM. KLM now analyses GEnx-1B on-wing data using PROGNOS for ENGINE, which analyses engine data based on statistics. Application of AM to the same data might lead to additional insight for KLM.

12.2.2. On-wing influences

The data used in this section is gathered on-wing, instead of in a controlled test cell environment. This causes additional phenomena to be present, influencing the measurements taken by the engine. As AM is a form of deterministic GPA, all changes to the measurements will directly cause changes to the outcome of the analysis. In this section the different mechanisms which influence on-wing measurements will be described.

The application of AM in GSP assumes that the engine is in a steady-state condition at the moment measurements are taken. In the test cell this assumption can assumed to be true, as the engine is given sufficient time to settle before measurements are taken. Furthermore it can be assumed that the ambient conditions remain constant over the duration of the test. On-wing the steady-state assumption will not fully hold. In order to save engine life, the power setting is reduced when possible [34]. Furthermore the ambient conditions are changing, as the aircraft is moving when the measurements are taken. The GE software taking the snapshots of the engine its condition will likely try to take the measurements at a point at which the engine is in near steady-state conditions. However, unsteady effects will still influence the measurements.

In the test cell a special bellmouth inlet is installed, to ensure uniform inflow to the fan at the tested conditions. On-wing a different inlet is used, designed to facilitate maximum pressure recovery at all conditions encountered during flight. A different inlet, combined with varying inlet flows lead to an increased amount of uncertainty on the conditions at the fan face. The pressure and temperature measurements at the fan face are used, to reduce the effect that the different inlet has on using the model (Chapter 6). It is unknown however if the flow encountered by the fan is as uniform on-wing as it is in the test cell. This can influence the performance of the engine, thus affecting the AM component. The inlet is designed to prevent this as much as possible, therefore the effects are considered to be small [42].

Cooling flows in the test cell and on-wing are assumed to be equal. As the Boeing 787 is a bleedless aircraft [28], no customer bleed flows to the aircraft are present. Only one additional bleed system is installed on-wing in comparison with the test cell: nacelle and booster anti-icing (BAI). When the nacelle anti ice is turned on the BAI also activates. The bleed air comes from the 7th HPC stage. In the data selection care has been taken to remove all snapshots in which the anti-ice system is activated, to keep the conditions as close as possible to those encountered in the test cell.

Installed on the engine are two Variable Frequency Starter Generators (VFSGs), providing electrical power to the aircraft during flight. The VFSGs are connected to the N2 shaft through a fixed gear gearbox, drawing power from the HPT. Both VFSGs in total extract 692 HP of power from the HPT. This is about 0.77% percent of the total power delivered by the HPT. This is double the amount of power take-off (PTO) than used in previous research, likely due to the large amount of electrical systems on the Boeing 787. The effects on the GPA analysis however are still considered to be very small. The PTO is added as a fixed amount to the on-wing GPA analysis.

12.2.3. Gathered data

Data has been obtained for all GEnx-1B engines in operation within the AFKL fleet on the 3rd of April 2018. In total 32 engines were in operation, 10 on AF aircraft, 22 on KLM aircraft. Take-off snapshots have been collected for all engines, starting from the moment they were installed on the aircraft on which they are operating on the 3rd of April 2018. For some engines this means that only a few snapshots are available, as they just entered service or because they were reinstalled after a shopvisit. In total 20,719 snapshots are available.

Some snapshots have been removed from the dataset before the analysis has been started. As mentioned in Section 12.2.2 all snapshots in which de-icing was activated have been removed. Furthermore all snapshots taken at over 3000 ft have been removed, as it was deemed that the conditions in which the engines operate at those altitudes differ significantly from those as encountered in the test cell at sea level. In essence this resulted in removing 5 airports from the dataset. Finally all snapshots referring to AF flights have been removed, as these have been operated in a different way, usually being used on short-haul flights, leading to much lower power settings being used. The model has not been tuned for these ranges, which is left as an recommendation. 12,034 snapshots remained in the dataset after cleaning.

12.2.4. Results

In this section the results of the AM analysis using on-wing measurements are shown. Not all available snapshots have been analysed, this section merely serves as an outlook on the possibilities of using GSP in an operational environment. Previous research has already investigated the possibility of using on-wing data[34, 35, 37]. Unique for the GEnx-1B fleet is that all engines collect data on-wing, unlike for the other engines in service at KLM. This makes analysing on-wing data all the more interesting.

The first engines of which on-wing results are analysed are the 95xxx6 and 95xxx7, both installed on the PH-BHH a KLM 787-9. Take-offs are available starting the 1st of September 2016 until the 3rd of April 2018. With the aircraft delivered on the 26th of August 2016, the engines are considered to be new and in good condition at the start of their first flight. For the 95xxx6 831 snapshots are analysed, for the 95xxx7 850. The difference in the amount of take-offs is also present in the original unfiltered dataset.

First the workings of the AM module with on-wing data is investigated further. Although already done in Chapter 8 for the reference engine (95xxx3), many more snapshots are available for some other engines, including snapshots taken at different conditions and power settings. The model has been tuned to simulate an engine in these on-wing conditions. The engine used to analyse this is the 95xxx7.

95xxx7

Results for the 95xxx7 are shown in Fig. 12.4, as a reference case the first available take-off for the 95xxx7 is chosen. By choosing an on-wing measurement as a reference point the unknown effects from Section 12.2.2 are compensated for by the Calibration Factors (CFs). The CFs for this analysis are shown in Table 12.5. All CFs are found to be near 1, indicating that only small adaptions to the model have been needed to align it with the reference dataset. The larger the CFs are, the larger the adaptions to the model have been, which might introduce additional errors into the analysis. The ambient conditions and power setting for the first available take-off are highly similar to those in the test cell for the design point measurement.

Table 12.5: Calibration factors for the 95xxx7 first available take-off

TT25	TT3	PS3	N2	TT49	WF
0.998	0.982	0.972	1.002	1.000	1.036

As expected the results for the 95xxx7 look equal to those found for the reference engine, albeit with more scatter due to the larger amount of snapshots available. The computed condition deviations are almost independent of the corrected component spool speed. The mass flow deviation for the HPC again shows the most scatter. Furthermore some relation with corrected spool speed is visible in Fig. 12.4d at higher spool speeds, indicating slight modelling errors.

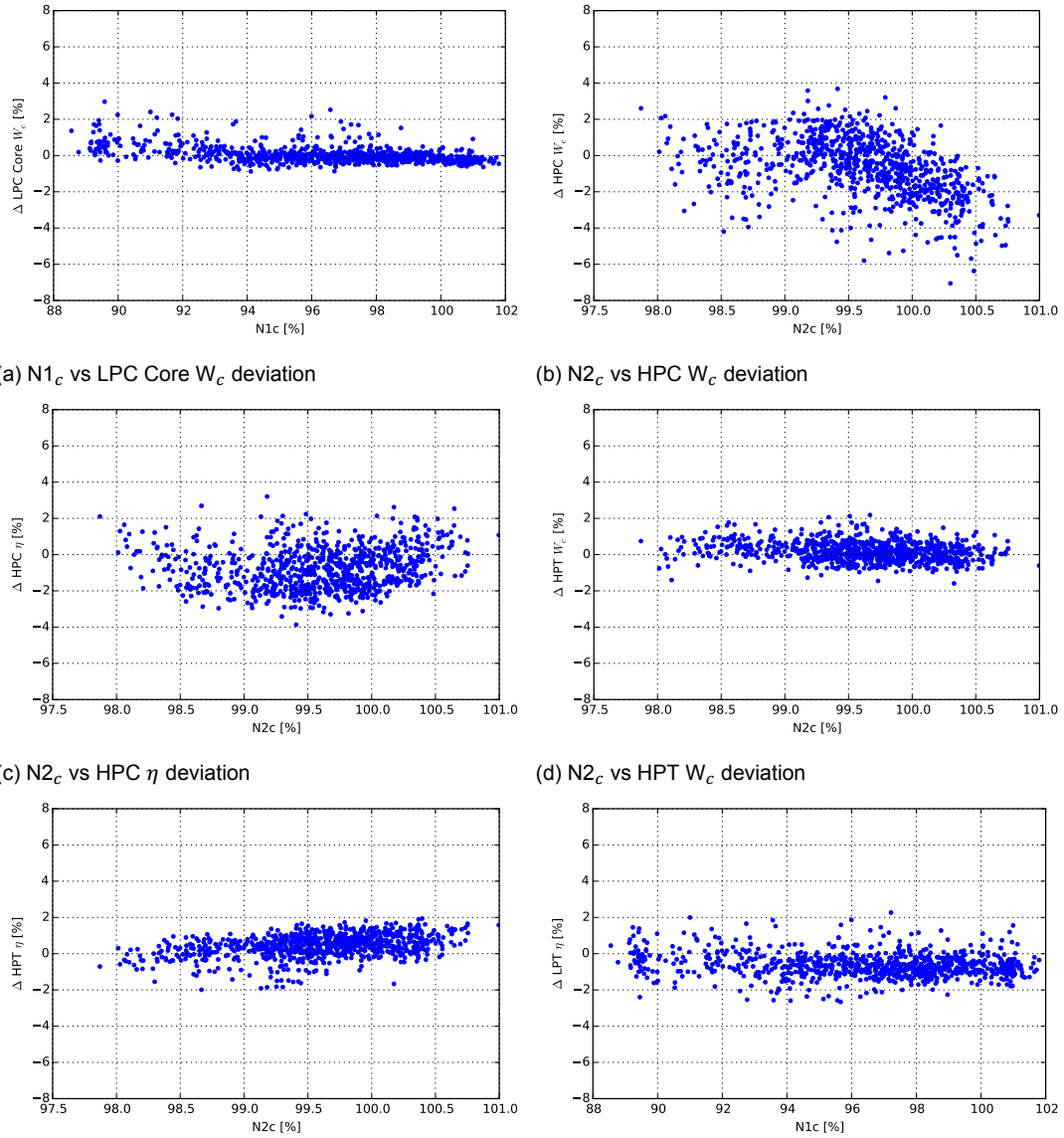

(a) $N1_c$ vs LPC Core W_c deviation

(b) $N2_c$ vs HPC W_c deviation

(c) $N2_c$ vs HPC η deviation

(d) $N2_c$ vs HPT W_c deviation

(e) $N2_c$ vs HPT η deviation

(f) $N1_c$ vs LPT η deviation

Figure 12.4: Accuracy of the model in simulating the engine condition for the 95xxx7, reference is the first available take-off snapshot

It is of interest to see if the results of Fig. 12.4 can be used to give an indication of the condition of the engine over time. This would allow for monitoring the engine throughout its operational lifetime. Therefore the results of Fig. 12.4 have been plotted in chronological order in Fig. 12.5.

$$A_i = \begin{cases} x_1 & \text{when } i = 1 \\ \alpha \cdot x_i + (1-\alpha)\, x_{i-1} & \text{when } i > 1 \end{cases} \tag{12.1}$$

Again scatter is present in the results. To make trends more visible an Exponentially Weighted Moving Average (EWMA) is plotted [34]. The EWMA is computed by Eq. (12.1). Here A_i is the EWMA value at time i, x the computed value and α a weighting coefficient between 0 and 1. With a higher value for α recent observations are given more weight. In this case a value of 0.1 has been chosen, as it is assumed that changes in gas turbine condition are slow, hence not too much weight must be given to a recent measurement.

Two different kind of trends are visible in Fig. 12.5, slow moving and periodic. Figures 12.5d to 12.5f

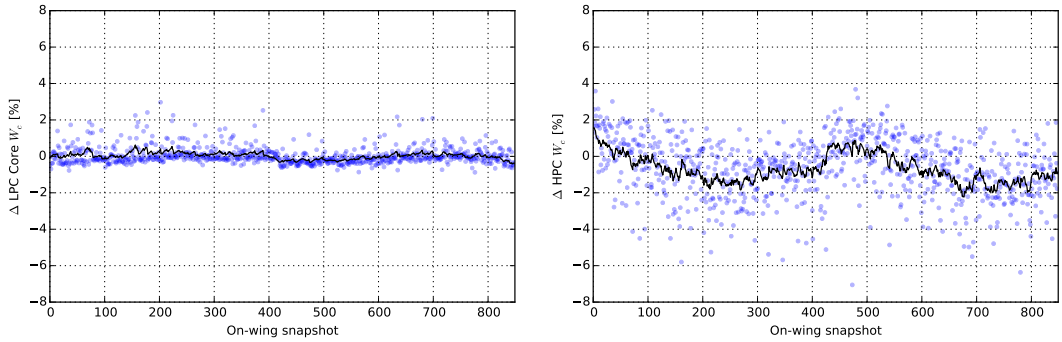

(a) Time vs LPC Core W_c deviation

(b) Time vs HPC W_c deviation

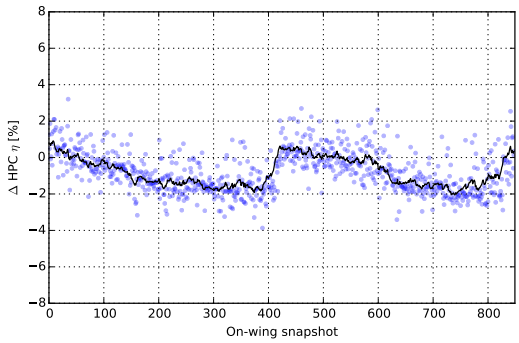

(c) Time vs HPC η deviation

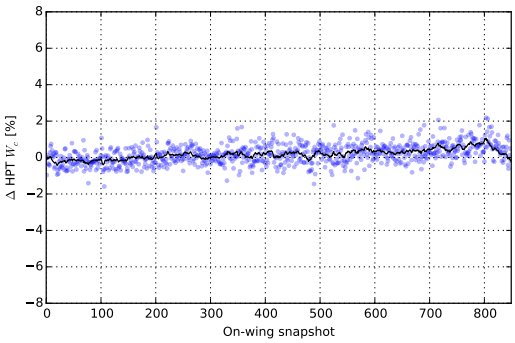

(d) Time vs HPT W_c deviation

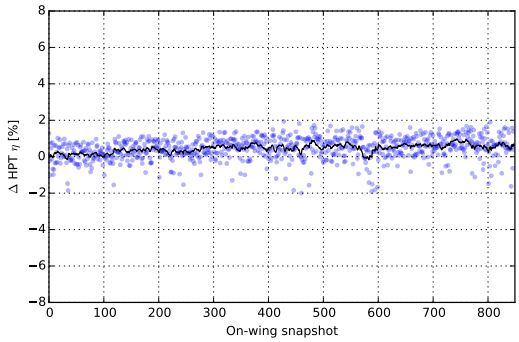

(e) Time vs HPT η deviation

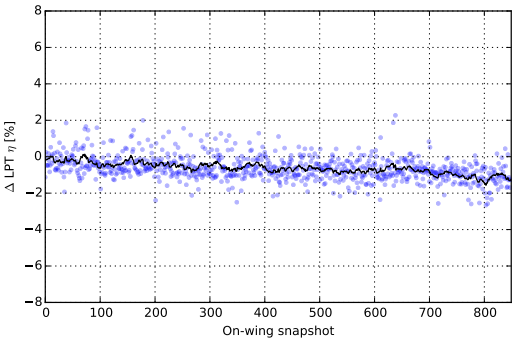

(f) Time vs LPT η deviation

Figure 12.5: Changes in engine condition over time for the 95xxx7, an EWMA is used for trending of the results. Reference is the first available take-off snapshot

show slowly changing conditions of the turbines. The mass flow capacity of the HPT is slowly increasing, possibly due to material removal in the stators [6, 16, 21]. For the LPT mass flow the opposite result is found, with a decrease in corrected mass flow capacity.This is a realistic effect, even though it was found in previous chapters that the LPT results would most likely not be valid. The HPT isentropic efficiency is found to slowly increase with time, an explanation for this might be an increase in N2 speed over time.

The results for the HPC show more rapid changes in condition as shown in Figs. 12.5b and 12.5c. A rapid increase in efficiency is found at around 400 take-offs, with another increase starting near 800 take-offs. Only one explanation is possible for this rapid increase, which is a water wash of the engine. Using water and a detergent the engine is cleaned in this procedure, removing fouling from its inner components. Using aircraft maintenance documents it has been confirmed that the engine has received a water wash around the 420th snapshot. As the compressors are most effected by fouling, especially the HPC due to the higher temperatures [6], it is likely that these components also experience the biggest improvement due to a water wash.

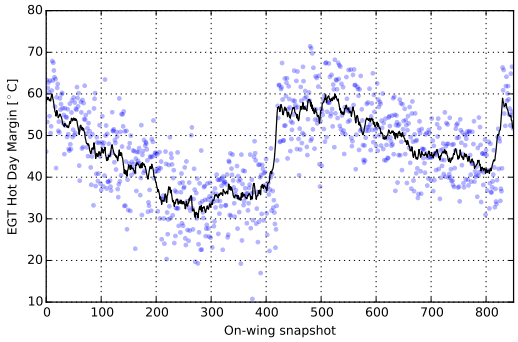

Figure 12.6: EGTHDM as computed by the GEnx-1B internal software for the 95xxx7

The mass flow capacity of the HPC sees a similar improvement due to the water wash. The results also show more scatter, as is also visible in Fig. 12.4b, due to which the EWMA is influenced more, adapting to general changes slower. The mass flow capacity decreases, then stays constant only to increase again due to the water wash. Whereas the efficiency is returned to a new like state, the mass flow capacity stays slightly reduced. This is likely due to fouling which has been unremovable and the run-in of seals in the HPC.

The LPC mass flow deviation in Fig. 12.5a shows a small jump around 400 take-offs. This is likely related to the same water wash, the effects of which on the LPC are limited. A drop in mass flow capacity is not as expected, possibly this is due to smearing of the HPC results as no PS25 measurement is available.

It is interesting to investigate how the component condition deviations as computed by GSP relate to the Hot Day EGT Margin (EGTHDM) as computed by the engine itself using GE software and knowledge. The EGTHDM is plotted in Fig. 12.6. Note that the margins are higher than reported for test cell results, this is because the EGT redline on-wing is higher than in the test cell. A pattern very similar to those as found for the HPC in Fig. 12.5 is visible, including a large amount of scatter. Combining these images leads to the conclusion that the HPC is responsible for most of the performance loss in terms of EGT margin when on-wing. This is also confirmed by GEnx-1B Type Engineers at KLM ES. Combining this with results from Chapter 11 it is concluded that the results as computed for the HPC by the AM component are correct.

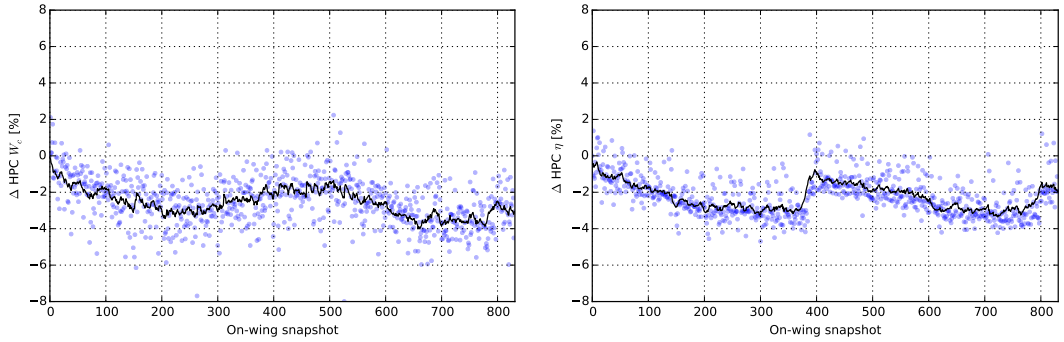

(a) Time vs HPC W_c deviation

(b) Time vs HPC η deviation

Figure 12.7: Changes in HPC condition over time for the 95xxx6, an EWMA is used for trending of the results. Reference is the first available take-off snapshot

95xxx6 and the influence of CFs

The 95xxx6 is installed on the same aircraft as the 95xxx7, hence it is assumed that it has experienced a similar life. Furthermore it is build, judging from the serial number, just before the 95xxx7. Based on this it is expected that the performance of both engines is similar. In Fig. 12.7 the condition of the HPC is shown. The associated CFs are shown in Table 12.6.

Table 12.6: Calibration factors for the 95xxx6 first available take-off

TT25	TT3	PS3	N2	TT49	WF
0.983	0.971	0.968	1.011	0.987	1.004

Comparing Figs. 12.5 and 12.7 leads to two interesting observations. First of all the shape of the curves is almost equal, however slightly shifted to the left. This is likely due to a different timing of the water wash for this engine, as only one engine is washed at a time. The second observation is that the curves are shifted down slightly, starting just below zero rather than above. This could be due to the actual deterioration of the engine, or due to the calibration of the AM module. This will be investigated next.

Scatter is present in all on-wing results investigated, showing that the operating conditions affect the AM procedure, but also the EGTHDM computation in the engine itself. From this it can only be concluded that the operating conditions will also influence the computation of the CFs and hence the reference dataset. To illustrate this Table 12.7 shows the computed CFs for three different take-offs. The first available take-off for the 95xxx6 and the first and second take-off for the 95xxx7. It was found that one earlier take-off was available for the 95xxx7. It strikes that the CFs for each day are highly similar. This leads to the conclusion that the CFs not only calibrate for the unknown installation effects of Section 12.2.2, but also for the influence of the operating conditions. This makes selection of the reference take-off more precarious, especially if the performance of several engines is to be compared, as the absolute value of the deterioration differs depending on the CFs.

Table 12.7: Calibration factor comparison

ESN	Date	TT25	TT3	PS3	N2	TT49	WF
95xxx7	01-09-2016	0.998	0.982	0.972	1.002	1.000	1.036
95xxx7	02-09-2016	0.985	0.972	0.968	1.011	0.988	1.018
95xxx6	02-09-2016	0.983	0.971	0.968	1.011	0.987	1.004

The influence of the CFs is investigated using the 95xxx7. In Figs. 12.8a and 12.8b the differences in computed HPC condition computed using two different reference cases are visible. It is clear that the conditions are shifted downwards when the second take-off is used as a reference case. This is about equal to the results found in Fig. 12.7, likely due to similar CFs. The question remains which of the two cases is the most correct. Considering Figs. 12.8c and 12.8d it is found that using the second take-off as a reference case a constant deviation from zero is found for the PS3 and TT49 deviation. It is deemed highly unlikely that an engine its performance during two years will differ significantly from its first take-off. From this it is concluded that the results using the first take-off are more reliable.

In general the following conclusions are drawn. It is important to carefully select the reference measurement, as this can greatly influence the calibration factors. The calibration factors must be close to one, as was also concluded in previous research. Finally the performance deviations must be near zero, at least at the start, for the most reliable results. Differences in the CFs are likely also contributed to small errors in the component maps.

Comparison of the 95xxx6 and 95xxx7

Using the information from the previous section a comparison is made between the 95xxx6 and 95xxx7 HPCs, using the same reference case. The results of this are located in Fig. 12.9 on Page 77. Here it is found that the condition of both HPCs changes in the same way, with the water wash for the 95xxx6 happening slightly earlier. The efficiency deviation followswater wash the same pattern for both engines, however the reduction in corrected mass flow capacity for the 95xxx6 seems slightly higher after the second water wash.

Located in Fig. 12.10 are the EGTHDMs as computed by the engines. It is clearly visible that the 95xxx6 is water washed earlier. It is also visible that less margin is regained by washing the engine for the 95xxx6 than for the 95xxx7. This is also visible in the TT49 deviation in GSP. It is suspected that this is due to a slightly more deteriorated HPT on the 95xxx6, visible in Fig. 12.11. This also gives more credibility to the results for the 95xxx1 in the test cell, as analysed in Section 12.1.4.

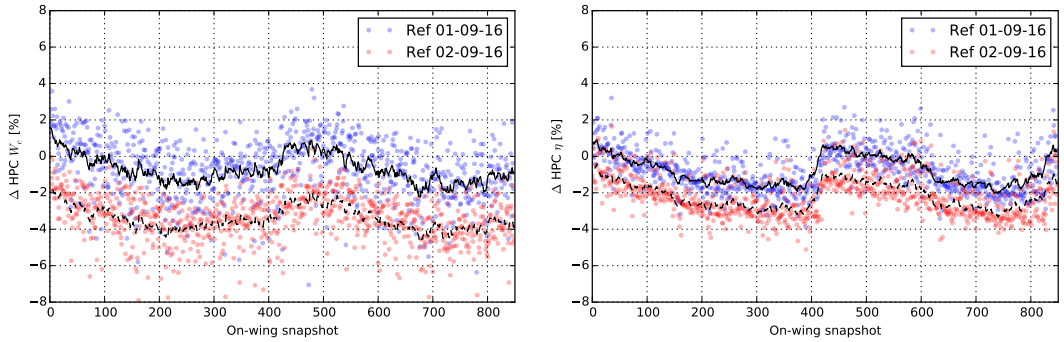

(a) Time vs HPC W_c deviation

(b) Time vs HPC η deviation

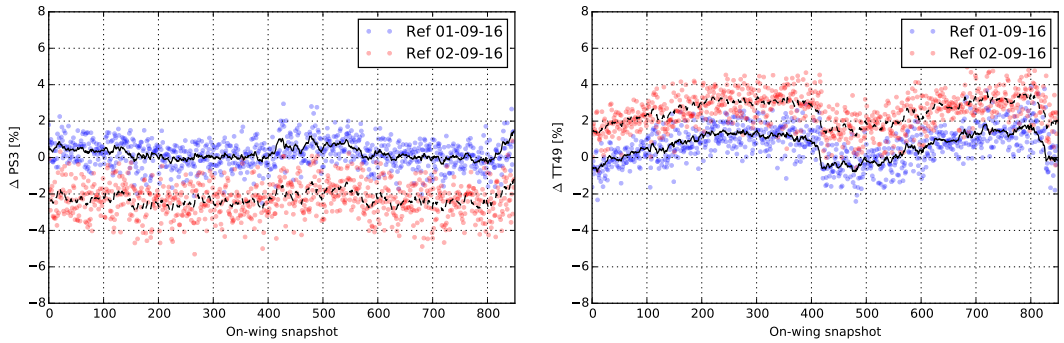

(c) Time vs PS3 deviation

(d) Time vs TT49 deviation

Figure 12.8: Condition of the 95xxx7, computed using two different reference cases

12.2.5. Analysis using a single reference case

The comparison between the 95xxx6 and 95xxx7 showed that good AM results can be obtained by analysing an engine with a reference case from a different engine. Furthermore it was found that the reference case selection can greatly vary the AM results, while being influenced by the operating conditions at the moment of measuring. Verbist has shown in previous research that good AM results can be obtained using a different reference engine, or using an average reference dataset [34]. In this section it will be investigated if it is possible to analyse all engines in the KLM fleet using the 95xxx7 as a reference engine.

Comparing two older engines

The first use case involves the comparison of two engines which were not new at the moment of the first available take-off, the 95xxx8 and 95xxx9. Again the HPC conditions are deemed the most interesting and are shown in Fig. 12.12. The EGTHDM as computed by the engines are located in Fig. 12.13.

In Fig. 12.12 it is visible that the computed condition deviations do not start at or near zero as was the case in the previous sections. Comparing Figs. 12.10 and 12.13 provides an explanation for this phenomena. The EGTHDM for the 95xxx8 and 95xxx9 start around 40 to 45°C, whereas the margins for the other two engines start around 60°C. It is found in Fig. 12.10 that the margin drops to 40°C after around 200 take-offs. In Fig. 12.9 is it found that the component conditions at around 200 take-offs are comparable to the starting conditions in Fig. 12.12.

Differences between the 95xxx8 and 95xxx9 are expected due to engine-to-engine differences and varying operational lives. Not all differences in EGTHDM can be contributed to differences in HPC condition. The analysis also shows that the HPT of the 95xxx8 is in better condition than the 95xxx9 HPT, contributing to the EGTHDM difference. The jump in EGTHDM around 300 and 350 snapshots is likely due to a water wash and visible in Fig. 12.9b.

From the above analysis some conclusions can be drawn. First of all it is possible to analyse two engines which are not as new in their first available snapshot. This is beneficial for when engines will be analysed later in life. Furthermore it shows that the component conditions can still be related to the EGTHDM of the reference engine. The computed condition deviations are likely correct. Finally it is

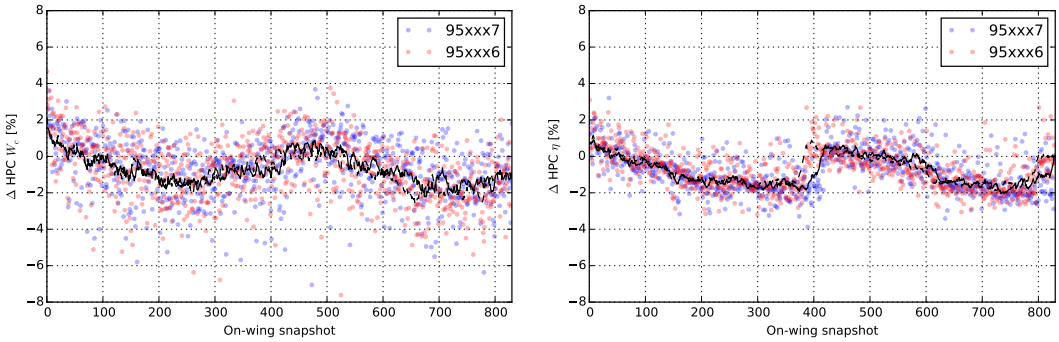

(a) Time vs HPC W_c deviation (b) Time vs HPC η deviation

Figure 12.9: Comparison of the computed conditions of the 95xxx6 and 95xxx7 HPC, reference is the first available take-off snapshot of the 95xxx7

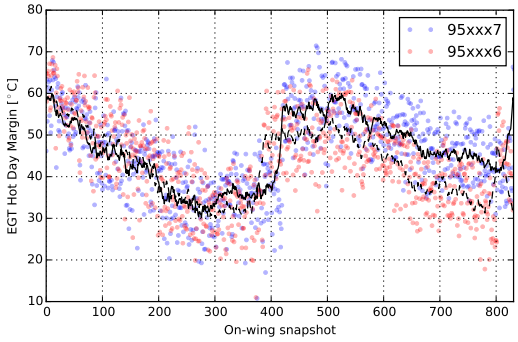

Figure 12.10: EGTHDM as computed by the GEnx-1B internal software for the 95xxx6 and 95xxx6

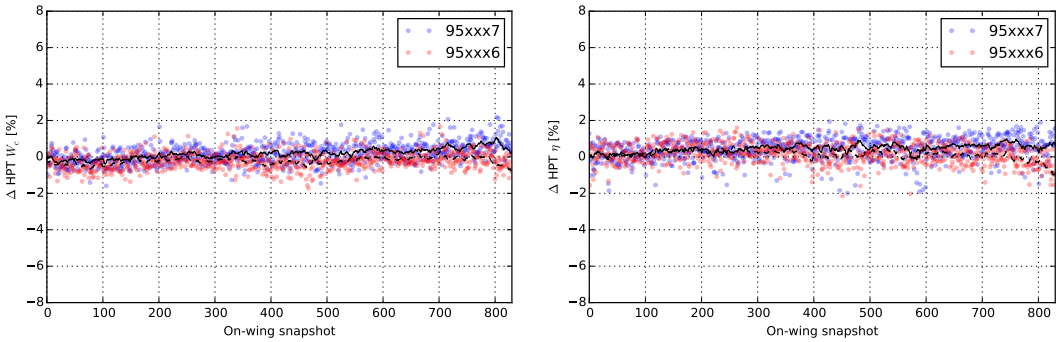

(a) Time vs HPT W_c deviation (b) Time vs HPT η deviation

Figure 12.11: Comparison of the computed conditions of the 95xxx6 and 95xxx7 HPT, reference is the first available take-off snapshot of the 95xxx7

concluded that to say something about the condition deviation of a specific engine over time, it might be easier to shift the whole graph up or down so that the EWMA starts at zero. This gives a clearer representation of the deterioration of a specific engine over time. This is especially useful if a reference engine is used which is not closely related to the analysed engine, as the change in time is of interest, not the absolute difference between the two engines.

Analysing all data

The above analysis can be repeated with any two engines, whether installed on the same aircraft or not. It is of interest to check if it is possible to analyse all engines using the first available take-off of the 95xxx7 and to compare their performance. This will however lead to an unpractical analysis, due

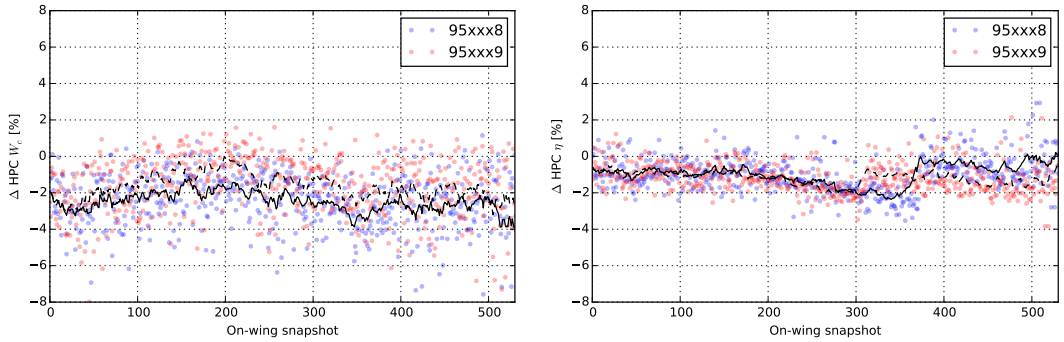

(a) Time vs HPC W_c deviation

(b) Time vs HPC η deviation

Figure 12.12: Comparison of the computed conditions of the 95xxx8 and 95xxx9 HPC, reference is the first available take-off snapshot of the 95xxx7

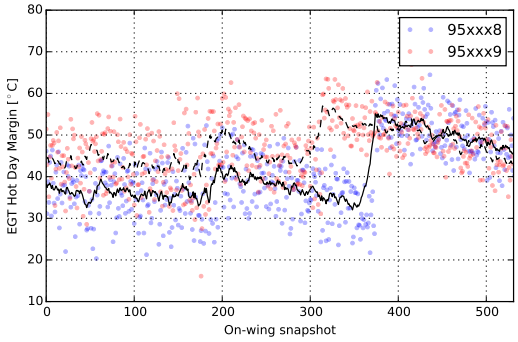

Figure 12.13: EGTHDM as computed by the GEnx-1B internal software for the 95xxx8 and 95xxx9

to the sheer amount of combinations available. Therefore it is decided to use a different approach.

All available take-offs have been analysed using the same reference engine, the first available take-off of the 95xxx7. The computed component condition deviations have been plotted against the calculated EGTHDM in Fig. 12.14. The data for the reference engine has been plotted separately in red. The location of the reference point is shown using a cross of dashed black lines.

In Fig. 12.14 clear trends between HPC condition and EGTHDM are visible, as was expected from Section 12.2.4. Furthermore it is observed that the trend for the reference engine is similar for all parameters as it is for the other engines. It must be remembered that the blue data points outnumber the red ones by more than 10,000. As the observed trends are equal, it is likely that the reference case can be used to analyse all on-wing data points, as long as the conclusions from the previous section are taken into account.

From a maintenance point of view it is can be concluded that restoring the HPC to as new condition has the greatest effect on the EGTHDM, as seen by the large gradients in Figs. 12.14b and 12.14c. The other components have a smaller effect on the margin, however from the above analyses it was seen that an underperforming component in combination with HPC deterioration will result in a lower EGTHDM. This however is not visible in this figure.

Figure 12.14 can also be used to draw conclusions on the condition of the 95xxx7 in comparison to the other engines in the fleet. The data points corresponding to the 95xxx7 lie in the middle of the point cloud, showing average performance of the engine. The range of EGTHDMs over which the 95xxx7 operates is normal for the GEnx-1B in operation at KLM. Some engines perform better, likely due to manufacturing differences, or a highly beneficial operating environment. The lower end of the margins is reached by the engine, after which a water wash is applied. It is likely that this point is about equal for all KLM engines.

The reference point in Fig. 12.14 is indicated using a black dashed cross. It is found that the EGTHDM is average in the reference point, although it was expected from Fig. 12.6 that the margin would be higher. Close inspection of Fig. 12.6 however reveals that the first point, the reference point,

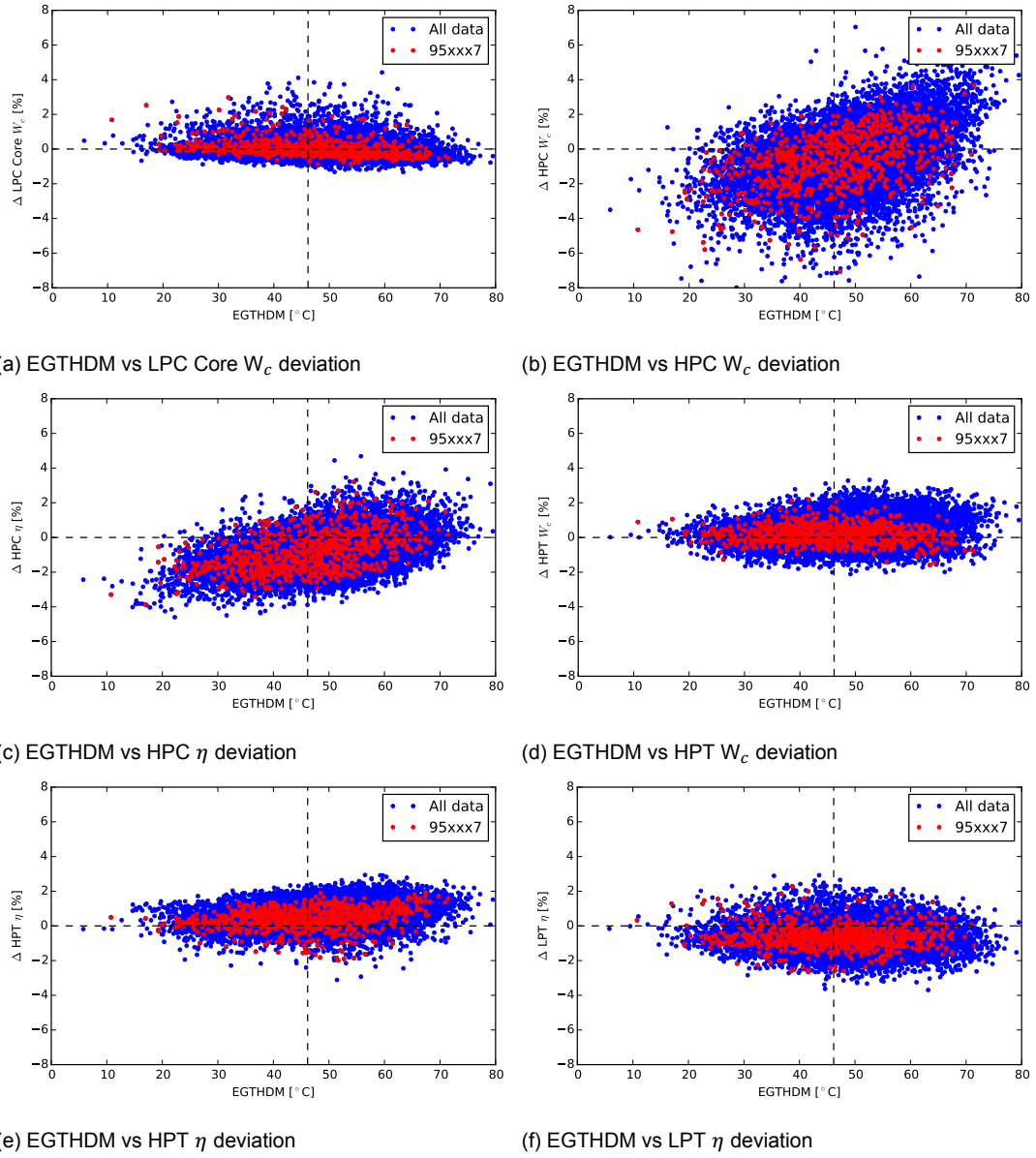

(a) EGTHDM vs LPC Core W_c deviation

(b) EGTHDM vs HPC W_c deviation

(c) EGTHDM vs HPC η deviation

(d) EGTHDM vs HPT W_c deviation

(e) EGTHDM vs HPT η deviation

(f) EGTHDM vs LPT η deviation

Figure 12.14: Relation between EGTHDM and component condition for all engines, reference is the first available take-off snapshot of the 95xxx7. The location of the reference point is shown with the black dashed lines

lies lower than the computed EWMA. This is most likely the reason that the EWMAs in Fig. 12.9 do not start at zero. As a reference point however an average point is likely to perform better, as it lies in the middle of the observed range which is to be analysed. This lowers the chance of operating points being encountered which lie out of the modelled range. The LPC, HPC and HPT mass flow deviation in the reference point is average, although the results of the HPC show a large amount of (expected) scatter. The HPC and LPT efficiency is found to be lower for most other operating points, likely decreasing with time. The HPT efficiency however is found to increase.

Overall it can be concluded that using a single reference case to compare all engines is possible. No strange results are encountered in Fig. 12.14 or any of the previous analyses using the 95xxx7 as a reference case. The chosen case seems a good choice due to the CFs close to unity and the average EGTHDM. Analysing all engines with one reference allows for easy comparison of the performance of different engines. Tracking the performance of a specific engine will likely require some additional computations moving to make sure that the EWMA starts at zero, or will require the use of a reference point specific for that engine.

Table 12.8: Calibration factors for the 95xxx3 first available take-off

TT25	TT3	PS3	N2	TT49	WF
0.992	0.968	0.940	1.014	1.002	1.004

Revisiting the 95xxx3

With the knowledge gained in this chapter it is interesting to revisit the 95xxx3, the reference engine on which the map tuning has been based in Chapter 8. In Figs. 8.1 and 8.2 relations were found between condition and performance deviations and corrected spool speed. Furthermore a shift from zero was observed for several parameters. It was suspected that the shift was due to the CFs. The CFs are shown in Table 12.8, where it is found that the PS3 CF is much smaller than for the engines analysed above.

Table 12.8 shows a comparison for the on-wing AM results for the 95xxx3, using either the 95xxx7 reference set as used above, or its own first take-off. A change in reference measurement set slightly removes the shift from zero for the PS3, TT49 and HPC efficiency deviations. Furthermore the dependency on spool speed is slightly reduced. For the HPC W_c deviations the relation with corrected spool speed seems slightly stronger.

From this analysis it is concluded that the model performs better than expected, when calibrated correctly. it must also be concluded that different CFs not only shift the results, but also change the relation between Nc_c and the computed deviations.

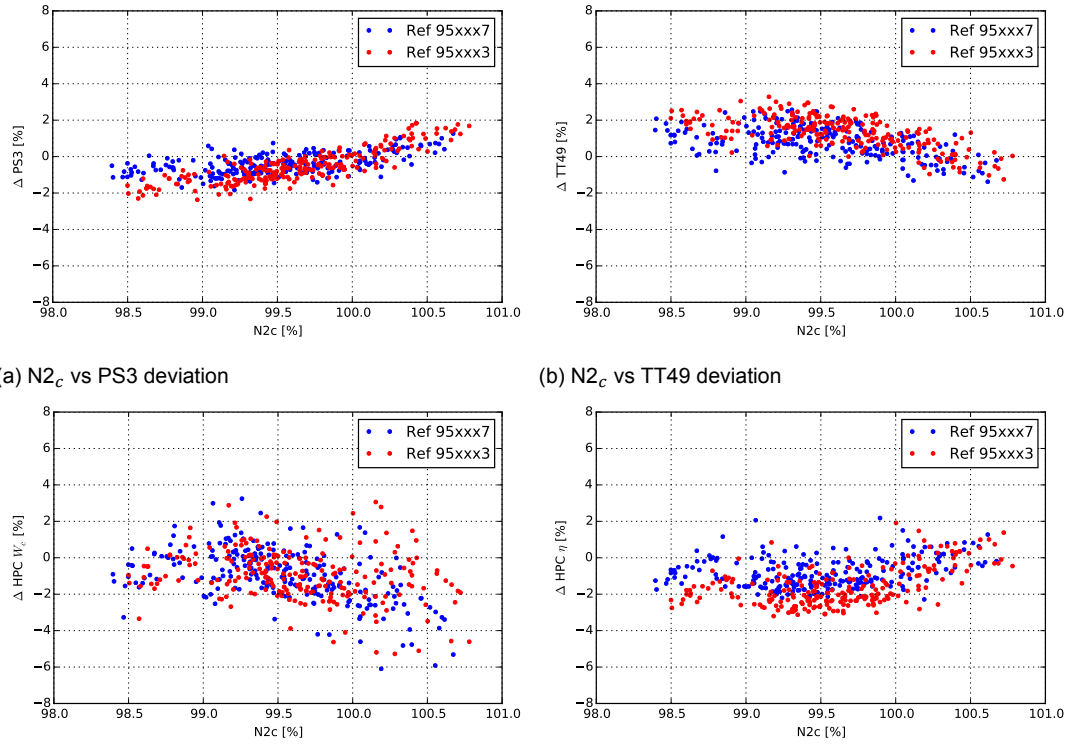

(a) $N2_c$ vs PS3 deviation

(b) $N2_c$ vs TT49 deviation

(c) $N2_c$ vs HPC W_c deviation

(d) $N2_c$ vs HPC η deviation

Figure 12.15: Comparison of the computed conditions of the 95xxx3 (reference engine) using two different reference datasets

12.3. Conclusions

This chapter has investigated the use of the GEnx-1B GSP model in combination with the GSP AM component and data collected from engines in operation. In general results for both the test cell and on-wing results are positive, leading to plausible explanations for the found component conditions. Validation of these results however remains impossible for both test cell and on-wing results.

It is concluded that the AM component is working with different reference engines and different power settings, investigated using test cell data. Small differences however exist, likely due to small modelling errors in the component maps. The analyses stay useful. It was also found that the results might depend on the parameters included in the analysis, as expected from literature [23, 41]. This increases the complexity of using AM in analysing test cell or on-wing results. In case of the CF6-80 model this added difficulty was not present due to the large amount of measurements taken inside the engine. Differences introduced due to different power settings being analysed, or different reference engines, are small and will likely not influence using the AM component in an operational setting.

On-wing measurements have been shown to include quite some scatter, as these measurements are influenced by more uncertainties than test cell measurements. From literature it was found that for on-wing measurements it is best to also select an on-wing reference point [34]. In this research it was found that the impact this scatter has on the reference point selection influences the CFs, strongly influencing the results of the analysis. Care must therefore be taken in selecting the reference data set. The 95xxx7 first take-off is found to be a good candidate for an on-wing reference set.

It is possible to compare the conditions of engines on-wing and to track their condition over time. Using a single reference case makes the analysis clearer, as AM is a form of differential GPA. Tracking the performance of a single engine, finding its ‘absolute’ performance deterioration will require the use of an adequate reference dataset, measured around the first take-off of that engine. It is also possible to shift the curves, such that the start corresponds to zero deterioration. More experience with the deterioration of GEnx-1B engines on-wing is likely required to fully reap the benefits of applying AM to on-wing data.

13

Conclusions and recommendations

This chapters forms the end of the report, summarising the conclusions made and milestones met throughout the report. Furthermore a look is taken towards future research with a number of recommendations.

13.1. Conclusions

Throughout the report several conclusions have been drawn, either on the modelling of the GEnx-1B or on the use of the model for GPA. Below these conclusions will be repeated, to form an overview of the report.

- Fewer gas path measurements are available on the GEnx-1B than on its predecessors, lacking a pressure measurement after the booster, after the HPT and in the fan bypass duct. Furthermore a TT5 measurement is not available. This has influenced both the modelling of the GEnx-1B and the application of the AM component in analysing GEnx-1B measurements.
- A design point model has been created, modelling the reference engine in the test cell at TO power setting. A reference engine has been chosen, which had the most average performance of all engines tested at the time of writing. Assumptions have been made on component performance to compensate for missing measurements. Furthermore assumptions have been made on the precise location of the pressure measurement and the gas path area, to convert static pressure measurements to total pressure, increasing the overall uncertainty. Overall the measured parameters have been replicated within +/- 0.0050% accuracy. The computed component design conditions match closely to both GE promotional material and open literature, leading to a high degree of certainty about the model.
- The off-design performance of the GEnx-1B has been modelled by tuning the LPC, HPC, and HPT component maps as were available for the CF6-80C2, as the GEnx-1B component maps are unavailable outside the OEM environment. This has been effective, although time consuming. The goal has been to match the measurements taken in the engine, for the MC power setting in the test cell and for on-wing data available for the reference engine. The MC point is simulated within +/-0.1% of the measured values. The on-wing data points showed some scatter originating from variability in real-life operating conditions, due to which it was not possible to simulate all points with the same accuracy. Instead the choice has been made to remove any dependencies between the performance and condition deviations as computed by GSP and the corrected spool speed of the component, as the condition of a component is not dependent on the power setting. Overall this has been successful, with small dependencies on the spool speed remaining for the deviation of PS3 and TT49. The condition of the HPC showed the most scatter, which could not be removed by further tuning of the maps.
- Having fewer measurements available on the GEnx-1B also influenced the tuning of the component maps. Especially those for the LPC and HPC, as the behaviour of the booster is not fully

known and the inlet conditions of the HPC are not fully defined. This increases the uncertainty involved with tuning the maps and likely also increases the scatter found for the component conditions.

- The effect of not having a PS25, PT49 and PS14 measurement available when analysing an engine using AM has been investigated using a model of the GE CF6-80C2. The CF6-80C2 model has been used in previous studies and had been shown to provide accurate condition analyses. Lack of a PT49 measurement leads to unreliable computed condition deviations for the LPT, as LPT deterioration will be attributed to a reduction in HPT efficiency. Removing the other two measurements from the dataset led to a slight shift in the results, likely reducing the accuracy of the analysis. Overall it was concluded that AM can still be used for analysing the engine condition, as the LPT is not as sensitive to deterioration as other components. This conclusion will also prove useful when in the future the CFMI LEAP-1B will be maintained by KLM ES, as on this engine the same parameters are measured as on the GEnx-1B.
- The sensitivity of the AM analysis to measurement error has been investigated using a Monte Carlo analysis. The HPC and HPT are the most sensitive to deviations in measurements. From the analysis it is concluded that the accuracy of a single snapshot used in the AM component is high enough, especially if a snapshot consists of averaged measurements. The differences in sensitivity between the different components is important to know, such that the results can be interpreted better.
- The workings of the AM component in combination with the GEnx-1B model has been tested further using simulated deterioration data. The LPT results are found to be unreliable. Furthermore having a deteriorated fan will hamper the on-wing results. The fan and LPT however are not as sensitive to deterioration as the other components. The conditions of the other components can be detected well, leading to a positive conclusion on the use of the model for GPA purposes.
- Analysis of test cell results with the AM component has been used to verify its functionality. Results changed slightly dependent on reference power setting, engine or on the power setting analysis. Overall however the picture painted by the results was the same, which is the most important in the MRO environment. The results found by the AM component correlate well with the EGT margins computed for the engines. From this it is concluded that the model can be used to analyse a GEnx-1B in the test cell. Analysis is made more complex by the fewer available gas path measurements. Depending on the set of component conditions varied by the AM component the results differ. Not including the suspected root cause of the performance deviations will lead to less reliable results.
- As a final test the AM component has been used to analyse on-wing measurements of different engines in the KLM fleet. On-wing measurements show quite some scatter, influencing the computed component conditions. Scatter also influenced the computation of the Calibration Factors (CFs) used to align the model with the reference measurement set, strongly influencing the outcome of the analysis. Care must therefore be taken when selecting a reference data set. This is a drawback of having a physics based model, which is calibrated based on a single reference point. A suggestion has been made for an on-wing measurement set which can be used to analyse all other engines. This showed promising results, allowing engines to be compared over time tracking their performance. The effects of water washing engines was clearly visible in the data, being correctly attributed to an improvement of HPC performance. Overall the AM component can be used to make an assessment of the condition of an engine while in operation.

13.2. Recommendations

Although this research has lead to a working GSP model of the GEnx-1B, which can be used to analyse both test cell and on-wing results, more work is still to be done. Furthermore the model can be used for further analysis in the future. Below some recommendations are given for improvements and future applications.

- When tuning the component maps the lines of constant speed re-labelled and moved. It is however also possible to change the shape of the lines themselves. It is possible that this will lead

to a more accurate representation of the GEnx-1B performance, removing the relations found between corrected spool speed and computed deviations.

- As was concluded above the lack of a PS25 measurement lead to an increase in uncertainty and difficulty when tuning the component maps. The GEnx-1B has been delivered with a PS25 pressure measurement, however this has been removed in a software update of the EEC. A pressure tap however is still available. It is recommended to find a way to connect this pressure tap to the test cell measurement system, to find a way to measure the pressure ratio of the LPC core in the test cell. This information would be highly valuable in improving the component maps.
- It is recommended to measure one engine at more power settings than required by GE in the test cell. By varying the power settings over the ranges encountered on-wing more information can be obtained on how the engines behaves at different settings in a more controlled environment. This would also allow for a correct estimation on the variation of engine thrust, allowing for a more accurate bypass map. Combined with the recommendation to try to add a PS25 measurement above, this would greatly improve the certainty with which the component maps are modelled.
- If the component maps are tuned again, it is recommended to increase the range of power settings over which they are tuned. Doing so would also allow for the analysis of AF engines, which have been mainly used on short-haul flights, requiring lower power settings at take-off.
- In this research only the 74/75/P2 rated GEnx-1B is modelled, as in use on KLM its Boeing 787-9s. The engine can however be rated at different power settings, which is done by some of KLM ES its customers. Furthermore it is possible that the 787-10 which KLM will receive in the near future will be flown with a differently rated engine. Analysing engines with a different rating has not been investigated in this thesis. It is recommended that this is done in the future by KLM to further extend the use of AM, also to its third party clients.
- Currently only a few engines have been inducted in the shop at KLM ES, all for Quick Turns (QTs). In the future engines will also come into the shop for a Performance Restoration Shop Visit (PRSV). During a PRSV the performance of an engine is restored, by repairing or replacing certain components. This does not happen in a QT. It is of interest to investigate if this performance improvement can be shown using GSP, by comparing on-wing data before the shop visit, and test cell data and on-wing data after the shop visit. If this can be done on a larger scale the effectivity of shop visits can be assessed, and the condition of the engine before it enters the shop can be determined better. This can aid in defining the work scope to be carried out during the shop visit. If a high level of detail can be achieved, the information collected on-wing might even be used to already start ordering components which will have to be replaced, reducing the time needed for maintenance. It is therefore recommended to use AM more frequently throughout the engine its life, analysing the data before and after shop visits when these start happening. This will be a very interesting starting point for future research.
- In order to fully benefit from the possibilities of applying AM regularly it is important to incorporate AM into the work flow at KLM. When this is done the benefits stated above can be achieved. In order to do this a solution needs to be build into GSP which allows for easy analysis of GEnx-1B data. Currently this is not yet possible, separate Python files have been written to transform the GEnx-1B data files into text files which can be read into GSP. Furthermore separate Python scripts have been written to analyse the AM data. When included in GSP this process would be easier to implement in the daily work flow of KLM. Ideally the AM analysis can be automated and performed periodically using downloaded engine data.

Bibliography

[1] P A Beishuizen. Improving compressor maps of the GE CF6-80C2 engine. Master's thesis, Delft University of Technology, 2008.

[2] S El Bouazzaoui. Modeling of a gsp diagnostic tool for the CFM56-7B engines. Master's thesis, Delft University of Technology, 2008.

[3] D Y Davis and E M Stearns. Energy efficient engine: Flight propulsion system final design and analysis. Technical Report NASA CR-168219, NASA and GE, August 1985.

[4] FM Dekking, C Kraaikamp, HP Lophuaä, and LE Meester. *A modern introduction to probability and statistics*. Springer, 2005.

[5] D M den Haan. GSP gas path analysis on CF6-80 engines at KLM engine services. Master's thesis, Delft University of Technology, 2010.

[6] P C Escher. *Pythia: An Object-Oriented Gas Path Analysis Computer Program for General Applications*. PhD thesis, Cranfield University, 1995.

[7] European Aviation Safety Agency. Type certification data sheet for engine genx series engines, 2016.

[8] *Technologies for the Next Engine Generation*, 2014. GE Aviation.

[9] General Electric Aviation. GEnx high bypass turbofan. `https://www.geaviation.com/sites/default/files/datasheet-genx.pdf`.

[10] General Electric Aviation. GEnx-1b turbofan engine installation manual. Technical Report GEK 112856, General Electric Aviation, October 2011.

[11] General Electric Aviation. Air france industries - test cell #1 correlation for genx-1b model engine. Technical report, General Electric Aviation, Feb 2017.

[12] General Electric Aviation. GEnx-1B workscope planning guide. Technical Report GEK 114098, General Electric Aviation, July 2017.

[13] General Electric Aviation. GEnx-1B engine manual. Technical Report GEK 112851, General Electric Aviation, 2018.

[14] GSP Development Team. *GSP 11 User Manual*. National Aerospace Laboratory NLR, October 2013.

[15] GSP team. Gas turbine simulation program. `https://www.gspteam.com/`.

[16] R Kurtz and K Brun. Degradation in gas turbine systems. *ASME Journal of Engineering for Gas Turbines and Power*, 123(1):70–77, 2000.

[17] Y G Li. Performance-analysis-based gas turbine diagnostics: A review. *Proceedings of the Institution of Mechanical Engineers, Part A: Journal of Power and Energy*, 216(5):363–377, 2002.

[18] YG Li, P Pilidis, and MA Newby. An adaptation approach for gas turbine design-point performance simulation. *ASME Journal of Engineering for Gas Turbines and Power*, 128(4):789–795, 2005.

[19] L Marinai, D Probert, and R Singh. Prospects for aero gas-turbine diagnostics: a review. *Applied Energy*, 79(1):109–126, 2004.

[20] NASA. A giant step in jetliner propulsion. `https://spinoff.nasa.com/spinoff1996/30.html`.

[21] SOT Ogaji, S Sampath, R Singh, and SD Probert. Parameter selection for diagnosing a gas-turbine's performance-deterioration. *Applied Energy*, 73(1):25–46, 2002.

[22] M Oostveen. Development of GPA functionality in GSP. Master's thesis, Delft University of Technology, 2004.

[23] H Pieters. Gas path analysis with GSP for the GEM42 turboshaft engine. Master's thesis, Delft University of Technology, 2005.

[24] AG Rao. AE4-238 aero engine technology lecture 2: Engine calculations. Lecture Slides Delft University of Technology, 2014.

[25] AG Rao. AE4-238 aero engine technology lecture 5: Intake and exhaust. Lecture Slides Delft University of Technology, 2014.

[26] HIH Saravanamuttoo, GFC Rogers, H Cohen, and PV Straznicky. *Gas Turbine Theory*. Pearson Education, 6 edition, 2009.

[27] Several authors and contributors. Performance prediction and simulation of gas turbine engine operation. Technical report, Research and Technology Organisation NATO, 2002. RTO-TR-044.

[28] M Sinnett. 787 no-bleed systems saving fuel and enhancing operational efficiencies. `http://www.boeing.com/commercial/aeromagazine/articles/qtr_4_07/AERO_Q407_article2.pdf`, 2007.

[29] A Stamatis, K Mathioudakis, and KD Papailiou. Adaptive simulation of gas turbine performance. *ASME Journal of Engineering for Gas Turbines and Power*, 112(2):168–175, 1990.

[30] CC Tonino. Analysis of post-overhaul engine performance at KLM engine services. Master's thesis, Delft University of Technology, 2013.

[31] JP van Buijtenen and WPJ Visser. Reader aero engine technology AE4238, October 2009.

[32] E van Dorp. Development and implementation of a GSP gas path analysis tool for gas turbine diagnostics. Master's thesis, Delft University of Technology, 2009.

[33] ML Verbist. Gsp modeling elements and numerical methods. Reader published as part of AE4203 Gas Turbine Simulation / Application, 2013.

[34] ML Verbist. *Gas Path Analysis for Enhanced Aero-Engine Condition Monitoring and Maintenance*. PhD thesis, Delft University of Technology, 2017.

[35] ML Verbist, WPJ Visser, JP van Buijtenen, and R Duivis. Gas path analysis on klm in-flight engine data. *ASME 2011 Turbo Expo: Turbine Technical Conference and Exposition*, Volume 3: Controls, Diagnostics and Instrumentation; Education; Electric Power; Microturbines and Small Turbomachinery; Solar Brayton and Rankine Cycle, 2011. GT2012-69688.

[36] ML Verbist, WPJ Visser, R Pecnik, and JP van Buijtenen. Component map tuning procedure using adaptive modeling. *ASME Turbo Expo 2012: Turbine Technical Conference and Exposition*, 1: Aircraft Engine; Ceramics; Coal, Biomass and Alternative Fuels; Controls, Diagnostics and Instrumentation:371–379, 2012. GT2012-69688.

[37] ML Verbist, WPJ Visser, and JP van Buijtenen. Experience with gas path analysis for on-wing turbofan condition monitoring. *ASME Journal of Engineering for Gas Turbines and Power*, 136(1), 2013.

[38] WPJ Visser. *Generic Analysis Methods for Gas Turbine Engine Performance*. PhD thesis, Delft University of Technology, 2015.

[39] WPJ Visser and MJ Broomhead. GSP a generic object-oriented gas turbine simulation environment. Technical report, Netherlands Aerospace Centre (NLR), 2000. NLR-TP-2000-267.

[40] WPJ Visser, O Kogenhop, and M Oostveen. A generic approach for gas turbine adaptive modeling. *ASME Journal of Engineering for Gas Turbines and Power*, 128(1):13–19, 2004.

[41] WPJ Visser, M Oostveen, H Pieters, and E van Dorp. Experience with gsp as a gas path analysis tool. *ASME Turbo Expo 2006: Power for Land, Sea, and Air*, Volume 2: Aircraft Engine; Ceramics; Coal, Biomass and Alternative Fuels; Controls, Diagnostics and Instrumentation; Environmental and Regulatory Affairs:175–182, 2006.

[42] R Vos. Advanced aircraft design I lecture 17: Engine intakes, exhausts and thrust reversers. Lecture Slides Delft University of Technology, 2014.

[43] PP Walsh and P Fletcher. *Gas Turbine Performance*. Blackwell Science Ltd, 2 edition, 2004.

[44] M Zedda and R Singh. Gas turbine engine and sensor fault diagnosis using optimization techniques. *Journal of Propulsion and Power*, 18(5):1019–1025, 2002.

A

Thesis assignment

Development of a GSP model of the GEnx engine for gas path analysis at KLM Engine Services
Propulsion & Power (FPP), Faculty of Aerospace Engineering

Introduction
Gas path analysis (GPA) with modern gas turbine simulation tools is a powerful means to diagnose gas turbine components. The GSP Gas Path Analysis (GPA) functionality is used on CF6-50, CF6-80 and CFM-56 engine data from the KLM Engine Services (ES) CF6 test bed to determine engine condition on the component level. In [37, 40, 41] results of this work are described. In addition, GSP GPA results from these engines have been trended and benefits further explored ([34, 38]). In [30], earlier work focused on trending of specifically the CF6-80 engine is described.

Recently, KLM ES has started to overhaul the new GEnx engine. For accurate test analysis and diagnostics, the GSP GPA tool is required. For GPA with GSP, a validated GSP performance model is required. With the GSP model and the TU Delft GSP Adaptive Modelling (AM) component, accurate non-linear gas path analysis using adaptive modelling can be applied. Provided a suitable data import method is available, then GPA can routinely be applied on GEnx test cell and on-wing data to assess engine condition on the component level, which offers great potential in terms of maintenance decision support and cost saving. As a first step, gas path analysis will be demonstrated using manual input of performance data into the GSP AM tool.

Key Objectives

- Development and validation of a GSP model of the GEnx-1B.
- Assessment of potential of GPA for test analysis of the GEnx engine.

Assignment
Your work will include the following elements:

1. A literature study on the latest developments of GPA and condition/performance trending tools and their application in aero-engine maintenance/overhaul environments.
2. Introduction to current KLM performance and condition methods.
3. Introduction to GSP and GSP GPA as applied to KLM CF6-80 and CFM-56 engines.
4. Development and validation of a GSP model of the GEnx-1B engine.
5. Assessment of the potential of GPA test analysis and diagnostics of the GEnx engine at KLM ES
6. Demonstration of GSP AM GPA on the GEnx engine using manual data input with either real data, or if not available, GSP simulated deteriorated engine data.

Report
Results of the work must be reported in English, with a copy of this assignment and an executive summary.

Coaching
The work will be performed in close collaboration with KLM Engine Services (Michel Nollet)

Date 28 November 2017

Professor, Prof. dr. ir. P. Colonna	Tutor, Dr. ir. W.P.J. Visser	Supervisor at KLM Michel Nollet

B

Additional simulated deterioration results

In this appendix the results the categories ‘III. Core+’, ’IV. Full-’ and ‘V. Full+”, containing simulated deterioration from Chapter 11 are shown. The cases are from Table 11.1, repeated here for clarity.

Table 11.1[repeated]: Simulated deterioration cases GEnx-1B

		LPC Core		LPC Bypass		HPC		HPT		LPT	
	Case	$\Delta\eta$	ΔW_c	$\Delta\eta$	ΔW_c	$\Delta\eta$	ΔW_c	η	W_c	η	W_c
I. Basics	1	-0.33%	-1%								
	2			-1%	-3%						
	3					-1%	-3%				
	4							-1%	-2%		
	5							-1%	2%		
	6									-1%	-2%
	7									-1%	2%
II. Core-	8	-0.33%	-1%			-1%	-3%				
	9							-1%	-2%	-1%	-2%
	10	-0.33%	-1%							-1%	-2%
	11					-1%	-3%	-1%	-2%		
	12	-0.33%	-1%			-1%	-3%	-1%	-2%		
	13	-0.33%	-1%			-1%	-3%	-1%	-2%	-1%	-2%
III. Core+	14							-1%	2%	-1%	2%
	15	-0.33%	-1%							-1%	2%
	16					-1%	-3%	-1%	2%		
	17	-0.33%	-1%			-1%	-3%	-1%	2%		
	18	-0.33%	-1%			-1%	-3%	-1%	2%	-1%	2%
IV. Full-	19	-0.33%	-1%	-1%	-3%	-1%	-3%				
	20			-1%	-3%			-1%	-2%	-1%	-2%
	21	-0.33%	-1%	-1%	-3%					-1%	-2%
	22			-1%	-3%	-1%	-3%	-1%	-2%		
	23	-0.33%	-1%	-1%	-3%	-1%	-3%	-1%	-2%		
	24	-0.33%	-1%	-1%	-3%	-1%	-3%	-1%	-2%	-1%	-2%
V. Full+	25			-1%	-3%			-1%	2%	-1%	2%
	26	-0.33%	-1%	-1%	-3%					-1%	2%
	27			-1%	-3%	-1%	-3%	-1%	2%		
	28	-0.33%	-1%	-1%	-3%	-1%	-3%	-1%	2%		
	29	-0.33%	-1%	-1%	-3%	-1%	-3%	-1%	2%	-1%	2%

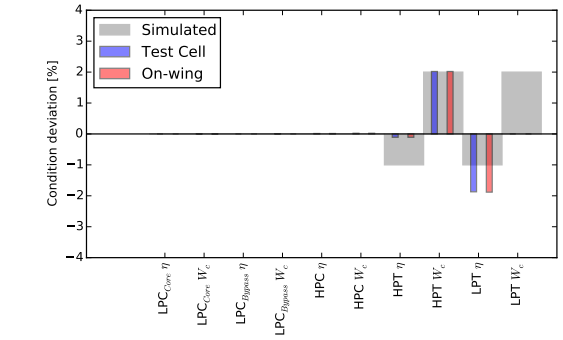

(a) Case 14

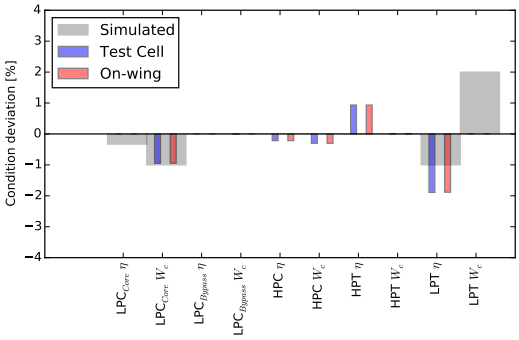

(b) Case 15

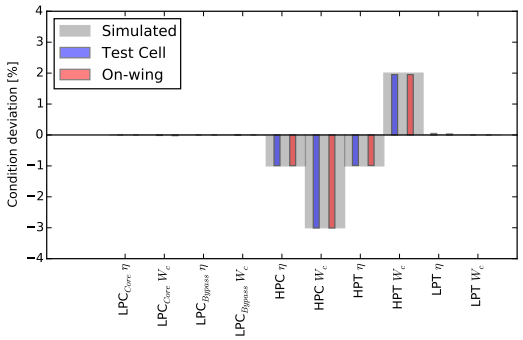

(c) Case 16

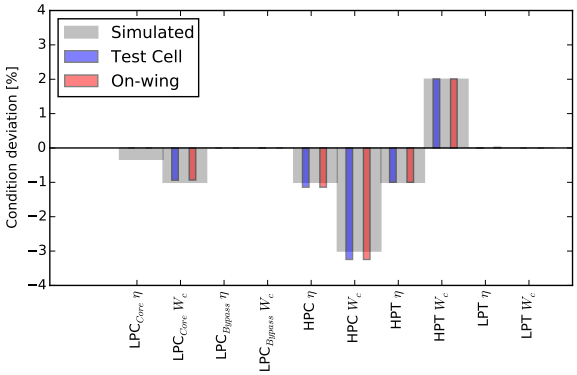

(d) Case 17

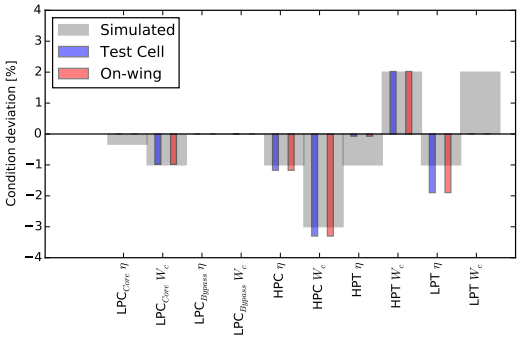

(e) Case 18

Figure B.1: Analysis of an engine with different types of simulated deterioration (‘III. Core+’ cases from Table 11.1) for either test cell or on-wing measurements

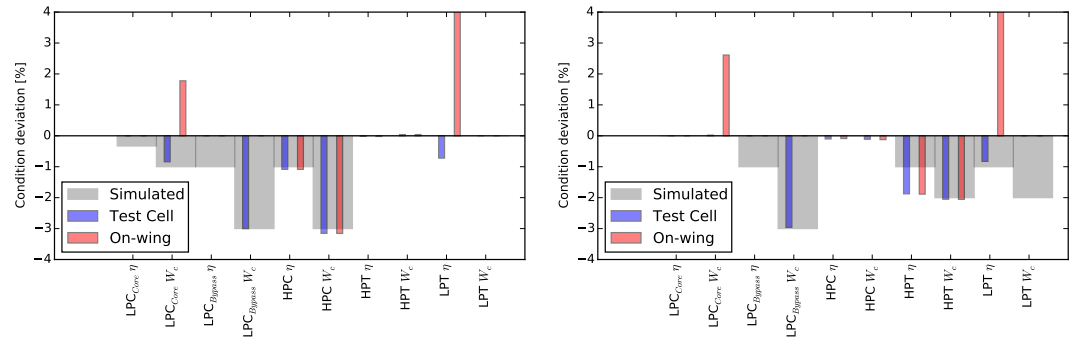

(a) Case 19

(b) Case 20

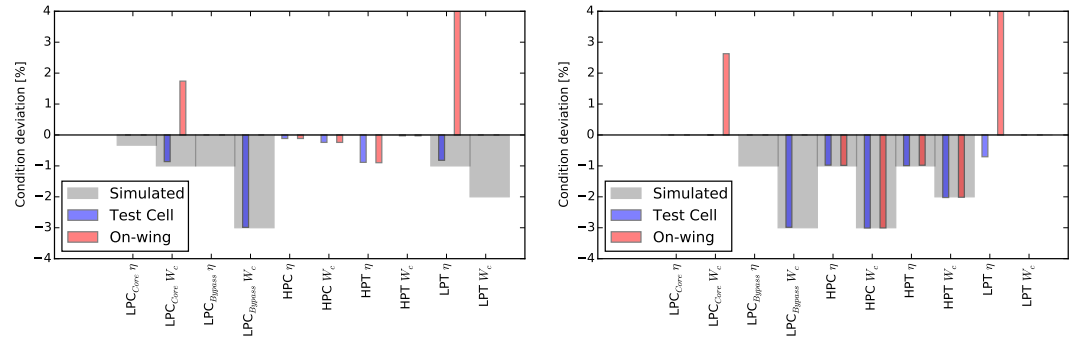

(c) Case 21

(d) Case 22

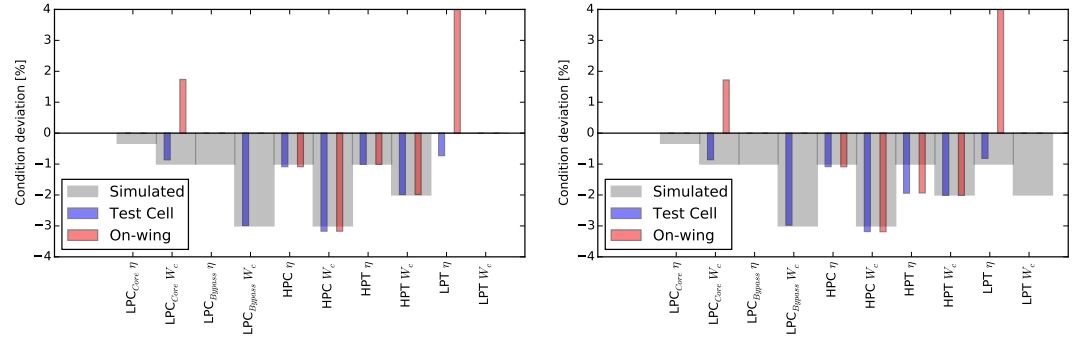

(e) Case 23

(f) Case 24

Figure B.2: Analysis of an engine with different types of simulated deterioration ('IV. Full-' cases from Table 11.1) for either test cell or on-wing measurements

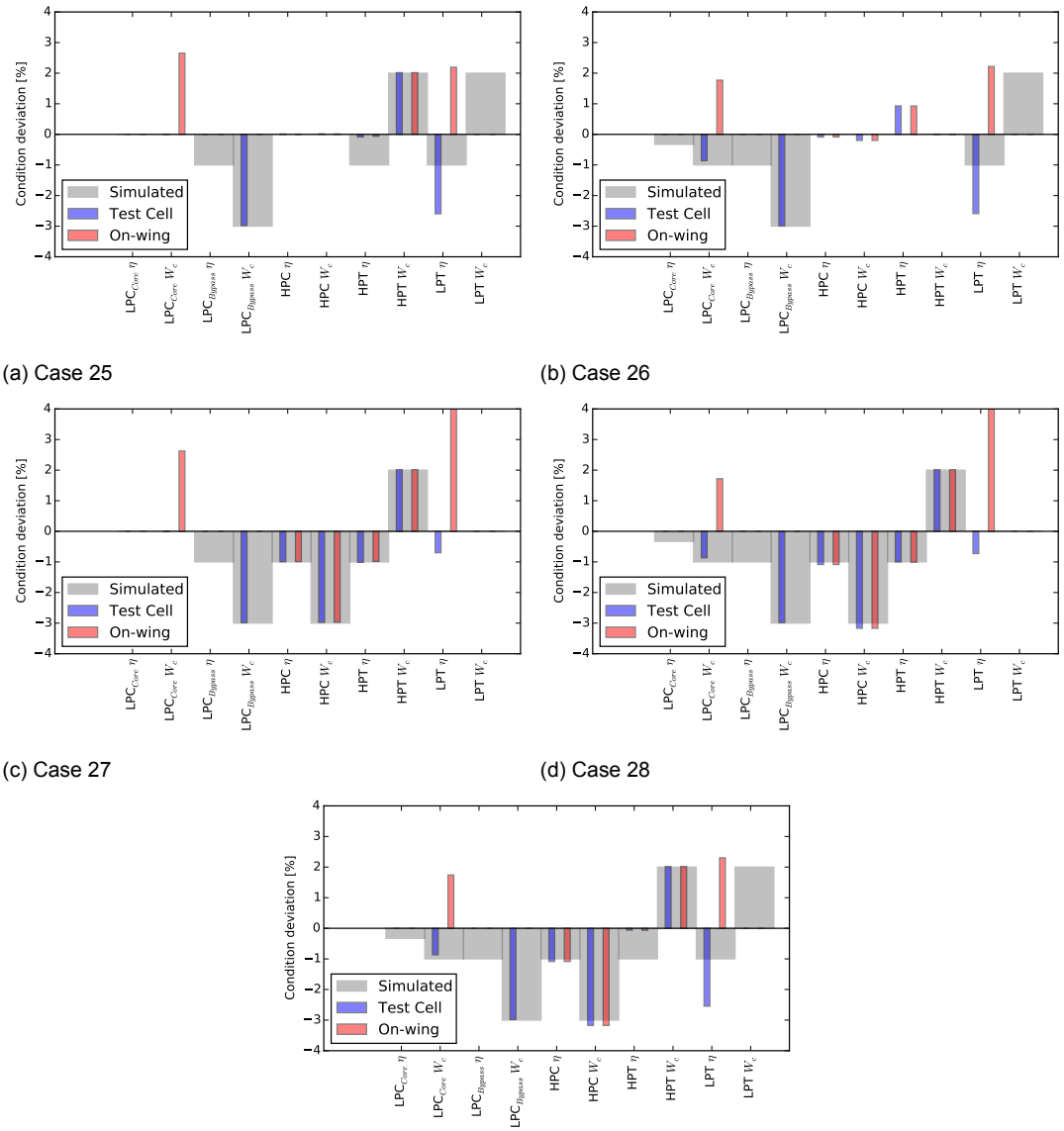

(a) Case 25

(b) Case 26

(c) Case 27

(d) Case 28

(e) Case 29

Figure B.3: Analysis of an engine with different types of simulated deterioration ('V. Full+' cases from Table 11.1) for either test cell or on-wing measurements

C

Thermodynamic principles of gas turbines

In this chapter the thermodynamic principles behind gas turbines are explained. This is followed by an example design point performance computation.

C.1. The ideal Joule-Brayton cycle

The thermodynamic cycle describing the thermodynamic process in the gas turbine is called the Joule-Brayton cycle [31]. Ignoring irreversibility effects and heat losses the ideal Joule-Brayton cycle consists of the following steps:

1. Isentropic compression
2. Isobaric heat addition
3. Isentropic expansion
4. Isobaric heat rejection

In the ideal cycle it is also assumed that the working fluid is an ideal gas, the properties, composition and mass flow of which does not change during the process. Furthermore it is assumed that there are no mechanical and pressure losses [31].

This process is also shown in Fig. C.1. The different processes take place continuously, the flow through the gas turbine does not come to a halt while flowing through the different stages.

The Joule-Brayton cycle can be both an open and a closed cycle. In a closed cycle the same working fluid circulates through the engine. In an open cycle new working fluid is drawn into the engine and heat rejection takes place outside the engine. In an open cycle the working fluid is usually atmospheric air, with heat rejection taking place in the atmosphere [31]. Both the open and closed cycle are shown in Fig. C.2.

An aircraft engine operates on an open Joule-Brayton cycle, with atmospheric air as the working fluid. Compression takes place inside the compressor, heat addition in the combustion chamber, expansion inside the turbine and heat rejection in the atmosphere.

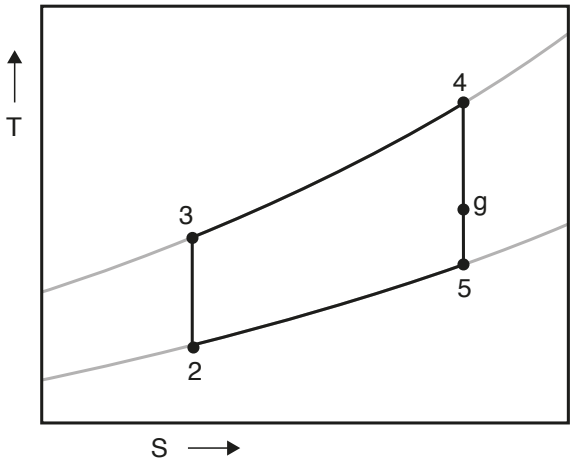

Figure C.1: T-S diagram of the ideal Joule-Brayton cyle [31][Redrawn]

In Figs. Fig. C.1 and Fig. C.2 a station g is indicated. In Fig. C.1 station is the point at which the distance between station 2 and 3 is equal to the distance 4-g. This represents the power needed to compress the air in the compressor. The residual power, distance g-5, represents the gas power, the power that can be extracted from the engine. The process 2-3-4-g is called the gas generator as is also indicated in Fig. C.2 [31].

The ideal simple cycle as described above can be extended with extra steps and components [26]. The cycle can be enhanced with for example a heat exchanger or intercooler. As these components are not used on the GEnx-1B, these additions will not be investigated further.

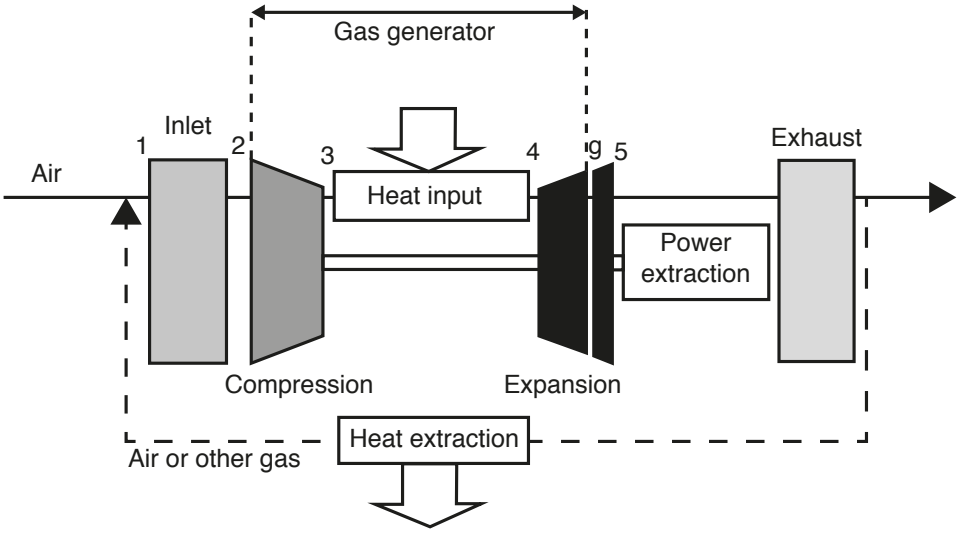

Figure C.2: Diagram of the open and closed cycle. The closed cycle is represented by the dashed line [31][Redrawn]

C.2. Real cycles

The process taking place inside a real engine differs from that of the ideal cycle as described in Appendix C.1. Irreversible effects cannot be ignored, changing the ideal steps. In this section the differences with the ideal cycle will be explained, followed by an overview of how the cycle calculations change.

C.2.1. Validity of the ideal cycle assumptions

In formulating the ideal cycle several assumptions have been made. In this section these assumptions will be investigated, to see how they hold in the real process.

The first assumption made ignores irreversibility effects. Due to this compression and expansion are assumed to be isentropic. In the real cycle however friction and other losses occur, making the process irreversible. This assumption can therefore not be held [31]. From this also follows that the differences in kinetic energies cannot necessarily be ignored [26].

Heat losses from the working fluid to the surroundings were also assumed to be nonexistent inside the gas turbine. This assumption can hold, as the steady-state heat exchange inside the engine is very small [31], having a negligible impact on performance.

The working fluid of the engine was assumed to be an ideal gas, with constant properties, composition and mass flow. This assumption partially holds. The working fluid can be assumed to behave as an ideal gas [31]. The properties however change. The specific heats of the working fluid and the ratio between them changes inside the engine, due to heat and in the case of internal combustion chemical reactions (change of composition) [26]. Changes due to pressure can be ignored [31]. The mass flow cannot always be assumed to be constant. The changes in mass flow due to fuel addition in the combustion chamber can safely be ignored [26, 31]. However, mass flow changes due to cooling flows or other bleed flows must be taken into account in order to make accurate cycle calculations [26].

Finally pressure and mechanical losses were assumed to be zero. Pressure losses are existent in the actual gas turbine, occurring due to friction and heat addition [26, 31]. Furthermore mechanical losses also occur due to friction and due to powering auxiliaries [26]. Powering the auxiliaries does not contribute to the power delivered by the engine, resulting in a mechanical loss.

It must be noted that the ideal cycle, as seen in Fig. C.1 does not result in an entropy increase, while producing useful work, which is not possible in a real system. Redrawing Fig. C.1 with the above changes in mind gives Fig. C.3, where it is visible that during the process entropy increases.

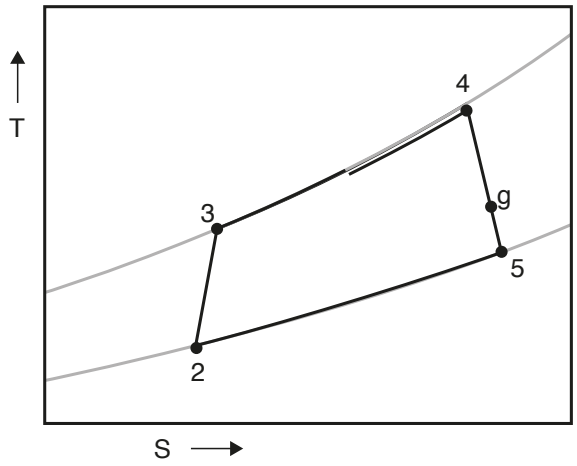

Figure C.3: T-S diagram of the Joule-Brayton cyle [31][Redrawn]

C.2.2. Effects on engine performance

The differences between the ideal and real cycle have their effects on the performance of the gas turbine, which will be described next.

Isentropic efficiencies

Due to reversible effects losses occur during compression and expansion in the real cycle when compared to the ideal isentropic processes. This is also shown in Fig. C.4. Here it is shown that in the actual process the same total pressure is reached at a higher total temperature than for the isentropic process. In addition an increase in entropy is visible in both processes. Using this information the isentropic efficiencies can be defined, Eqs. (C.1) and (C.2) [26]. Here η_c is the isentropic compressor efficiency and η_t the isentropic turbine efficiency. T refers to the temperature and h to the enthalpy at the different stations. The 0 subscripts refer to the total properties, is to the isentropic cases.

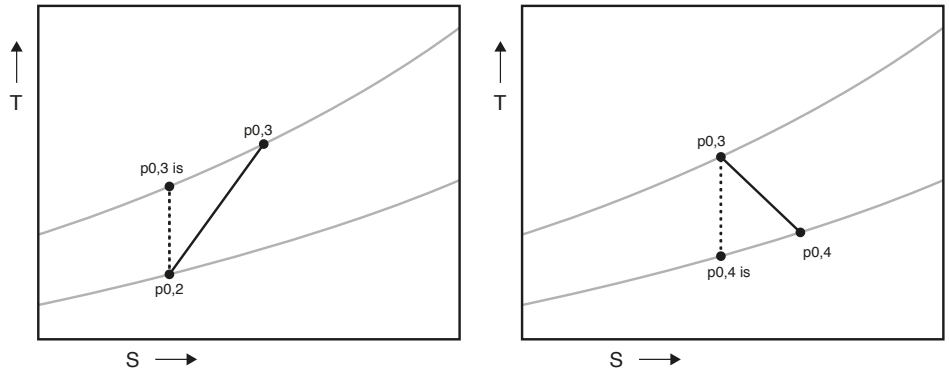

(a) Compression (b) Expansion

Figure C.4: Detailed view of the differences between the real and ideal cycle for compression and expansion [31][Redrawn]

$$\eta_c = \frac{h_{0,3,is} - h_{0,2}}{h_{0,3} - h_{0,2}} = \frac{T_{0,3,is} - T_{0,2}}{T_{0,3} - T_{0,2}} \tag{C.1}$$

$$\eta_t = \frac{h_{0,3,} - h_{0,4}}{h_{0,3} - h_{0,4,is}} = \frac{T_{0,3,} - T_{0,4}}{T_{0,3} - T_{0,4,is}} \tag{C.2}$$

Here use has been made of the assumption that the working fluid inside the gas turbine behaves as an ideal gas. Assuming that the specific heat at constant pressure, c_p, is constant, the relation between change in total enthalpy and total temperature in an ideal gas is given by Eq. (C.3). As the processes taking place in the compressor and turbine are adiabatic the numerator and denominator in Eqs. (C.1) and (C.2) represent a change in work [26].

$$\Delta h_0 = c_p \Delta T_0 \tag{C.3}$$

For the intake the ram efficiency, η_{ram} can be defined rather than the isentropic efficiency. The ram efficiency is given by Eq. (C.4) [25]. Its parameters are easier to measure, but can be used interchangeably with the isentropic efficiency up until Mach 0.8.

$$\eta_{ram} = \frac{p_{0,1} - p_0}{p_{0,0} - p_0} \tag{C.4}$$

Pressure losses
From Appendix C.2.1 follows that there are additional pressure losses in the gas turbine, for example in the combustion chamber. These are not added as efficiencies, but rather subtracted from the pressures at the beginning of the component. Pressure losses in ducts before the compressors and turbines are usually accounted for in the isentropic efficiencies [26].

Mechanical efficiency
As noted in Appendix C.2.1 mechanical losses occur due to friction. These are accounted for using the mechanical efficiency, defined in Eq. (C.5)[31]. Losses are usually small, in the order of 1% [26].

$$\eta_{mech} = \frac{\text{Turbine power} - \text{Mechanical losses}}{\text{Turbine power}} \tag{C.5}$$

Combustion efficiency
Although not the result of an assumption from Appendix C.2.1 the last efficiency that has to be accounted for is the combustion efficiency. Combustion takes place under less than ideal circumstances,

due to which the combustion process is incomplete. Furthermore not all heat is released into the working fluid, some is lost in heating the combustion chamber and its surroundings. These losses are taken into account using the combustion efficiency, η_{cc} defined in Eq. (C.6) [31]. Here $\dot{m}$ is the mass flow and LHV the Lower Heating Value. The subscript air refers to the air, or working fluid if no air is used and f to the fuel used for combustion. The numerator is the amount of energy added to the flow, the denominator the amount of energy available in the fuel in case of ideal combustion.

$$\eta_{cc} = \frac{\dot{m}_{air} c_{p,gas} \left(T_{0,4} - T_{0,3}\right)}{\dot{m}_f \mathrm{LHV}_f} \tag{C.6}$$

C.3. Design point performance

In this section an example calculation procedure is given for the design point performance of a generic gas turbine. Design point calculations are relatively straight forward and can usually be completed without the need for iteration [38]. Design point calculations follow the air through the engine from inlet to nozzle. In this section the design point calculations are shown [24, 26, 31]. The exact equations to be used depend on the parameters known. Different authors use different schemes, however the idea behind the equations is the same. The equations here are valid for a boosted twin-spool turbofan. The equations used are based on those used by Rao [24]. Station numbers are denoted in accordance with Aerospace Recommended Practice (ARP) 755A standard [43].

First the total ambient conditions have to be calculated, the total pressure and total temperature. This is done using Eqs. (C.7) and (C.8).

$$T_{0,am} = T_{am}\left(1 + \frac{\gamma_a - 1}{2} M^2\right) \tag{C.7}$$

$$p_{0,am} = p_{am}\left(\left(1 + \frac{\gamma_a - 1}{2} M^2\right)^{\frac{\gamma_a}{\gamma_a - 1}}\right) \tag{C.8}$$

The effect of the inlet is calculated next. The ambient properties do not change at the start of the inlet. The inlet is assumed to be adiabatic, see Appendix C.2.1, hence the total temperature remains constant over the inlet. The total pressure changes. The total pressure after the inlet is calculated using Eq. (C.9). Here η_{in} is the inlet isentropic efficiency.

$$p_{0,2} = p_{am}\left(\left(1 + \eta_{in} \frac{\gamma_a - 1}{2} M^2\right)^{\frac{\gamma_a}{\gamma_a - 1}}\right) \tag{C.9}$$

Next the fan will compress the flow, increasing the total pressure and temperature. The pressure increase is dictated by the Pressure Ratio (PR) shown in Eq. (C.10). The temperature increase is dictated by the isentropic compression equation, with the added isentropic efficiency, Eq. (C.11).

$$p_{0,21} = \mathrm{PR}_{fan} \cdot p_{0,2} \tag{C.10}$$

$$T_{0,21} = T_{0,2}\left(1 + \frac{1}{\eta_{fan}}\left(\left(\frac{p_{0,21}}{p_{0,2}}\right)^{\frac{\gamma_a - 1}{\gamma_a}} - 1\right)\right) \tag{C.11}$$

After the fan the airflow is split into the core and bypass flow. The bypass flow properties will not change anymore, no pressure losses in the duct are taken into account in these calculations. The bypass flow will return at the end of the calculations. The mass flow in both the core and bypass flow can be calculated using Eq. (C.12). Here it assumed that the bypass ratio (BPR) is known and either the total mass flow, core mass flow or bypass mass flow.

$$\mathrm{BPR} = \frac{\dot{m}_{bypass}}{\dot{m}_{core}} \tag{C.12}$$

The core flow continues through the booster and HPC. Through both components the total pressure and temperature rise. The same equations as for the fan can be used, Eqs. (C.10) and (C.11), replacing the fan PR and efficiency with those of the booster and HPC.

After the HPC the core flow goes through the combustion chamber. In the combustion chamber pressure losses occur due to friction and heat addition, see Appendix C.2.1. These losses are assumed to be known, hence the total pressure after the combustion chamber is given by Eq. (C.13). Assuming that the fuel mass flow is given the total temperature can be calculated with Eq. (C.14). Here η_{cc} is the combustion efficiency. If the total temperature after the combustion chamber is given, Eq. (C.14) can be rewritten to calculate the fuel mass flow. The total mass flow after the combustion chamber is given by Eq. (C.15).

$$p_{0,4} = p_{0,3} - \Delta p_{cc} \tag{C.13}$$

$$T_{0,4} = T_{0,3} + \frac{\dot{m}_f \mathrm{LHV}_f \eta_{cc}}{\dot{m}_{core} c_{p,gas}} \tag{C.14}$$

$$\dot{m}_{gas} = \dot{m}_4 = \dot{m}_{core} + \dot{m}_f \tag{C.15}$$

Next are the turbines. The turbines power the compressor connected to the same shaft. For the HPT this is the HPC. The HPT must provide the work needed by the HPC. Using Eq. (C.3) and the assumption of an adiabatic turbine, it is found that the work comes from a total temperature drop over the turbine. Taking the mechanical efficiency into account the total temperature after the HPC can be calculated using Eq. (C.16). Next the total pressure after the HPC is calculated using Eq. (C.17).

$$T_{0,45} = T_{0,4} - \frac{\dot{m}_{core} c_{p,a} \left(T_{0,3} - T_{0,25}\right)}{\eta_{mech} c_{p,g} \dot{m}_4} \tag{C.16}$$

$$p_{0,45} = p_{0,4} \left(1 - \frac{1}{\eta_{HPC}} \left(1 - \frac{T_{0,45}}{T_{0,4}}\right)\right)^{\frac{\gamma_g}{\gamma_g - 1}} \tag{C.17}$$

The pressure and temperature drop over the LPT can be calculated in the same way. For the LPT the work performed by the fan needs to be calculated as well, as the fan is connected to the same shaft as the booster and LPT.

As the flow has been expanded through both turbines it needs to be expelled through the nozzle. It must be checked first if the nozzle is choked, that is if sonic speeds are reached in the nozzle. This is true depending if Eq. (C.18) is true. Here η_j is the nozzle efficiency.

$$\frac{p_{0,7}}{p_{0,am}} \geq \frac{1}{\left(1 - \left(\frac{1}{\eta_j}\right)\left(\frac{\gamma_g - 1}{\gamma_g + 1}\right)\right)^{\frac{\gamma_g}{\gamma_g - 1}}} = \mathrm{PR}_{crit} \tag{C.18}$$

In case the nozzle is choked a shockwave is present in the nozzle. In this case Eqs. (C.19) to (C.24) are used to calculate the thrust produced by the core. The area in Eq. (C.24) is an approximation [26]. It is used to calculate the force caused by expanding the flow to ambient conditions outside of the engine [31].

$$T_8 = \frac{2T_{0,7}}{\gamma_g + 1} \tag{C.19}$$

$$p_8 = \frac{p_{0,7}}{\mathrm{PR}_{crit}} \tag{C.20}$$

$$v_8 = \sqrt{\gamma_g R T_8} \tag{C.21}$$

$$\rho_8 = \frac{p_8}{R T_8} \tag{C.22}$$

$$A_8 = \frac{\dot{m}_7}{\rho_8 v_8} \tag{C.23}$$

$$F_{core} = \dot{m}_7 \left(V_8 - V_0\right) + A_8 \left(p_8 - p_{am}\right) \tag{C.24}$$

In case the nozzle is not choked, the thrust produced can be calculated using Eqs. (C.25) to (C.27).

$$T_8 = T_{0,7}\left(1 - \eta_j\left(1 - \frac{p_{am}}{p_{0,7}}^{\frac{\gamma_g - 1}{\gamma}}\right)\right) \tag{C.25}$$

$$v_8 = \sqrt{2 c_{p,g}\left(T_{0,7} - T_8\right)} \tag{C.26}$$

$$F_{core} = \dot{m}_7 \left(V_8 - V_0\right) \tag{C.27}$$

The thrust for the bypass flow is found in the same way. The total thrust is found by adding the core and bypass thrust. Again it needs to be checked if the nozzle, in this case the bypass nozzle, is choked.

Using Eqs. (C.7) to (C.27) all gas path properties of the engine have been calculated. Using these properties the Specific Fuel Consumption (SFC) and efficiencies can be calculated. Note that in these calculations no use has been made of the physical properties of the engine components. The flow path areas are unknown (which are only needed for static property calculations [5]) shaft rotation speeds are not known et cetera.